ABSTRACT

INVESTIGATION OF SOLID POLYMERIC HOLLOW FIBER HEAT EXCHANGE DEVICES FOR USE IN THERMALLY-DRIVEN DESALINATION PROCESSES

by
Saskia Christian

The heat exchange between hot brine (4 wt% NaCl) and cold water as well as between condensing steam and cold water without direct fluid-fluid contact using modules made out of solid polymeric hollow fibers of polypropylene (PP) and polyetheretherketone (PEEK) has been studied. The solid hollow fiber dimensions were 425μm/575μm (ID/OD) for PP and 420μm/570μm (ID/OD) for PEEK. Extensive heat transfer measurements have been performed and the experimentally-determined overall heat transfer coefficients utilized to isolate the wall heat transfer coefficient, the inside heat transfer coefficient and the outside heat transfer coefficient. The heat exchange between hot brine and cold water was evaluated at hot brine temperatures between 82 ^{o}C and 99 ^{o}C and cold water temperatures between 5 ^{o}C and 41 ^{o}C. The tube-side Reynolds Number was varied in the range of 58-2464 and 3-160, respectively for the hot brine-cold water and condensing steam-cold water systems. The maximum U (overall heat transfer coefficient based on the inside area) values attained in the hot brine-cold water system for PEEK and PP-based modules were 1914 W/m^2-K and 2076 W/m^2-K, respectively. The maximum U value attained in the two-phase heat exchange system was 1700 W/m^2-K. Overall, the PP-based module HEPP2 showed the highest conductance per unit volume (CUV) value (2.92x10^6 W/m^3-K). The highest CUV value achieved was approximately 19 times higher than what can be achieved in conventional metallic shell and tube heat

exchangers. The results for hot brine-cold water heat exchange demonstrated thermal efficiencies very close to 97% and up to four transfer units for devices having height of transfer unit (HTU) values as low as 5 cm. Those results were attained under conditions of lower tube-side Reynolds numbers.

INVESTIGATION OF SOLID POLYMERIC HOLLOW FIBER HEAT EXCHANGE DEVICES FOR USE IN THERMALLY-DRIVEN DESALINATION PROCESSES

by
Saskia Christian

A Thesis
Submitted to the Faculty of
New Jersey Institute of Technology
in Partial Fulfillment of the Requirements for the Degree of
Master of Science in Chemical Engineering

Department of Chemical Engineering

August 2005

APPROVAL PAGE

INVESTIGATION OF SOLID POLYMERIC HOLLOW FIBER HEAT EXCHANGE DEVICES FOR USE IN THERMALLY-DRIVEN DESALINATION PROCESSES

Saskia Christian

8/9/05

Dr. Kamalesh Sirkar, Thesis Advisor — Date
Distinguished Professor of Chemical Engineering, NJIT
Foundation Professor, Membrane Separations

9/8/05

Dr. Marino Xanthos, Committee Member — Date
Professor of Chemical Engineering, NJIT

8/8/2005

Dr. Michael Huang, Committee Member — Date
Assistant Professor of Chemical Engineering, NJIT

BIOGRAPHICAL SKETCH

Author: Saskia Christian

Degree: Master of Science

Date: August 2005

Undergraduate and Graduate Education:

- Master of Science Degree in Chemical Engineering
  New Jersey Institute of Technology, Newark, NJ, 2005

- Bachelor of Science Degree in Chemical Engineering
  University of the West Indies, St. Augustine Campus, Trinidad and Tobago, 2001

Major: Chemical Engineering

This thesis is dedicated to my mother, Osme Minns. I extend my deepest expression of love and appreciation for the encouragement and the sacrifices she made throughout my graduate studies.

ACKNOWLEDGMENT

I extend my most profound gratitude to my advisor, Professor Kamalesh Sirkar for his invaluable assistance in the culmination of this thesis work. My sincerest appreciation is also extended to my thesis committee members, Professors Marino Xanthos and Michael Huang for their contributions.

A special thanks is given to Dr. Liming Song for his support throughout this study. I would like to thank the Van Houten Librarian, Mr. Bruce Slutsky for rendering assistance with the literature review search.

I also express my appreciation to my colleagues in the NJIT Membrane Separations Group for their encouragement and assistance over the years. I would like to acknowledge the financial support provided by ONR through two contracts N000140311002 (10/15/03 – 09/15/04) and N000140410810 (09/15/04 – 09/14/05).

Last, but certainly not the least, I would like to thank my mother and sister for their motivation throughout this project and my graduate studies.

LIST OF SYMBOLS

A	heat transfer area, m^2
A_i	inside heat transfer area, m^2
C	heat capacity rate, $\dot{m}C_p$, $W\ K^{-1}$
C^*	heat capacity ratio, Equation (3.14 c)
C_p	specific heat, $J\ kg^{-1}\ K^{-1}$
CUV_C	clean conductance per unit volume, $W\ m^{-3}\ K^{-1}$, Equation (3.25)
CUV_D	dirty conductance per unit volume, $W\ m^{-3}\ K^{-1}$
D	diameter, Equation (3.7 a)
D_i	inside fiber diameter
D_o	outside fiber diameter
D_s	shell inside diameter
D_1	diameter of central distribution tube with one fiber layer
D_4	diameter of central distribution tube with four fiber layers
D_T	tape thickness
D_{DT}	diameter of central distribution tube
$f_{Fanning}$	Fanning friction factor
g	gravitational constant, $9.81 m\ s^{-2}$
h_i	inside or tube-side heat transfer coefficient, $W\ m^{-2}\ K^{-1}$
h_o	outside or shell-side heat transfer coefficient, $W\ m^{-2}\ K^{-1}$
HTU	height of a transfer unit, cm
j_H	Colburn factor for heat transfer, $St\ Pr^{2/3}$

LIST OF SYMBOLS

k	thermal conductivity, W m^{-1} K^{-1}
K_{ent}	fiber entrance pressure loss coefficient
K_{ex}	fiber exit pressure loss coefficient
K_b	pressure loss coefficient related to the 90° bend
L	active fiber length, cm
L_{actual}	actual fiber length inside the module, cm
$\dot{m}$	mass flow rate, kg s^{-1}
N	number of fibers in module
Nu	Nusselt number, $\frac{hD}{k}$
Nu_{T3}	inside Nusselt number for the T3 boundary condition
NTU	number of transfer units, Equation (3.14 b)
NTU_{cf}	number of transfer units based on temperature correction factor, Equation (3.14 a)
N'_{HEPP1}	the number of fibers per layer in module HEPP1
ΔP	pressure drop across module, Pa
ΔP_{true}	the true pressure drop inside the fibers
ΔP_T	experimentally derived pressure drop
Pr	Prandtl number, $\frac{C_p \mu}{k}$
Q	rate of heat transfer, W
q_w	wall heat flux, W m^{-2}

LIST OF SYMBOLS

r	radial coordinate, m
r_i	inside radius, m
R	thermal resistance, $m^2 K W^{-1}$
Re_t	tube-side Reynolds Number, $\frac{D_i u_t \rho}{\mu}$
Re_s	shell-side Reynolds Number, $\frac{D_o u_s \rho}{\mu}$
s	thermal energy source number
S	uniform heat generation per unit volume
S*	sum of squares of the residuals of 1/U
St	Stanton number, $Nu / Re\,Pr$
T	temperature, K
T_{s1}	shell-side fluid inlet temperature, °C
T_{s2}	shell-side fluid outlet temperature, °C
T_{t1}	tube-side fluid inlet temperature, °C
T_{t2}	tube-side fluid outlet temperature, °C
T_a	surrounding medium temperature, K
U	overall heat transfer coefficient based on the inside area, $W m^{-2} K^{-1}$
U_o	overall heat transfer coefficient based on the outside area, $W m^{-2} K^{-1}$
V	volume, m^3
u_s	shell-side velocity, $cmmin^{-1}$
u_t	tube-side velocity, $cmmin^{-1}$

LIST OF SYMBOLS

x^*	dimensionless axial distance for hydrodynamically developing flow, $(x/D)/\mathrm{Re}$
Y_n	n^{th} eigenfunction
z	axial displacement, m
W_1	flow width based on the first fiber layer
W_4	flow width based on the fourth or last fiber layer

Greek Symbols

α	surface area/volume ratio based on the total module volume, m^2m^{-3}
ε	heat exchanger effectiveness factor, Equation (3.14 d)
θ	dimensionless temperature
λ_n	n^{th} eigenvalue
μ	dynamic viscosity, kg $m^{-1}s^{-1}$
ξ	dimensionless radial displacement, r/r_i
ρ	density
σ	ratio of inside fiber (core) free flow- area to compact heat exchanger frontal area

LIST OF SYMBOLS

Subscripts

b	bulk
ent	entrance
ex	exit
i	inside
in	inlet
lm	logarithmic mean
loc	local
o	outside
out	outlet
ov	overall
s	shell side
t	tube side
w	wall

TABLE OF CONTENTS

TABLE OF CONTENTS
(Continued)

LIST OF FIGURES

LIST OF FIGURES
(Continued)

LIST OF FIGURES
(Continued)

LIST OF FIGURES
(Continued)

LIST OF TABLES

LIST OF TABLES
(Continued)

LIST OF TABLES
(Continued)

CHAPTER 1

INTRODUCTION

1.1 Objective

Thermally-driven desalination processes involve heat exchange between hot brine and cold brine, distillate and cold brine and steam and cold/hot brine. This thesis investigates heat exchange rates in thermal desalination processes using solid polymeric hollow fiber-based heat exchange devices having either transverse or parallel flow mode. The utilization of metallic shell-and-tube heat exchangers in thermal desalination processes requires large capital investments as well as high costs for assembly and other fabrication aspects [El-Dessouky and Ettouney, 1999]. They also encounter considerable fouling and corrosion problems. To support the use of construction materials such as high steel alloys for the production of heat transfer surfaces in thermally-driven desalination processes, employment of corrosion control agents and frequent parts replacement are required to sustain high production rates [El-Dessouky and Ettouney, 1999].

The adoption of plastic heat exchangers (such as evaporators and condensers) for thermally-driven desalination processes is quite advantageous and is motivated by several factors such as ease of construction, lower erection cost and elimination of in-leakages [El-Dessouky and Ettouney, 1999]. Plastic heat exchangers built with smaller polymeric tubes made out of thermally, chemically stable, hydrophobic plastics are potentially excellent alternatives to metallic heat exchangers. These heat exchange systems are capable of attaining overall heat transfer coefficients comparable with metallic shell-and - tube heat exchange devices with a heat transfer area density (based on outside area) of approximately 1394 m^2/m^3 [Zarkadas and Sirkar, 2004]. Significant cost savings may be

attained through the use of these compact, lightweight, ultra-thin wall (75 μm) thick devices for liquid-liquid and vapor-liquid heat exchange. The ultrathin walls supply reasonably high wall heat transfer coefficient values. Although polymers possess low strength, low thermal conductivity and large thermal expansion (ten times greater than metals), their resistance to chemical attack at low temperatures and pressures and their low cost relative to that of metals outweigh these shortcomings [Reay, 1989]. The tube-side fluid in these polymeric tubular devices flows through a chemically inert flouropolymer wall and there is unidirectional shell and tube-side liquid flows. This unidirectional flow pattern facilitates full purging of the devices after batch operation [Zaheed and Jachuck, 2004].

In this study, the heat exchange characteristics of modules constructed out of solid, nonporous, hydrophobic hollow fine fibers of polypropylene (PP) and polyetheretherketone (PEEK) are investigated for hot brine-cold water and steam-cold water heat exchange. The PP fibers used can sustain temperatures of up to 105^0C and their wall conductive heat transfer coefficient is 2125 W/m^2-K based on a thermal conductivity of 0.17 W/m-K and a wall thickness of 75 μm. Polyetheretherketone (PEEK) has working temperatures in excess of 250°C and also exhibits resistance to most process fluids. The wall thermal conductivity of PEEK fibers is 0.25 W/m-K and the corresponding wall conductive heat transfer coefficient of the PEEK-based hollow fiber module (based on 75 μm thickness) used in this study is approximately 3300 W/m^2-K. Since the fiber walls are of nonporous nature, there is no pore fouling. The cold water to be heated flows on one side of the heat exchanger and the flowing hot brine or steam is cooled on the other side. The overall heat transfer coefficients as well as the inside and outside heat transfer coefficients obtained from analysis of experimental results are to be

characterized; the product of the overall heat transfer coefficient and heat exchanger surface area per unit volume for the test modules is to be compared with those obtained with metallic shell-and-tube heat exchangers. The heat transfer coefficients obtained from modules with shell-side crossflow arrangement are also to be compared with those obtained from modules with shell-side parallel flow arrangement. Other heat exchange performance indicators such as thermal effectiveness factor, number of transfer units (NTU), pressure drop per NTU and height of transfer unit (HTU) are also to be assessed in order to compare the heat exchange performances of the various test polymeric hollow fiber modules with those of conventional metallic shell-and-tube heat exchangers.

1.2 Background Information

Development and applications of metallic compact heat exchanger systems have significantly progressed over the years. Concurrently, compact polymer film-based heat exchange devices and polymeric shell-and-tube units have become quite useful for both single-phase and two-phase heat exchange applications.

Compact polymer film-based devices are critical to the growth of a new age of heat exchangers since they offer substantial savings in weight, space and cost; they also possess considerable corrosion resistance making them superior to their rival metallic heat exchangers. Polymeric heat exchangers of conventional shell-and-tube configuration have been employed in numerous applications in the desalination, biotechnology and environmental industries [El-Dessouky and Ettouney, 1999].

However, polymers have their shortcomings due to their low strength when compared to metals, their low wall thermal conductivities and their inability to sustain high temperatures metallic heat exchangers can easily tolerate [Reay, 1989]. The thermal

conductivities of polymeric materials fall in the range of 0.1- 0.4 Wm^{-1}-K^{-1} which is 100 to 300 times lower than that of metals; hence, this demands use of thin walled polymeric tubes or fibers for performance to be comparable to metallic rivals [El-Dessouky and Ettouney, 1999]. Atmospheric degradation can pose a major problem to polymers at moderate temperatures; hence, stabilizers need to be incorporated to guard against this effect [Reay, 1989]. In order for plastics to compete with their metal counterparts in heat exchanger applications, high temperature plastics with better mechanical attributes need to be developed.

Polymer film-based compact heat exchangers have been widely employed in plastic solar collectors for low temperature applications [Shah, 1997]. The heat transfer and pressure drop characteristics of a matrix of corrugated (to promote crossflow on shell side) 100 μm PEEK film in water-water system were investigated by Shah [1997]. Crossflow plate exchangers constructed out of cross-corrugated films of polyetheretherketone were also utilized to study heat exchange in a water-water system. These films had a channel wall thickness of 50 μm and yielded overall heat transfer coefficient values between 900 and 1000 W/m^2-K [Jachuck and Ramshaw, 1994]. Those values for the corrugated films were the highest overall heat transfer coefficients values ever reported in literature for film- based plastic heat exchangers in single-phase heat exchange applications.

Zaheed and Jachuck [2004] also reviewed the use of polymer compact heat exchangers with primary focus on the polymer film unit. Zaheed and Jachuck [2004] suggested polyvinylidene fluoride (PVDF)-based and PEEK- based thin films with hydrophobic super smooth surfaces as alternative materials of construction to metals in heat exchangers. However, those units unlike corrugated polymer film units did not deal

effectively with the inherently low thermal conductivity and the adoption of laminar flow regime to avoid high pressure drops. For wall thickness of 1mm, 0.9 mm and 0.8 mm, only overall heat transfer coefficients of 145, 160 and 175 W/m^2-K were attained, respectively. More recent designs of PVDF heat exchangers were successful in decreasing the wall thickness to a range of 0.5 -1 mm and increasing the heat exchange performance. However, none of the more recent designs for film-based heat exchangers yielded overall heat transfer coefficients comparable with those reported for corrugated films or those reported by Zarkadas and Sirkar [2004] for polymeric ultra-thin wall tubular heat exchangers.

Few studies were done to demonstrate the heat exchange performance of polymer-based tubular heat exchangers in liquid-liquid heat exchange systems. George Fischer Inc. had developed the Calorplast compact shell-and-tube heat exchanger featuring corrosion resistant material in a lightweight shell suitable for heat exchange in liquid-liquid applications [Zaheed and Jachuck, 2004]. Teflon shell-and-tube heat exchangers by Fluorotherm have been developed for efficient heat transfer in applications where chemical inertness to aggressive fluids matters the most [Zaheed and Jachuck, 2004]. Morcos and Shafey [1995] studied the use of turbulence enhancement devices in a PVC shell-and-tube heat exchanger for an aqueous/aqueous system and were able to augment the overall heat transfer by a factor of 3.5 using Reynolds number as high as 1000. Liu, Davidson and Mantell [2000] had investigated the feasibility of lowering the cost of solar water heating systems by using tube-in-shell heat exchangers fabricated out of crosslinked polyethylene (PEX) tubes and ultra-thin high temperature nylon (HTN) tubes. Liu, Davidson and Mantell [2000] had also compared the performance of polymer-based heat exchangers with copper shell-and-tube heat exchangers and concluded that

polymeric heat exchangers can supply thermal output similar to that of copper heat exchangers at a substantially lower cost. Although this study is related to heat exchange for liquid-liquid applications, it is not directly related to the idea presented in this study since potable water (liquid receiving heat) was passed through single walled tubes at a higher pressure than the collector heat transfer liquid.

El-Dessouky and Ettouney [1999] claimed that the overall heat transfer coefficient for polymeric heat exchangers with shell-and-tube configurations falls between 100 and 500 W/m^2-K for thermal desalination processes which is substantially lower than conventional metallic shell-and-tube heat exchangers, having values of up to 3300 W/m^2-K. Those results were obtained in heat exchangers having a wall thickness of 0.15- 0.44 mm, tube diameter of 1.5-6 mm, heat transfer area of 50 m^2 and a heat transfer area density of 600 m^2/m^3. The hollow fine fiber heat exchange devices used in the present study have a much lower wall thickness (75 μm), much smaller fiber diameter and comparable or substantially higher heat transfer area densities. These attributes potentially can lead to the achievement of overall heat transfer coefficients much higher than those previously reported values for plastic heat exchangers with larger polymeric tubes in desalination processes.

Solid, hydrophobic, fine, hollow fibers were not incorporated in the design of any of the aforementioned shell-and-tube polymer heat exchangers. There was only one study that investigated the heat exchange performance of polymer-based hollow fine fiber heat exchangers. Zarkadas and Sirkar [2004] proposed polymeric hollow fine fiber heat exchangers as an alternative for lower temperature and pressure applications. They tested the performance of a water-water system and an ethanol-water system in nonporous, hydrophobic polymeric hollow fine fiber heat exchangers. They achieved overall heat

transfer coefficients of 647-1314 Wm^{-2}-K^{-1} (based on outside fiber area) for the water-water system in a parallel flow configuration at the shell side of the devices and concluded that those results were larger than the values ever reported for liquid-liquid applications.

However, the present study extensively investigates the use of solid hollow hydrophobic fine fibers in heat exchange devices for liquid-liquid applications using devices having parallel flow configuration as well as crossflow configuration at the shell side. The plastic heat exchanger designs discussed earlier demonstrated heat exchange performance superior to that of their metal competitors but were not necessarily more compact than metallic heat exchangers. Hence, the much more compact solid nonporous polymeric hollow fiber heat exchangers used in this study are most likely to overcome this limitation. A different aqueous-aqueous system (brine, 4 wt % NaCl -cold water) is investigated in this thesis. PP- based and PEEK- based solid hollow fibers were tested extensively between 0°C and 99°C and at Re_t between 58 and 2464. This study will demonstrate that overall heat transfer coefficients much higher than 1314 W/m^2-K are attainable when PP-based and PEEK-based solid nonporous polymeric hollow fiber heat exchangers are employed in aqueous-aqueous systems for both parallel flow and crossflow arrangement on the shell side.

Compact two-phase heat exchangers can find applications in a number of industries (including the desalination industry). These applications can lead to a substantial reduction in energy consumption. That was demonstrated by M.Groll and R.Mertz [2004] who studied various aspects of evaporative heat transfer from enhanced surfaces of tubular heat exchangers. Cheng and Vandergeld [2005] showed how drop wise condensation heat transfer can be achieved in a polymer compact heat exchanger.

They investigated heat transfer and pressure drop characteristics of air/water and air-steam/water heat exchange in polymer-based compact heat exchanger made of polyvinylidene fluoride and concluded that the overall heat transfer coefficients of air-steam/water heat exchanger (150 to 600W/m^2-K) are higher than that of air/water exchange (80 to 130 W/m^2-K). El-Dessouky and Ettouney [1999] studied the use of thin-walled PTFE plastic compact heat exchangers for single effect thermal desalination processes with the primary focus on single effect mechanical vapor compression desalination. They compared the heat exchange and economical performance of shell-and-tube evaporators constructed out of metal with those constructed out of PTFE (polytetrafluoroethylene) plastic and concluded that the PTFE plastic heat exchangers have larger specific heat transfer areas and lower specific costs than metallic (titanium and high steel alloy) shell-and-tube evaporators. Polymer film-based plastic heat exchangers performing heat exchange by evaporation and condensation have been adopted in the desalination industry for purifying saline or brackish water.

Cross-corrugated polymer thin film heat exchangers have been employed as evaporators where gas and liquid flow in a crossflow pattern [Reay, 1989]. Franco and Giannini [2004] proposed a new kind of crossflow compact heat exchanger for the optimum thermal design of modular compact heat exchanger structure for heat recovery steam generators. Franco and Giannini claimed that this modular structure can substitute shell-and-tube structures since its design fosters better performance in terms of heat flow and energy losses, lower installation costs and weight costs. Franco and Giannini also reported that this new kind of compact heat exchanger can attain an area density higher than 500 m^2/m^3 compared to 100-200 m^2/m^3 of the shell-and-tube, metallic heat exchangers.

The present study also investigates the heat exchange performance of PP-based and PEEK-based polymeric, solid hollow fiber heat exchangers having either crossflow mode or parallel flow mode at the shell side of the devices in steam-water applications. The steam-water system was tested extensively between 100°C and 116°C and at Re_t between 3 and 160.

CHAPTER 2

METHODS FOR DETERMINING HEAT TRANSFER COEFFICIENTS

The solutions of forced convection heat transfer problems for laminar flow inside a circular tube or circular duct often involve an assumption of constant and prescribed wall temperature (constant outside convective resistance or constant temperature of the shell surrounding the fibers) or a constant heat flux. These problems are referred to in literature as Extended Graetz Problems and the solutions are expressed in the form of a series of eigenfunctions. All but a few of these extended solutions neglect the resistance to heat transfer at the wall. However, in the case of the polymeric hollow fibers, the fiber wall resistance is significant due to the low thermal conductivity of the polymers (for example, for PP, 0.17 W/m-K); hence, it cannot be ignored in the analysis. In these extended Graetz problems, there is an assumption of uniform fluid temperature at the inlet $z = 0$ and the fluid temperature is unaltered before the inlet by upstream conduction [Michelsen and Villadsen, 1974].

The heat transfer inside the polymeric tube wall is essentially one dimensional and axial thermal conduction can sometimes be neglected. Three different methods of determining the temperature profile inside the polymeric hollow fiber heat exchanger or the inside, outside and wall heat transfer coefficients are explored. These methods are the Conventional Convection Method, Hsu's Method and the Wilson Plot Method. The Sieder-Tate correlation is also examined but this method is only capable of isolating the inside or the tube-side heat transfer coefficients.

2.1 Conventional Convection Method

The circular tube thermal entrance problem for laminar flow through a closed conduit was initially studied by Graetz in 1883 and later by Nusselt in 1910 [Shah and London, 1978]. An incompressible fluid flowing through a circular tube (maintained at constant temperature), with constant physical properties, a fully developed laminar velocity profile and a thermally developing temperature profile was investigated by these pioneers. They derived the first three terms of an infinite series solution for hydrodynamically developed and thermally developing flow for the T boundary condition.

The Conventional Convection method regards the outside wall resistance and the outside convective resistance as one term and the energy equation pertaining to the tube-side liquid is solved [Zarkadas and Sirkar, 2004]. The T3 convective boundary condition is utilized: this assumes that the outside wall temperature of the circular duct is constant axially and that the heat flux is linearly proportional to the difference between the outside wall temperature and the inside wall temperature which can vary axially as well as peripherally [Shah and London, 1978]. However, the surface temperature variation needs to be considered in this approach since considerable surface temperature gradient exists in the solid hollow fiber modules. Different temperature distributions at the wall yields different values of the outside wall heat transfer coefficient hence, this constant wall temperature approach might be misleading.

The formula to evaluate asymptotic Nusselt number was correlated by Hickman as a result of employment of Laplace transform technique in the analysis of thermal entry length problem [Zarkadas and Sirkar, 2004]. The derived asymptotic Nusselt number for fully developed laminar flow was presented as $Nu_{T3} = 3.66$ and this value is applicable to

the case of negligible axial heat conduction, flow work and viscous dissipation within the fluid. The Hickman formula is given in Equation (2.1):

$$Nu_{T3} = \frac{(48/11) + Nu_w}{1 + (59/220)Nu_w} \tag{2.1}$$

$$Nu_w = \frac{U_w D_i}{k_i} \tag{2.2}$$

$$\frac{1}{U_w} = \frac{D_i}{D_o h_o} + \frac{D_i}{2k_w} ln\left(\frac{D_o}{D_i}\right) \tag{2.3}$$

The outside wall to fluid thermal resistance is incorporated in the $1/U_w$ term. Equation (2.1) yields Nu_{T3} values that fall in the range of 3.66 and 4.364. The lower limit of this Nusselt number range is the limiting Nusselt number corresponding to the constant wall temperature condition ($Nu_w = \infty$) and the upper limit is the limiting Nusselt number corresponding to the constant heat flux boundary condition $Nu_w = 0$. The reciprocal of the lumped resistance term $1/U_w$ is the wall heat transfer coefficient and this is calculated based on the inside fiber area. The overall Nusselt number is also calculated based on the inside fiber area since the overall heat transfer coefficient (U) calculations performed for all the runs are based on the tube side of the polymeric heat exchanger only. The overall Nusselt number can be calculated using Equation (2.4):

$$\frac{1}{Nu_{ov}} = \frac{k_i}{UD_i} = \frac{1}{Nu_{T3}} + \frac{1}{Nu_w} \tag{2.4}$$

$$where\ U = \frac{Q}{A_i \Delta T_{lm}} \tag{2.5}$$

$$\frac{1}{U} = \frac{1}{h_i} + \frac{1}{U_w} \tag{2.6}$$

$$\text{where } h_i = \frac{Nu_{T3} k_i}{d_i} \tag{2.7}$$

The expression for Nu_{T3} in Equation (2.1) is then substituted into Equation (2.4) and the second order polynomial expression in terms of Nu_w is then obtained in Equation (2.8):

$$\left[1-\frac{59}{220}Nu_{ov}\right]Nu_w^{\,2}+\left[\frac{48}{11}-2Nu_{ov}\right]Nu_w-\left[\frac{48}{11}\right]Nu_{ov}=0 \qquad (2.8)$$

This quadratic equation is then solved and it produces a positive and a negative root. Only the positive root is considered as the wall Nusselt number. The wall heat transfer coefficient is then calculated from Equation (2.2) and this is then substituted into Equation (2.3) to obtain the outside heat transfer coefficient, h_o.

2.2 Hsu's Method

Hsu's method (the extended Graetz problem with fluid axial heat conduction consideration) and the Leveque type solution have also been developed to address thermally developing laminar flow inside a circular duct utilizing the thermal boundary condition of the third kind. The Leveque solution utilizes the similarity transformation technique and is based on the premise that in the downstream region close to the point of a step change, the temperature changes are confined to a boundary layer that is thin compared to the momentum boundary layer [Shah and London, 1978]. It also neglects any curvature effects in the region close to the wall. This method is only applicable in a very restricted thermal entrance region near x* (dimensionless distance in the flow direction for the thermal entrance region heat transfer) = 0; it yields large errors far from the entrance region. However, Hsu's method of solving the extended Graetz problem is more complete since it accounts for axial heat conduction within the fluid (Peclet number > 50) except for the immediate neighborhood of the thermal entrance region [Shah and London, 1978].

Hsu solved the thermally developing laminar T3 problem by taking into account simultaneous wall convective heat transfer and a uniform internal heat generation source [Hsu, 1971]. The fluid flowing with a fully established laminar velocity profile is assumed to have constant temperature T_o in the vicinity of the thermal entrance region ($z<0$). At $z = 0$, there is onset of uniform heat generation per unit volume S. Simultaneously convective heat transfer occurs through the tube wall to the shell-side fluid which is maintained at a constant temperature T_a hence, constant outside convective resistance is assumed [Hsu, 1971]. As in the case of the classical Graetz problem, this analysis is based on the assumptions of constant physical properties and incompressible fluid flow with negligible viscous dissipation. Unlike the Conventional Convection method, Hsu's method takes into account the axial conduction within both the fluid and tube wall and does not regard the outside convective resistance and wall convective resistance as one lumped term. In essence the wall temperature or the wall heat flux is not treated as a constant. The overall heat transfer coefficient is based on the resistance of the wall and the resistance between the wall and the surrounding shell-side fluid. The following is the tube-side energy equation in dimensionless form along with its appropriate transformed boundary conditions:

$$(1-\xi^2)\frac{\partial\theta}{\partial z} = \frac{1}{r_i\ (\mathrm{Re}\,\mathrm{Pr})}\left(\frac{\partial^2\theta}{\partial\xi^2} + \frac{1}{\xi}\frac{\partial\theta}{\partial\xi} + S\right) \tag{2.9}$$

where the boundary conditions are given in Equations (2.10), (2.11) and (2.12):

$$At\ \ z = 0\ ,\ \theta = 1 - \frac{T_a}{T_{in}} \tag{2.10}$$

$$For\ z>0\ at\ \xi = \frac{r}{r_i} = 0,\ \frac{\partial\theta}{\partial\xi} = 0 \tag{2.11}$$

$$For\ z = 0\ \ at\ \xi = 1,\ -\frac{\partial\theta}{\partial\xi} = \frac{Nu_w}{2}\theta \tag{2.12}$$

The energy equation and the associated boundary conditions are transformed by letting:

$$\theta = \frac{T(\xi, z) - T_a}{T_{in}} \tag{2.13}$$

where T is a function of radial (ξ) and axial (z) displacement. The dimensionless radial displacement and the source term are defined in Equation (2.14):

$$\xi = \frac{r}{r_i} \quad \text{and} \quad S = \frac{sr_i^2}{kT_{in}} \tag{2.14}$$

$$\theta = \frac{T(z,\xi) - T_a}{T_o} \tag{2.15}$$

$$= -\frac{S\xi^2}{4} + \frac{S}{2}\left[\frac{2}{Nu_w} + \frac{1}{2}\right]$$

$$+ \sum_{n=1}^{\infty} C_n Y_n \exp\left[-\frac{\lambda_n^2 z}{r_o^2 \,\mathrm{Re}\,\mathrm{Pr}}\right]$$

and

$$\theta_b = \frac{T_b - T_a}{T_{in}} = \tag{2.16}$$

$$4\left[\frac{S}{24} + \frac{S}{4Nu_w} + \frac{Nu_w}{2}\sum_{n=1}^{\infty}\frac{C_n Y_n(1)}{\lambda_n^2} exp\left(\frac{\lambda_n^2 z}{r_i RePr}\right)\right]$$

where λ_n and Y_n are the eigenvalues and eigenfunctions, respectively.

The heat flux at the tube wall is expressed in Equation (2.17):

$$q_w = U_w T_{in}\left[\frac{S}{Nu_w}\right] + \sum_{n=1}^{\infty} C_n Y_n(1)\ exp\left[-\frac{\lambda_n{}^2 z}{\mathrm{Re}\,\mathrm{Pr}\, r_i}\right] \tag{2.17}$$

Equation (2.18) is the governing equation:

$$\frac{d^2Y_n}{d\xi^2} + \frac{1}{\xi}\frac{dY_n}{d\xi} + \lambda_n{}^2(1-\xi^2)Y_n = 0 \tag{2.18}$$

Equation (2.18) satisfies the following boundary conditions:

$$\frac{dY_n}{d\xi} = 0 \ \ at \ \ \xi = 0 \tag{2.19}$$

$$-\frac{dY_n}{d\xi} = \frac{Nu_w}{2} Y_n \ \ at \ \ \xi = 1 \tag{2.20}$$

The coefficients in the Sturm Liouville system can be computed from the relationships defined in Equation (2.21), Equation (2.22) and Equation (2.23):

$$C_n = I_n\left[1 - \frac{T_a}{T_{in}}\right] + SG_n \tag{2.21}$$

where

$$I_n = \frac{\int_0^1 \xi\,(1-\xi^2)\,Y_n d\xi}{\int_0^1 \xi(1-\xi^2)\,Y_n{}^2 d\xi} = \frac{\left[Nu_w/2\right] Y_n(1)}{\lambda_n{}^2\left[\int_0^1 \xi(1-\xi^2)\,Y_n{}^2 d\xi\right]} \tag{2.22}$$

$$G_n = \frac{\int_0^1 \left[\frac{\xi^2}{4} - \frac{1}{2}\left(\frac{2}{Nu_w} + \frac{1}{2}\right)\right]\xi(1-\xi^2)Y_n d\xi}{\int_0^1 \xi(1-\xi^2)Y_n^2 d\xi} \tag{2.23}$$

$$= \frac{-\int_0^1 \xi Y_n d\xi}{\lambda_n^2 \int_0^1 \xi(1-\xi^2)Y_n^2 d\xi}$$

Using the expression for the bulk fluid temperature and the expression for heat flux at the tube wall, an expression for the local Nusselt number is derived in Equation (2.24):

$$Nu_{T3,local} = \frac{q_w}{T_b - T_w}\frac{2r_i}{k_i} \tag{2.24}$$

The average inside Nusselt number is then calculated by integrating the local Nusselt Number over the effective length of the heat exchanger:

$$Nu_{T3,average} = \frac{1}{L}\int_0^L Nu_{T3,local}\, dz \tag{2.25}$$

The eigenvalues and eigenfunctions are calculated by solving the governing equation and the associated boundary conditions stated earlier. The governing equation is a Sturm Liouville type problem. The eigenvalues are determined such that the $\frac{dY_n}{d\xi} = 0$ at $\xi = 0$ and the eigenfunctions or eigenvectors compensate for the guess value of $Y_n(0)$. The temperature profile is obtained by solving the initial value problem. The two techniques utilized to solve this problem are the Fourth Order Runge Kutta Method and the Secant method. The solution is initiated by assuming an approximate value for the eigenfunction at the lower boundary. Numerical integration is then performed between $\xi = 0$ and $\xi = 1$

by a fourth order Runge Kutta method. The secant method is carried out on the convective boundary condition at $\xi = 1$. A better approximation to the eigenvalue is calculated by using the results of previous integrations and the difference is tested between these approximations against a pre-assigned error using the false position Newton Raphson iteration (secant method).

2.3 Wilson Plot

The Wilson Plot Method (1915) is one of the methods used to determine the values of the inside heat transfer coefficient, the outside heat transfer coefficient and the wall heat transfer coefficient [Klein and Kessler, 2001]. "The Wilson's Plot term has come to be used for various related approximate methods for determining the relationships between the temperature difference and the heat flux for either side of a heat exchanger from measurements of the overall temperature difference between the two fluids and the heat transfer rate between them. This avoids the often difficult task of measuring the temperature of the wall separating the fluids" [Rose, 2004].

Heat transfer in thermally driven desalination processes incorporates the tube-side resistance, the wall resistance and the shell-side resistance. Generally when conventional heat transfer equipment is analyzed, constant wall temperature or a constant wall heat flux boundary condition is assumed. The wall resistance for such equipment is negligible since the thermal conductivity of these metallic shell-and-tube exchangers is high. However, in the case of polymeric tubular devices, the magnitude of the thermal conductivity is low hence, reasonable wall thermal resistance occurs.

Besides the wall thermal resistance to heat transfer, the resistances for the tube side and shell side generate temperature gradients close to the wall of the hollow fiber.

The heat transfer resistances across the thermal boundary layers are significantly influenced by the fluid hydrodynamic parameters. The heat transfer coefficients dictate the heat transfer rates for the shell-side and tube-side liquids in the hollow fiber module. The shell-side liquid flow is assumed to be primarily of fully developed laminar flow regime. In some instances, this transitional flow regime can be augmented to turbulent flow. The tube-side fluid is channeled through very thin hollow fibers (small diameter hollow fibers) hence, it is assumed to be of laminar and fully developed laminar flow types. The overall heat transfer resistance R_{ov} is essentially the summation of the resistances in series related to the shell-side and tube-side fluid:

$$R_{OV} = R_i + R_W + R_O \tag{2.26}$$

$$1/U = \sum R_{ov} = [1/h_i(D_i/D_O)] + [R_W\ A_O/A_{ln}] + [1/h_O] \tag{2.27}$$

where the subscripts i, w and o refer to inside, wall and outside, respectively.

For an outside heat transfer coefficient (h_o), the Nu can be expressed in the correlation given in Equation (2.28) where a, b and c are constants:

$$Nu = a(\mathrm{Re}^b, \mathrm{Pr}^c) \tag{2.28}$$

Klein and Kessler [2001] have reviewed heat transfer correlations published for heat transfer studies for flow outside tubular devices and concluded that the values for b ranged approximately from 0.33 to 0.93. The b values for polymeric hollow fibers fall close to the upper bound due to the single-phase fully developed laminar flow forced convection behavior. Following from Equation (2.28), Nusselt number on the shell side (equivalent to $h_o d_s/k$) is directly proportional to the shell-side velocity raised to the exponent b.

Therefore,

$$h_o = Au_s^{\ b} \tag{2.29}$$

where h_o is the shell-side heat transfer coefficient, u_s is the shell-side fluid velocity and A is the constant related to the geometry of the hollow fiber module.

The Wilson's Plot method is utilized to correlate shell-side heat transfer data since no specific shell-side correlation has been derived in the past. The overall heat transfer coefficient is calculated for several shell-side velocity values at constant maximum tube-side velocity (constant tube-side thermal resistance) and 1/U is plotted versus $1/u_s^{\ b}$. This is illustrated in the figure below. The value of the exponent b is selected by linear regression to yield the best straight-line fit for the data. The resultant intercept of the straight line represents the infinite shell-side velocity at which the shell-side thermal resistance is zero. The intercept is essentially $1/h_i\ (D_i/D_o) + R_w$. The outside or shell-side thermal resistance at a certain shell-side velocity can be derived by deducting the resultant intercept from the value of 1/U that is specific to that velocity.

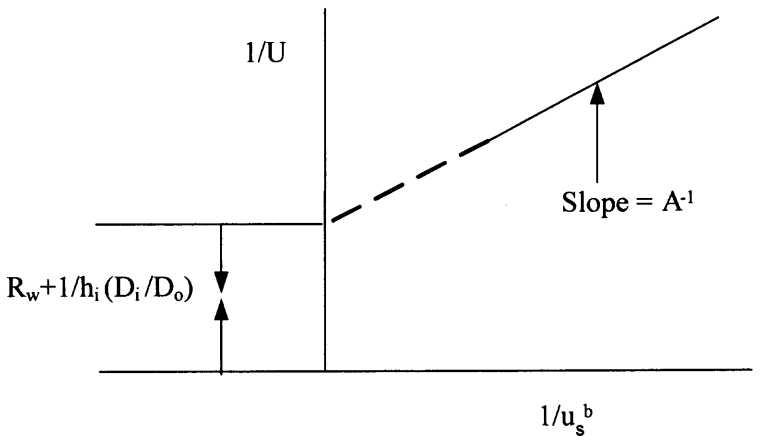

Figure 2.1 Principle of Wilson Plot.

In the case of constant tube-side flow parameter with shell-side velocity variation, two constants are unknown (A and $1/h_i$ (D_i/D_o)) and one constant is known (b). The first unknown constant A is linear and can be deduced from the slope of the straight line in the plot depicted in the previous figure. The second unknown constant $1/h_i$ (D_i/D_o) is also linear. The best straight line is designated by linear regression technique to minimize S*, the sum of the squares of the residuals of 1/U [Rose, 2004].

$$S^* = \sum \left[\frac{1}{U_{calc}} - \frac{1}{U_{obs}} \right]^2 = \tag{2.30}$$

$$\sum \left[\frac{u_s^{-b}}{A} + R_w \left(\frac{A_o}{A_{ln}} \right) + \frac{1}{h_i \left(D_i / D_o \right)} - \frac{1}{U_{obs}} \right]^2$$

For minimum S*,

$$\frac{\partial S^*}{\partial (1/h_i (D_i/D_o))} = 0, \quad \frac{\partial S^*}{\partial (1/A)} = 0 \tag{2.31}$$

In this method, equal weight is assigned to all data points. The U_{obs} values for points with lower shell-side velocities would be more accurate due to the greater temperature change of the fluid on the shell side [Rose, 2004]. This would bring about an increase in the level of accuracy with which the heat values are determined.

This same method is employed to correlate the tube-side heat transfer experimental data even though correlations for tube side have been established earlier (for example, the Sieder-Tate correlation for laminar flow inside a circular duct).

2.4 Sieder-Tate Correlation

This correlation is used to calculate the tube-side heat transfer coefficients in the polymeric hollow fiber heat exchangers. Sieder and Tate formulated an equation for streamline flow region where Re <2100 after developing correlation of heating and cooling fluids in horizontal and vertical tubes [Kern, 1950]. This equation is given in Equation (2.32):

$$Nu = \frac{h_i D}{k} = 1.86\left[\left(\frac{Du_t\rho}{\mu}\right)\left(\frac{C_p\mu}{k}\right)\left(\frac{D}{L}\right)\right]^{1/3}\left(\frac{\mu}{\mu_w}\right)^{0.14} \qquad (2.32)$$

This correlation is more applicable to fluid flow in laminar regime and not fully developed laminar flow. In the majority of the runs the shell-side and tube-side liquids' Reynolds numbers were in the fully developed laminar regime or the mixed, subcritical flow regime (10^3 <Re < 10^4) [Zukauskas, 1972]. Hence, use of this correlation is not necessarily the best approach in predicting the inside heat transfer coefficients. The Sieder-Tate correlation is useful for the prediction of inside heat transfer coefficients when RePr (D/L) >10.

CHAPTER 3

EXPERIMENTAL

3.1 Approach

Cold tap water was used as the cooling medium on the tube side or on the shell side. Hot 4 wt % sodium chloride feed solution was circulated on the shell side or on the tube side of the polymeric hollow fiber heat exchangers to study the heat exchange between hot brine (4 wt % NaCl) and cold water using PP-based and PEEK-based hollow fiber modules (Figure 3.1) fabricated at NJIT laboratories (by Dr. Baoan Li and Dr. Liming Song). Steam was also circulated on the lumen side and cooling water passed on the shell side to study the heat exchange between condensing steam and cold water using the same hollow fiber modules. Solid PP and PEEK hollow fiber modules built using fibers having ID/OD 425 μm/575 μm and 420 μm/570 μm, respectively and transverse flow / parallel flow configuration were utilized to study heat transfer characteristics between hot brine and cold water and between steam and cold water. These modules contained anywhere between 79 and 400 fibers. They were fabricated with the fiber length varying between 18.0-21.5 cm and an effective surface area between 193-960 cm^2 (Table 3.1a) based on the internal diameter of the fiber. The shells of the modules comprised of transparent polypropylene tubing and the dimensions of the tubing are also summarized in Table 3.1b.

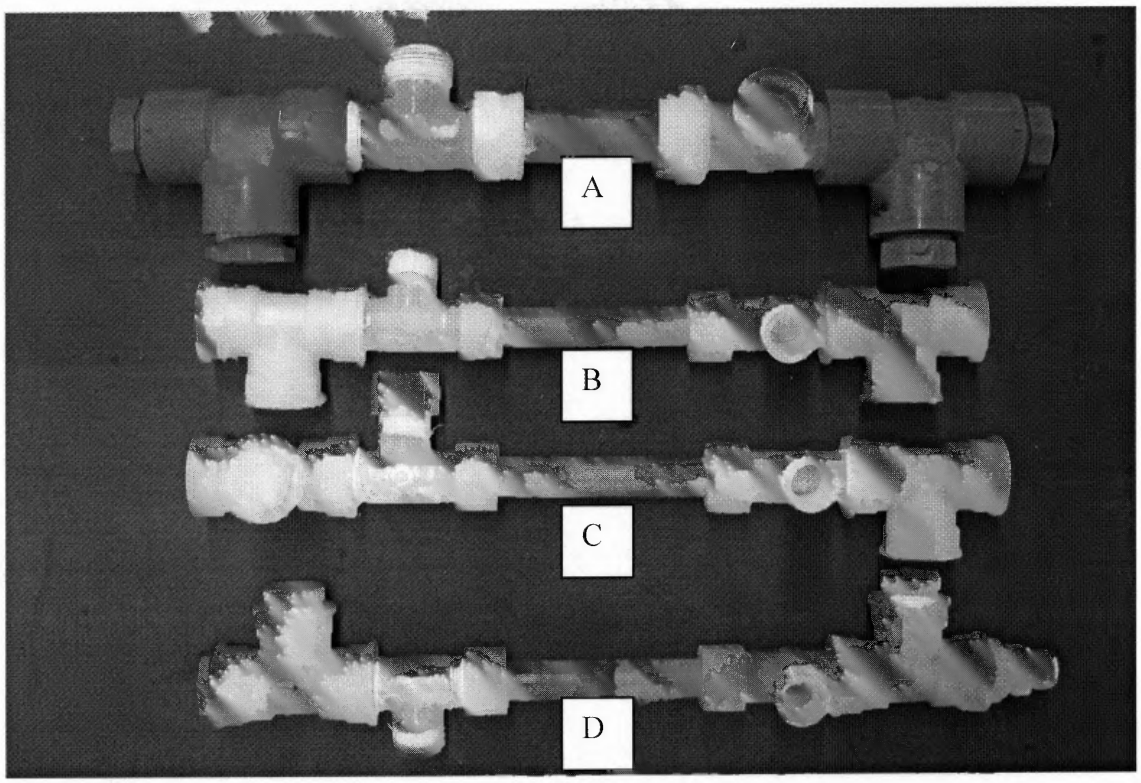

Figure 3.1 PP-based and PEEK-based transverse/parallel flow modules developed at NJIT Center for Membrane Technologies (A: HEPP2, B: HEPP1, C: HEPP3 and D: HEPEEK2).

Table 3.1a Hollow Fiber Membrane modules: Geometrical dimensions of fibers

Module	**HEPP1**	**HEPP2**	**HEPP3**	**HEPEEK 2**
Support Membrane Material	PP	PP	PP	PEEK
Fiber OD/Capillary OD, μm	575	575	575	570
Fiber ID/Capillary ID, μm	425	425	425	420
Wall thickness, μm	75	75	75	75
No. of fibers/capillaries	79	400	200	79
Effective fiber length, cm	18.5	18.0	21.5	18.5
Actual fiber length inside the module, cm	25	27.5	28.5	26.7
Effective membrane surface area, cm^2	195	960.8	573.8	193
Effective membrane surface area per unit volume (α) *, m^2m^{-3}	531	1404	1345	537
Effective cross-sectional area for shell side with crossflow, cm^2	15.5	17.5	21.5	15.9
Effective cross-sectional area for shell side with parallel flow, cm^2	1.28	2.05	0.98	1.29

* α values calculated based on shell inside diameter and fiber inside diameter

Table 3.1 b Hollow Fiber Membrane modules: Geometrical dimensions of modules and other information

Module	**HEPP1**	**HEPP2**	**HEPP3**	**HEPEEK 2**
Internal dimensions of module frame (cm)	Shell Material: PP; ID: 1.59	Shell Material: PP; ID: 2.2	Shell Material: PP; ID: 1.59	Shell Material: PEEK; ID: 1.59
Distribution tube inside diameter (cm)	0.48	0.60	0.48	0.48
Distribution Tube outside diameter (cm)	0.79	0.95	0.79	0.79
Packing fraction of fibers	0.137	0.247	0.180	0.135
Shell-side flow configuration	Transverse Flow/Parallel Flow			
Potting material	Epoxy			Epoxy
Fiber form	Knitted array			Single strands

3.2 Chemicals, Materials and Equipment

The chemicals, materials and equipment used in the experiments are listed below:

Chemicals:

- 4 wt % sodium chloride feed solution
- Tap water

Materials:

- Omega Flex translucent Polypropylene tubing with ID/OD: 0.625 inches/0.75 inches, (Model TYPP-178-100, Omega Engineering Inc.)
- Solid Polypropylene Hollow fibers (ID/OD: 425 μm /575 μm) fabricated by Celgard, Charlotte, NC.
- Solid PEEK Hollow fibers (ID/OD: 420 μm /570 μm) fabricated by Texloc Ltd., Forth Worth, Texas.
- Solid Polypropylene Hollow Fiber Modules fabricated at New Jersey Institute of Technology (refer to Table 3.1a and Table 3.1b for detailed specifications of these modules)

Equipment:

- Orion Conductivity Meter (Model 115, Orion Research, Beverly, M.A)
- Four Channel Thermocouple (Model 94461-30, Serial 020800857, Sper Scientific Ltd, Scottsdale, AZ)
- Immersion Heater, 1500W, 115V (Model 08516-74)
- Steam Generator, 20 kW, 240V, 100psi (Model MBA20B3, Serial SS-86837), Sussman Automatic Corporation, Long Island City, NY
- Centrifugal Pump, 178 W, 2700/3200rpm (Model TE-4-MD-HC, Type U62, Little Giant Pump Corporation, Oklahoma City, Oklahoma)

- Pressure gauges, 0-15psi (Model M35/901, Noshok)
- NPT ½ ″ Three Way Valve (Model 06472-47)
- 2 micron, 20 inch PP sediment cartridges
- 20″ Filter Housing, High Temperature
- Stopwatch

3.3 Experimental Setup and Procedure

3.3.1 Setup

The experimental apparatus used to study the heat exchange between 4 wt % hot brine and tap water and between steam and tap water is shown in Figures 3.2 and 3.3.

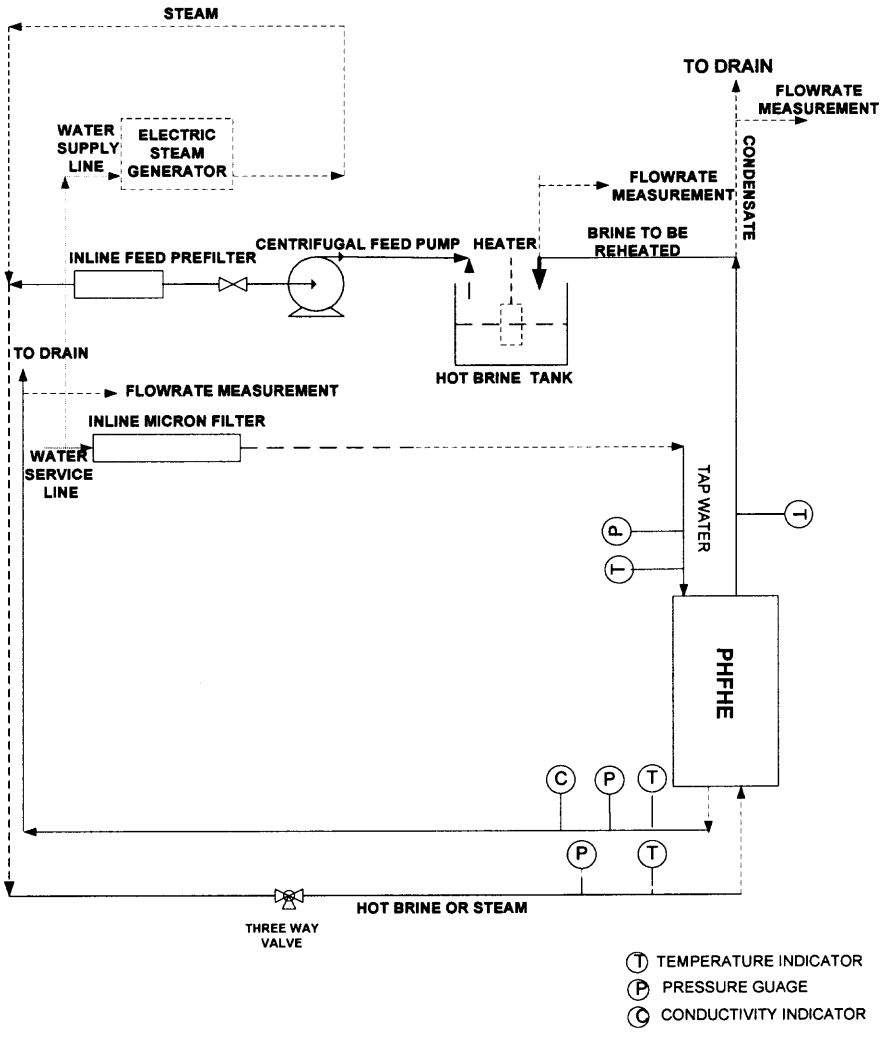

Figure 3.2 Experimental schematic for heat transfer measurements in PHFHEs.

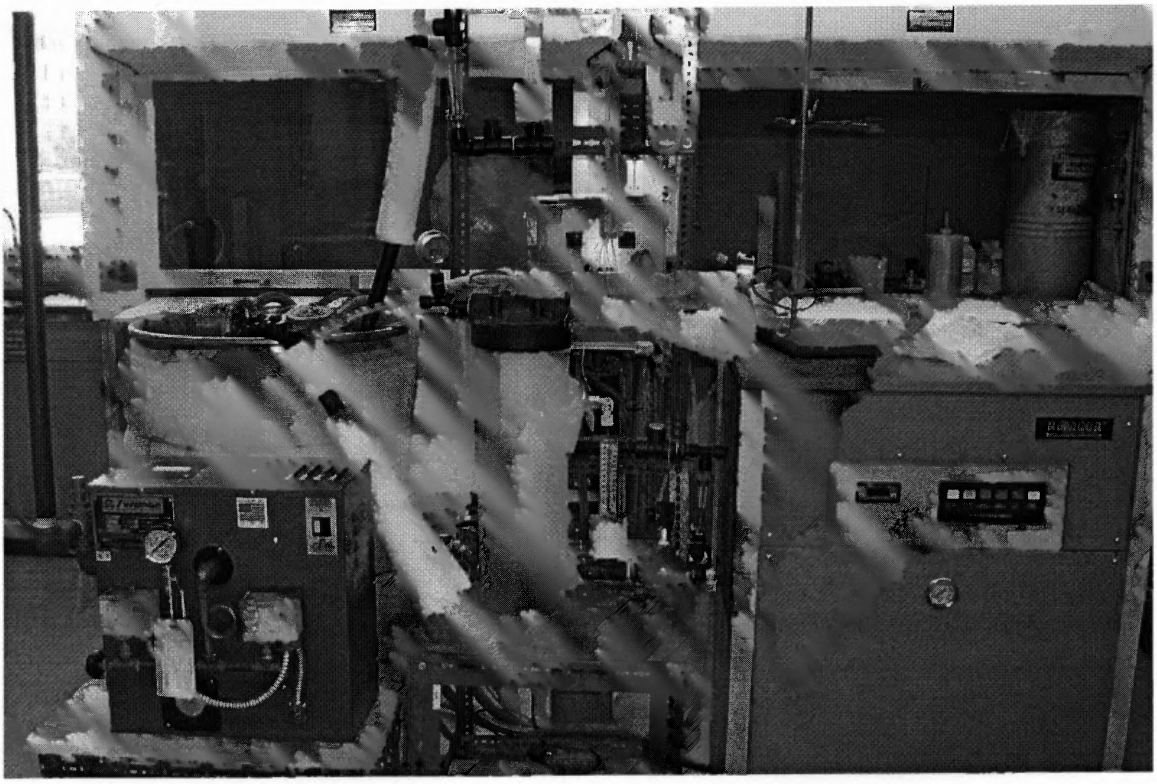

Figure 3.3 Photo of the Experimental setup.

3.3.2 Procedure

In all experiments, the orientation of the hollow fiber module was horizontal. The piping was well insulated to mitigate heat loss from the system. The feed solution heated to a temperature of approximately 91°C by two 1500 W immersion heaters, was introduced on the shell side or the tube side from a hot brine storage tank by a centrifugal pump (2700/3200 rpm, Model TE-4-MD-HC, Little Giant Pump Corporation, Oklahoma City, Oklahoma) at a constant flow rate. The system flow rates were varied in the range of 258–11000 ml/min. At the shell outlet or tube outlet, the feed solution was circulated back to the feed storage tank and was reheated. Tap water was filtered through a sediment filter to remove any particulate matter prior to it being introduced on the shell side or the lumen side of the hollow fiber modules. The shell-side liquid either flowed along the fibers (parallel flow configuration) or flowed uniformly through the many circumferential holes in the central distribution tube, outside of and perpendicular to the fibers in the module (crossflow configuration). The inlet and the outlet temperatures of the shell-side and tube-side liquid streams were measured with a four-channel thermocouple (Model 94461-30, Serial 020800857, Sper Scientific Ltd, Scottsdale, AZ) with an accuracy of $\pm 0.2^{\circ}C$.

In any given experiment, the flow rate of a liquid stream on one side of the tubular heat exchanger was varied, while that of the liquid stream on the other side was kept constant for several entrance temperatures of the feed stream. The flow rates of the shell-side and tube-side outlet streams were derived by measuring the time necessary to collect a particular liquid volume. At the maximum feed flow rate, 7-13 different cooling liquid flow rates were utilized, commencing from either the highest or lowest possible cooling liquid flow rate. During each run, both the feed and cooling liquid flow rates

were measured at least twice. The inlet temperature of the feed solution was varied between 82-99°C and the coolant inlet temperature was varied between 5-41°C. The values of the inlet and outlet temperatures of the liquid streams, the outlet flow rates of the liquid streams, the inlet and exit pressure readings for tube side and shell side and the electrical conductivity or salt concentration of the cooling liquid outlet stream were recorded approximately every 20 minutes. Steady state conditions were assumed to be attained when the readings of the flow rates of the cooling water, hot brine and the four inlet and outlet temperatures reached constant values. Pressure gauges having an increment of 0.1 kPa were utilized to measure the pressure head at the tube inlet and shell inlet. A conductivity meter (Model No.115, Orion Research, Beverly, M.A) was used to measure the salt conductivity of the cooling liquid exit stream. These steady inlet temperatures, outlet temperatures and flow rates of the brine feed and tap water were recorded for the calculation of the heat transfer rate. To obtain accurate measurements of the true tube-side pressure drop, the modules were disconnected from the setup shown in Figure 3.3 and connected to the cold water supply with pressure gauges located at tube-side entrance and tube-side exit.

In the case of the experiments conducted with steam as feed, steam was introduced at a low temperature (212 to 232°F) to the tube side of the hollow fiber module while cold tap water was passed on the shell side of the module. The steam was produced by a steam generator, 20 kW, 240 V, 100 psi (Model MBA20B3, Serial SS-86837, Sussman Automatic Corporation, Long Island City, NY). Experiments were run for both parallel flow and crossflow configuration on the shell side using PP-based and PEEK-based modules. Measurements of the inlet and outlet tube and shell-side temperatures, shell-side and tube-side pressure drop and outlet shell and tube-side flow

rates were taken in the same manner as in the case of those experiments conducted with hot brine as feed.

3.4 Data Reduction

3.4.1 Calculation of Physical and Transport Properties

Experimentally observed inlet and outlet temperatures for the shell-side and tube-side liquids were used to determine the density, viscosity and thermal conductivity of the liquids in each run using the following correlations developed from thermodynamic properties data for water between 0°C and 100°C in Appendix F11, F51 and E11 of [Weast, 1978-1979]. The averages of the inlet and outlet of the tube-side and shell-side liquid temperatures are substituted in the following correlations.

For density,

$$\rho = 10^{-8}T_{av}^{3} - 6\times10^{-6}T_{av}^{2} - 3\times10^{-6}T_{av} + 1.003 \quad (g/cm^3) \tag{3.1}$$

For dynamic or absolute viscosity,

$$\mu = -0.4607 \ln T_{av} + 2.3669 \quad (g/cm^2s) \tag{3.2}$$

For thermal conductivity,

$$k = -0.0097T_{av}^{2} + 2.1662T_{av} + 559.2 \quad (mW/m\text{-}K) \tag{3.3}$$

The Prandtl numbers for tube-side and shell-side liquids are determined from Equation (3.4):

$$\mathrm{Pr} = \mu C_p / k \tag{3.4}$$

where C_p (the specific heat capacity of water) is 4.18 J/g-°C.

The diameter-based tube-side Reynolds number Re_t is determined from the following definition:

$$Re_t = \frac{\rho u_t D_i}{\mu} \tag{3.5 a}$$

where D_i is the inside fiber diameter and u_t is the linear velocity for tube-side parallel flow:

$$u_t = \frac{Q}{A_t} \tag{3.5 b}$$

$$= \frac{\text{Brine or Cold water flow rate}}{\text{Open area for flow through tube side}}$$

where $A_i = N \pi D_i^2/4$ and N is the number of fibers in the module.

The diameter-based shell-side Reynolds number Re_s is determined from Equation (3.6 a):

$$Re_s = \frac{\rho u_s D_o}{\mu} \tag{3.6 a}$$

where u_s is the shell-side linear velocity for parallel flow on the shell side or shell-side interstitial velocity for crossflow on the shell side and D_o is the outside fiber diameter:

$$u_s = \frac{Q}{A_s} \tag{3.6 b}$$

$$= \frac{\text{Brine or Cold water flow rate}}{\text{Open area for flow through shell side}}$$

$$A_S = L(W\text{-}N'D_O) \tag{3.6 c}$$

Here N' represents the number of fibers per layer, W is the total flow width for the first fiber layer and L is the active fiber length. N'_{HEPP1} and $N'_{HEPEEK2} = 40$ fibers and N'_{HEPP2} and $N'_{HEPP3} = 50$ fibers. Figure 3.4 provides further details.

$W = \pi D = \pi$ [2(Thickness of tape (D_T) used to make fiber layers) +2 (Inside Radius of Distribution Tube(D_{DT})) + D_o)] (3.7 a)

Here D_T = 0.14 cm, D_{DT} = 0.475 cm and D_o = 0.0575 cm. When there are a number of fiber layers, the value of W is changed. The values of W that have been used for different modules are based on layer 1 only and are as follows: HEPP2 = 3.60 cm; HEPP1 = 3.14 cm; HEPP3 = 3.289 cm; HEPEEK2 = 3.14 cm. The variation is primarily due to the fact that the tape thickness and D_{DT} may be different. However it should be noted that the value of the free cross-sectional area for shell side in crossflow mode changes with the fiber layers. For HEPP2 (200 fibers in 4 layers), the outside fiber diameter D_o (0.0575cm) is changed at the very least by a factor of 4; therefore,

$W_4 - W_1 = \pi D_4 - \pi D_1 = \Delta W = \pi \Delta D =$ (3.7 b)
π [0.14 cm + (0.475 x 2) cm + (0.0575x 4) cm]
$-\pi$ [0.14 cm+ (0.475 x 2) cm+ 0.0575 cm]

Therefore, % change in $W = \frac{0.54}{3.60} x100 = 15$. The new open area LW based on four fiber layers (module HEPP2) for flow through the shell side is calculated in Equation (3.7c):

New Frame Cross- sectional area – Fiber Projected Area = $L\,\pi D_4 - L\,N'_{HEPP2}\,D_o$ = 75-[18 x 50 x 0.0575] (3.7 c)
= 75-52 = 23 cm^2

The original open area LW based on the first fiber layer (module HEPP2) for flow through the shell side is calculated in Equation (3.7 d):

Original Frame Cross-sectional area – Fiber Projected Area = 65-52 =13 cm^2 (3.7 d)

Therefore, % change in open area for module HEPP2 = $\frac{10}{13}$ x 100 = 76.

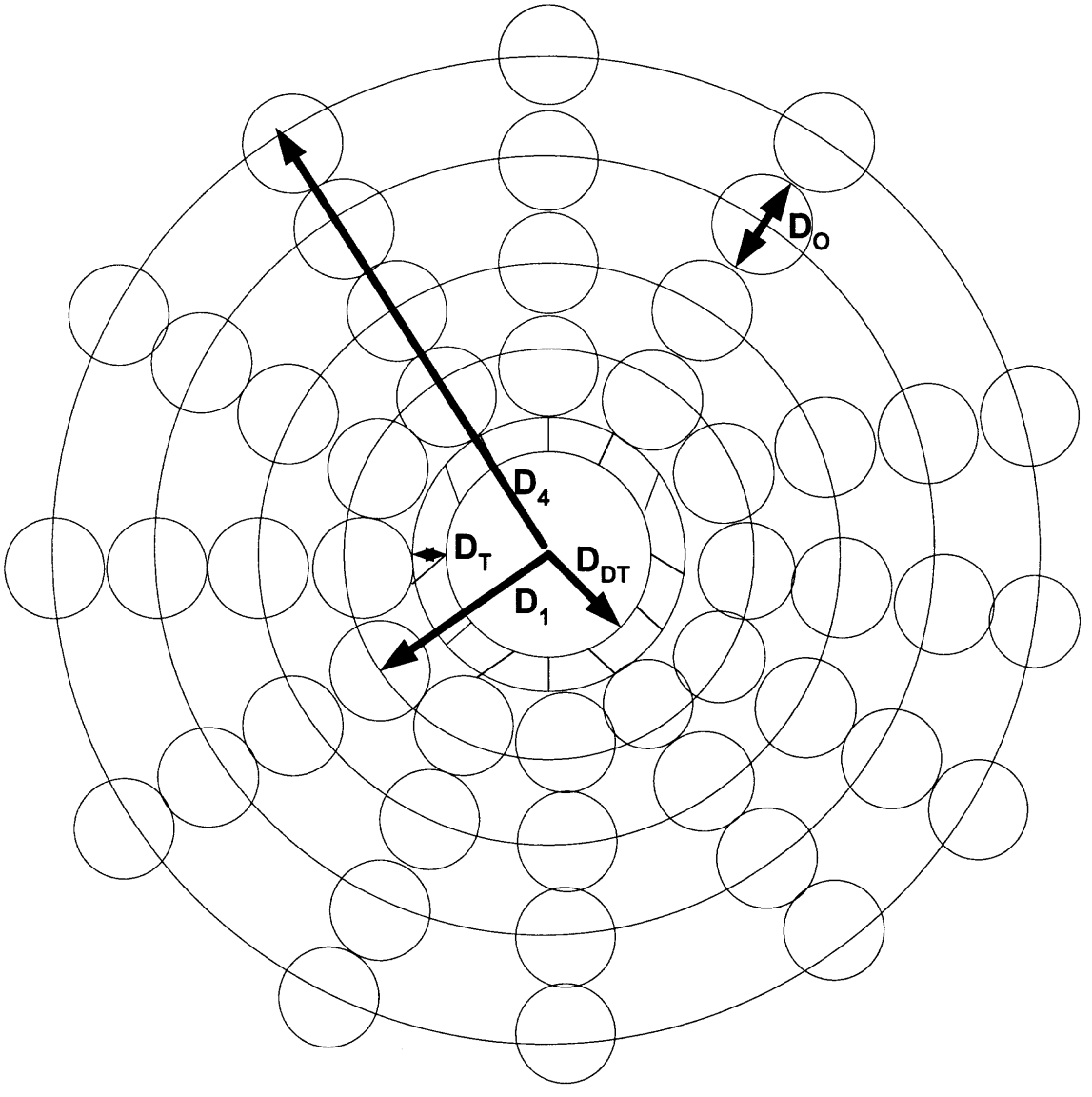

Figure 3.4 Placement of hollow fibers around the central distribution tube in crossflow modules based on PP and PEEK hollow fibers (not drawn to scale).

The Nusselt number is only determined for the tube side. For laminar flow inside the polymeric hollow fiber module,

$$Nu = \frac{h_i D_i}{k} = 1.86\left[\left(\frac{D u_t \rho}{\mu}\right)\left(\frac{C_p \mu}{k}\right)\left(\frac{D}{L}\right)\right]^{1/3}\left(\frac{\mu}{\mu_w}\right)^{0.14} \qquad (3.7e)$$

where μ_w is the liquid viscosity evaluated at the tube wall temperature. The term $\left[\frac{\mu}{\mu_w}\right]^{0.14}$ is negligible for membrane applications.

3.4.2 Total Rate of Heat Exchange Between the Shell-side and Tube-side Liquids

The total rate of heat transfer between the hot brine and cold water is defined by the hot and cold liquid flow rates and their entering and exit temperatures. The total rate of heat transfer between the shell-side and tube-side liquids, Q, is obtained from Equation (3.8):

$$Q = C_H (T_{H1}-T_{H2}) = C_c (T_{C2}-T_{C1}) \qquad (3.8)$$

where $C_H = \dot{m} C_{pH}$ is the capacity rate of hot brine and $C_C = \dot{m} C_{pC}$ is the capacity rate of the cold water. One assumes here no heat loss to the surrounding. The local overall heat transfer coefficient based on the inside area is calculated using Equation (3.9):

$$dQ = U\, dA_i\, (T_H - T_C) \qquad (3.9)$$

The Q value for the tube-side stream is used since it does not have heat loss to the surrounding. The discrepancy in the Q values for the shell-side and tube-side liquids were less than 12%. The heat exchanger surface area necessary to satisfy the specification of Equation (3.9) is calculated by integrating the heat transfer rate equation over the area of

the tubular heat exchanger [Cheremisinoff, 1984]. For a constant overall heat transfer coefficient,

$$Q = U \int_{A_i} (T_H - T_C) dA_i \tag{3.10}$$

The effective temperature difference averaged over the total heat exchanger contact surface area is:

$$\Delta T_M = \frac{1}{A_i} \int_{A_i} (T_H - T_C) dA_i \tag{3.11}$$

This effective mean temperature difference is equivalent to the logarithmic mean temperature difference (LMTD) in the case of modules with the shell side in parallel flow mode. This temperature difference is also given by Equation (3.12):

$$\Delta T_{lm} = \frac{\Delta T_1 - \Delta T_2}{ln\left[\frac{\Delta T_1}{\Delta T_2}\right]} \tag{3.12}$$

where $\Delta T_1 = T_{H1} - T_{C1}$ *and* $\Delta T_2 = T_{H2} - T_{c1}$.

3.4.3 The Effectiveness-NTU Method

The heat exchanger effectiveness ε for modules with crossflow or parallel flow mode on the shell side is calculated using Equation (3.13):

$$\begin{aligned} \varepsilon &= \frac{\text{actual rate of heat transfer}}{\text{maximum possible heat transfer rate}} \\ &= \frac{Q_{actual}}{Q_{\max}} = \frac{UA_i \Delta T_{lm}}{C_{\min}(T_{H1} - T_{C1})} \\ &= \frac{U_o A_o \Delta T_{lm}}{C_{\min}(T_{H1} - T_{C1})} \end{aligned} \tag{3.13}$$

The maximum possible heat transfer Q_{max} occurs in a countercurrent heat exchanger of infinite area if one liquid undergoes a temperature change equivalent to the maximum temperature change available [Cheremisinoff, 1984]. Q_{max} is calculated based on the liquid (shell or tube side) having the smaller capacity rate in each run.

3.4.4 Determination of Temperature Correction Factor (F)

The Logarithmic Mean Temperature Difference Method is utilized to calculate the logarithmic mean temperature difference correction factor F for crossflow since the inlet and outlet temperatures for the shell-side and tube-side liquid streams are known. For heat exchangers with crossflow at shell side, F generally falls within the range of 0.75-1.00. This factor is calculated by Equation (3.14a):

$$F = \frac{NTU_{cf}}{NTU} = \frac{\varepsilon(t_{t1} - t_{s1})}{NTU\ \Delta T_{lm}} = \frac{1}{NTU(1-C^*)} \ln\left[\frac{1-C^*\varepsilon}{1-\varepsilon}\right] \quad (3.14\ a)$$

where $NTU = U_o A_o / C_{min}$ (3.14 b)

C^* *(heat capacity rate ratio)* $= \dfrac{C_{min}}{C_{max}}$ (3.14 c)

and $\varepsilon = \dfrac{t_{t2} - t_{t1}}{t_{s1} - t_{t1}}$ (3.14 d)

where ε is the thermal effectiveness factor. The Equation (3.14a) holds for $C^* \neq 1$.

This factor F = φ (P, R, flow arrangement) is then employed in the following equation to calculate the true overall heat transfer coefficient for shell-side crossflow configuration:

$$q = U A_i F \Delta T_{lm} \quad (3.15)$$

where $F = \Delta T_M / \Delta T_{lm}$ (3.16)

3.4.5 Determination of the Number of Transfer Units (NTU) and Height of Transfer Unit (HTU)

$$NTU = \frac{UA}{C_{\min}} = \frac{U_o A_o}{C_{\min}} \tag{3.17}$$

$$HTU = \frac{L}{NTU} \tag{3.18}$$

where L is the effective length of the heat exchange device.

3.4.6 Determination of Tube-side Fanning Friction Factor

The Fanning friction factor is obtained from the following relationship for thermally developing laminar flow utilizing tube-side pressure drop measurements taken during the runs:

$$f_{Fanning} = \frac{\Delta P}{L_{actual}} \frac{D_i}{2\rho u_t^2} \tag{3.19}$$

The tube-side pressure drop obtained from the experiment needs to be corrected for entrance and exit effects and hydrodynamic entrance effects for a short duct. The true tube-side pressure drop (ΔP_{true}) is calculated by deducting the pressure drop across the 90° miter bend (with vanes) located at the exit of the PHFHE (ΔP_3), the entrance pressure loss (ΔP_{ent}) and the exit pressure loss (ΔP_{ex}) from the experimentally derived tube-side pressure drop (ΔP_T). Both the entrance and exit pressure losses were derived based on the literature graph (entrance and exit pressure loss coefficients for a multiple circular tube heat exchanger core with abrupt contraction entrance and abrupt expansion exit vs. σ), Equation (3.20) and Equation (3.21) [Kays and London, 1984]:

$$\Delta P_{ent} = \rho \frac{u_t^2}{2}(1-\sigma) + K_{ent}\frac{\rho u_t^2}{2} \tag{3.20}$$

$$\Delta P_{ex} = \rho \frac{u_t^2}{2}(1-\sigma) - K_{ex}\frac{\rho u_t^2}{2} \tag{3.21}$$

where u_t represents the velocity inside the fibers. Further the ΔP for the 90^0 miter bend is calculated using Equation (3.22):

$$\Delta P_3 = \frac{K_b \rho u_t^2}{2g} \tag{3.22}$$

where the value of K_b corresponding to 90^o miter bend vanes is 0.2 [Roberson and Crowe, 1985].

Therefore, the true pressure drop inside the fibers ΔP_{true} is calculated by Equation (3.23):

$$\Delta P_{true} = \Delta P_T - \Delta P_{ent} - \Delta P_{ex} - \Delta P_3 \tag{3.23}$$

3.4.7 Calculation of Heat Transfer Area Density and CUV (Conductance per Unit Volume)

Heat transfer area density α is calculated using Equation (3.24):

$$\alpha = \frac{A_i}{V} = \frac{4ND_i}{D_s^2} \tag{3.24}$$

where A_i is the tube/fiber inside area in the volume V of the heat exchanger module.

The Overall Conductance per unit volume (CUV) is calculated by Equation (3.25):

$$CUV = CUV_C = \alpha U \tag{3.25}$$

where U is the overall heat transfer coefficient for the hot brine-cold water system calculated based on the inside membrane surface area.

3.4.8 Sample Calculation for Wilson's Plot Method

Experimentally-determined overall heat transfer coefficients for HEPP3 module (crossflow on the shell side) with tube-side hot brine flow and shell-side cooling water flow were used to isolate the inside, outside and wall heat transfer coefficients. Linear regression analysis was performed on the first data set in the pair (Figures 3.5 and 3.6) where the tube-side hot brine flow rate was constant (at or close to the maximum attainable tube-side flow rate); linear regression analysis was performed as well on the second data set in the pair (Figures 3.7 and 3.8) where the tube- side hot brine flow rate was varied and the shell-side interstitial velocity was held constant. A value of 0.845 for exponent b yielded the 'best' straight line for both 1/U vs. $1/u_s^b$ and $1/h_o$ vs. $1/u_s^b$ plots in the first data set and a value of 0.93 for exponent b yielded the best straight line for both 1/U vs. $1/u_t^b$ and $1/h_i$ vs. $1/u_t^b$ plots in the second data set. As illustrated in Figures 3.4, 3.5, 3.6 and 3.7, the second data set had a much better fit than the first data set due to its much higher regression coefficient (R^2=0.989). The values of the exponents also confirm that the velocities for the tube-side and shell-side liquids were such that the flows were in the fully developed laminar flow regime. The inside and outside heat transfer coefficients were obtained from the equation of the straight line in $1/h_i$ vs $1/u_t^b$ and $1/h_o$ vs $1/u_s^b$ plots at maximum fixed tube-side liquid velocity and maximum fixed shell-side liquid velocity, respectively.

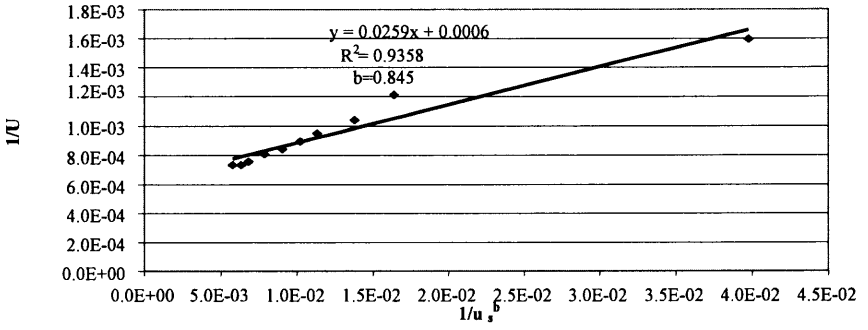

U Variation: 627-1363 w/m² K
Tube-side (Hot Brine,4%NaCl)Linear Velocity: 9736cm/min(Re ₜ:2132)
Inlet Hot Brine (4%NaCl) Temperature: 98°C
Inlet Cooling Water Temperature: 10° C
Shell-side (Cooling Water) Interstitial Velocity Variation: 45-447cm/min(Re ₛ:5-39)
Shell-side Configuration: Crossflow

Figure 3.5 Variation of 1/U with $1/u_s^b$ for Module HEPP3 with Shell-side Cooling Water Flow and Tube-side Hot Brine Flow.

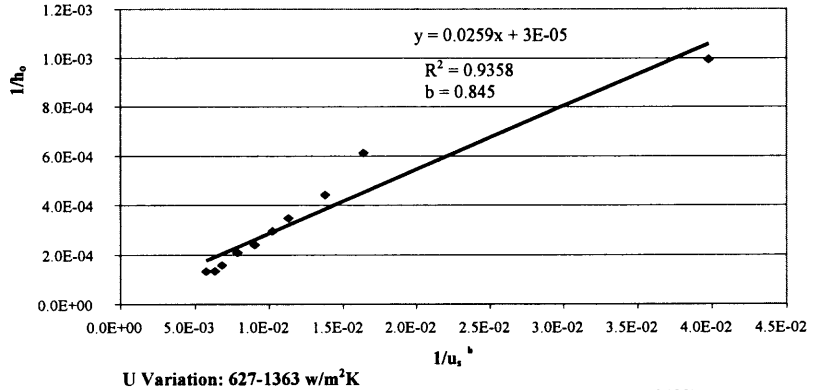

U Variation: 627-1363 w/m²K
Tube-side (Hot Brine,4%NaCl) Linear Velocity: 9736cm/min(Re ₜ: 2132)
Inlet Hot Brine (4%NaCl) Temperature: 98°C
Inlet Cooling Water Temperature: 10°C
Shell-side (Cooling Water) Interstitial Velocity Variation: 45-447cm/min (Re$_s$: 5-39)
Shell-side Configuration: Crossflow

Figure 3.6 Variation of $1/h_o$ with $1/u_s^b$ for Module HEPP3 with Shell-side Cooling Water Flow and Tube-side Hot Brine Flow.

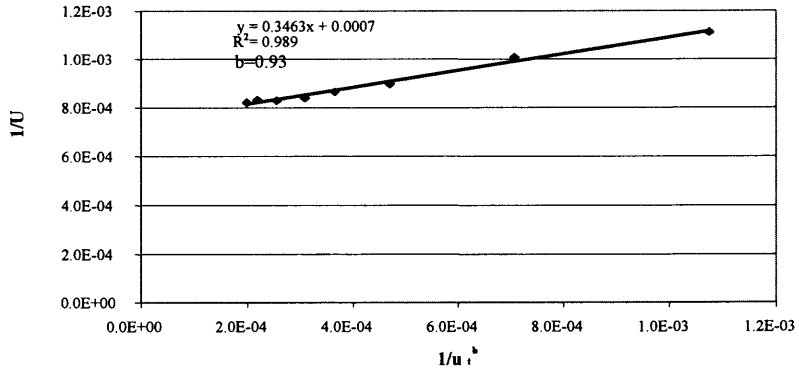

U Variation: 899-1218 w/m²K
Tube-side (Hot Brine,4%NaCl) Linear Velocity Variation:1555-9547cm/min(Re_t : 218-2025)
Inlet Hot Brine (4%NaCl) Temperature: 96°C
Inlet Cooling water Temperature: 8°C
Shell-side (Cooling water) Interstitial Velocity: 312cm/min (Re_s: 24)
Shell-side Configuration: Crossflow

Figure 3.7 Variation of 1/U with $1/u_t^b$ for module HEPP3 with shell-side cooling water flow and tube-side hot brine flow.

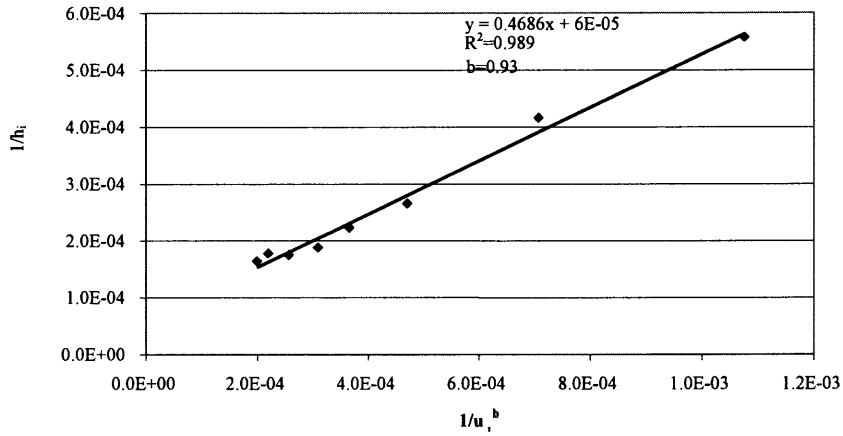

U Variation: 899-1218 w/m²K
Tube-side (Hot Brine,4%NaCl) Linear Velocity Variation:1555-9547cm/min (Re_t:218-2025)
Inlet Hot Brine (4%NaCl) Temperature: 96°C
Inlet Cooling water Temperature: 8°C
Shell-side (Cooling water) Interstitial Velocity: 312cm/min (Re_s: 24)
Shell-side Configuration: Crossflow

Figure 3.8 Variation of $1/h_i$ with $1/u_t^b$ for module HEPP3 with shell-side cooling water flow and tube-side hot brine flow.

CHAPTER 4

RESULTS AND DISCUSSION

Four tubular crossflow/parallel flow hollow fiber modules were thoroughly investigated for their heat exchange performance with hot brine (4 wt % NaCl)/cold water flowing either in crossflow over the outside surface of the hollow fibers or flowing parallel to and outside the surface of the hollow fibers and cold water / hot brine (4 wt % NaCl) flowing within the hollow fiber bore. The condensing steam-cold water system was not extensively studied; hence, the primary emphasis will be on heat transfer results obtained from the hot brine-cold water system.

Tables 3.1a and 3.1b summarize the characteristics of the four different modules tested (3 PP-based modules and 1 PEEK-based module having roughly the same hydraulic diameter as that of the PP-based modules). Table 4.1 lists the observed range of experimentally-determined overall heat transfer coefficients and the corresponding tube-side and shell-side Reynolds numbers for the four modules. Detailed performances of the modules were investigated for four different test run configurations having either crossflow or parallel flow on the shell side namely: variation of shell-side hot brine flow with constant tube-side cooling water flow, variation of tube-side hot brine flow with constant shell-side cooling water flow, variation of shell-side cooling water flow with constant tube-side hot brine flow and variation of tube-side cooling water flow with constant shell-side hot brine flow.

The tube-side, shell-side and wall heat transfer coefficients were determined by two methods, namely Wilson's Plot and Conventional Convection (refer to Table 4.2 and

Tables E.1 to E.4, respectively). The tube-side, shell-side and wall heat transfer coefficients determined by these two methods were compared to determine if they are similar. The Sieder-Tate correlation was only utilized to calculate the inside heat transfer

Table 4.1 Summary of Test Results for Liquid-Liquid Heat Exchange

Test Run Configuration	**Overall Heat Transfer Coefficient U (W/m^2-K)**			
	HEPP1	**HEPP2**	**HEPP3**	**HEPEEK2**
Vary hot brine flow rate on the shell side, fix cooling water flow rate on the tube side	450-1936[a] 509-1620[b]	1539-2032[a] 707-1239[b]	1165-1706[a] 321-1000[b]	1530-1782[a] 1408-1682[b]
Fix hot brine flow rate on the shell side, vary cooling water flow rate on tube side	490-1828[b]	723-2014[a] 505-1220 [b]	1325-1706[a] 319-1025[b]	944-1929[a] 1487-1642[b]
Vary cooling water flow rate on shell side, fix hot brine flow rate on tube side		911-2076[a] 669-1524[b]	793-1799 [a] 627-1363[b]	1043-1914[a] 535-1369[b]
Fix cooling water flow rate on shell side, vary hot brine flow rate on tube side	1100-1465[b]	1146-1913[a] 941-1423[b]	871-1727[a] 899-1218[b]	864-1364[b]
	Reynolds Number			
Vary hot brine flow rate on shell side, fix cooling water flow rate on tube side	Re_t : 498[a] Re_s : 24-1446[a] Re_t : 425[b] Re_s: 2-75[b]	Re_t : 790[a] Re_s :667-1649[a] Re_t : 600[b] Re_s : 39-200[b]	Re_t : 789[a] Re_s:316-2567[a] Re_t : 674[b] Re_s : 6.4-92[b]	Re_t:1219[a] Re_s:334-2772[a] Re_t: 1176[b] Re_s: 51-130[b]
Fix hot brine flow rate on shell side, vary cooling water flow rate on tube side	Re_t : 58-1376[b] Re_s :78[b]	Re_t : 67-992[a] Re_s : 1797[a] Re_t : 66-639[b] Re_s : 224[b]	Re_t :410-828[a] Re_s: 2661[a] Re_t : 96-730[b] Re_s : 93[b]	Re_t:433-1571[a] Re_s:3110[a] Re_t:486-1211[b] Re_s: 134[b]
Vary cooling water flow rate on shell side, fix hot brine flow rate on tube side		Re_t :2377[a] Re_s :83-490[a] Re_t :2464[b] Re_s :4-50[b]	Re_t : 1844[a] Re_s : 81-825[a] Re_t : 2132[b] Re_s : 5-39[b]	Re_t:1639[a] Re_s:85-951[a] Re_t: 1397[b] Re_s: 4.36-57[b]
Fix cooling water flow rate on shell side, vary hot brine flow rate on tube side	Re_t:153-2232[b] Re_s :34[b]	Re_t : 402[a] Re_s : 172-2315[a] Re_t : 264-2425[b] Re_s : 50[b]	Re_t:125-1779[a] Re_s: 650[a] Re_t:218-2025[b] Re_s: 24.29[b]	Re_t:239-1300[b] Re_s: 55[b]

[a] Shell side with Parallel Flow Arrangement [b] Shell side with Crossflow Arrangement , Tube side , Shell side

coefficients; then these values were compared with the inside heat transfer coefficients isolated by the Conventional Convection and the Wilson's Plot Methods.

The various heat exchange performance indicators such as U, thermal effectiveness factor, HTU, NTU and pressure drop per NTU were also examined during the assessment of the performances of the test modules. The heat exchange performances of the modules were also compared to those of conventional metallic shell-and-tube heat exchangers and plastic shell-and-tube heat exchangers reported in literature. The U_o values (based on outside fiber area) for the test modules are presented in Table B.1 (Appendix B) in order to compare the tested PHFHEs with previously tested PHFHEs, film-based and conventional metallic shell-and-tube heat exchangers. The overall heat transfer coefficients for the condensing steam-cold water system are reported in Appendix G for the PP-based and PEEK-based modules.

The working temperature ranges of the hot brine and cold water in the hot brine-cold water system were 82-99°C and 5-41°C, respectively. The working temperature ranges of the condensing steam and cold water in the steam-cold water system were 100-116°C and 7-23°C, respectively. The steam pressure was in the range of 0-15 psig (0-1.034 x 10^5 kPag). Almost all graphs depicting U variation with linear or interstitial velocity demonstrate the same trend (increase in U with increasing velocity followed by flattening of the curve due to U limitation attributed to the wall thermal resistance). The reproducibility of the data trend clearly suggests that all test run configurations exhibit essentially the same behavior regardless of the module type and the flow pattern on the shell side.

The differences in the performance of the PP-based modules are primarily due to the difference in the number of fibers and the packing density since the gross flow patterns in the different modules were likely to be identical (transverse/parallel flow on shell side), the substrate fibers were the same and the characteristic fiber dimensions (fiber ID and fiber OD) did not change with the module. The membrane area was increased by increasing the total number of fibers while holding the fiber length constant [Klein and Kessler, 2001]. Since module HEPP2 housed more than twice the number of fibers housed in HEPP1 for roughly the same fiber length, the membrane area was substantially higher in HEPP2. As a result, the fiber packing fraction was considerably higher ($0.247 > 0.137$) and the projected heat exchange performance or the overall heat transfer coefficient for HEPP2 was substantially greater than that of HEPP1. This is demonstrated in the overall heat transfer coefficient values quoted in Table 4.1 and Table B.1.

The packing density of HEPP2 is 0.247 which is substantially higher than that of HEPP3 (0.180). HEPP2 yielded also higher shell-side heat transfer coefficients than HEPP3. The greater effect of channeling on shell-side heat transfer in the HEPP3 module is due to its lower packing fraction. Since the shell-side liquid flow is poorly distributed among the fibers in the HEPP3 module, heat transfer is significantly hindered by relatively stagnant regions. This poor distribution of the shell-side liquid resulted in poor use of the available surface area. It is necessary to approach a packing density of 0.63 to maximize the fiber surface area to volume ratio of the module and the heat transfer coefficient per unit flow rate [Kakac, Shah and Bergles, 1983].

The spacing arrangement of the fibers on the shell side also significantly impacts the shell-side heat transfer coefficient. Unlike the PP fibers, the PEEK fibers were not potted in such a way to accommodate regular spacing on the shell side; hence, there was considerable bypassing. That in turn lowered the shell-side heat transfer coefficient in the HEPEEK2 module and consequently the overall heat transfer coefficient. The highest attained overall heat transfer coefficient for the PEEK-based module was around 1914 W/m^2-K. This value unlike predictions based on the wall thermal conductivity of PEEK fiber is lower than the highest achieved overall heat transfer coefficient for the PP-based modules (2076W/m^2-K). Tables G1 to G5 also demonstrate that the PP-based modules approached a higher overall heat transfer coefficient (1700 W/m^2-K) than the HEPEEK2 module (1500 W/m^2-K) for the steam/cold water system.

According to the results presented in Table B.1 for the aqueous-aqueous system, polymeric hollow fiber heat exchangers are superior to conventional metallic shell-and-tube heat exchangers in terms of conductance per unit volume (CUV) and overall heat transfer coefficient. Table B.1 demonstrates that the highest CUV value attained by polymeric hollow fiber heat exchangers is approximately 19 times higher than the highest CUV_D value for metallic shell-and-tube heat exchangers. Fouling factors are only incorporated in the determination of the CUV values for the metallic shell-and-tube heat exchangers since there is no significant effect of fouling on the heat exchange performance of polymeric hollow fiber heat exchangers. Table B.1 also shows that the CUV_C value for PEEK plate heat exchanger (polymer film-based) is equivalent to the maximum attained CUV_C value for the PEEK-based polymeric hollow fiber heat exchanger tested. However, the overall heat transfer coefficient for the PEEK plate heat

exchanger (900 W/m^2-K) is substantially lower than the maximum experimentally-derived overall heat transfer coefficient (1914 W/m^2-K) for the PEEK-based hollow fiber module. The highest CUV_C value attained for HEPP1, HEPP2, HEPP3 and HEPEEK2 modules were $1.03x10^6$, $2.92x10^6$, $2.29x10^6$ and $1.04x10^6$ W/m^3–K, respectively. Overall, HEPP2 has the highest CUV_C value due to its highest packing density. Table 4.1 also shows that HEPP2 has the highest overall heat transfer coefficient hence, HEPP2 is the most efficient heat exchanger studied in terms of U and CUV_C. The maximum value of HEPP2 overall heat transfer coefficient U_0 (1534W/m^2-K) was also the highest U_0 value ever reported for plastic heat exchangers and conventional metallic shell-and-tube heat exchangers in liquid-liquid heat exchange systems.

The tube-side flow regime significantly impacts heat transfer. The flow regime in the tube side of the polymeric hollow fiber heat exchange devices is of developing laminar and fully developed laminar flow types unlike the regime on the tube side of conventional shell-and-tube heat exchangers (which generally varies from laminar to turbulent). This is evident from the values of the tube-side Reynolds numbers for all the modules identified in Table 4.1. The majority of the test runs had maximum tube-side Reynolds number slightly below or above 1000. The values of the power index b for the tube-side velocities used in Wilson's Plot fell in the range of 0.77-1.00. The tube-side Reynolds Numbers were in the range of 58-2464 and 3-160, respectively for the hot brine-cold water and the condensing steam-cold water system. The developing or fully developed laminar type tube-side flow is attributed to the very small lumen diameter; laminar flow serves to eliminate excessively high pressure drop due to typically high flow resistance along the hollow fine fibers.

The shell-side Reynolds Numbers for shell-side crossflow mode and for shell-side parallel flow mode for the hot brine-cold water system studied were in the range of 2-200 and 24-3110, respectively. In the case of the hot brine/cold water system, shell-side Reynolds numbers significantly above 1000 were most prevalent. For the steam-cold water system, the shell-side Reynolds Numbers for the shell-side crossflow mode and shell-side parallel flow mode were in the range of 3-90 and 21-630, respectively.

Crossflow on the shell side has been known to introduce flow which augments turbulence. This flow with a higher degree of mixing on the shell side generates superior heat transfer which facilitates higher overall heat transfer coefficients [Zaheed and Jachuck, 2004]. However, contrary to predictions, Table 4.1 shows that parallel flow on the shell side yielded comparable or higher overall heat transfer coefficients at higher shell-side liquid velocities than crossflow on shell side (where the shell-side liquid velocities mostly fell in developing laminar flow region). The substantially lower shell-side Reynolds Number is responsible for this observed behavior. Table 4.1 also shows that for parallel flow on the shell side, the HEPP2 module had a significantly higher maximum overall heat transfer coefficient value than that of the HEPEEK2 module.

Higher shell-side heat transfer coefficients were also obtained for the majority of the test run configurations when hot brine (less viscous liquid) was placed on tube side and cooling water (the more viscous liquid) was placed on shell side. The shell-side liquid flow was kept in turbulent regime or the transition region (mixed flow) resulting in higher shell-side heat transfer coefficients for parallel flow on shell side. This is demonstrated in Tables 4.2 for HEPP3 module with parallel flow on shell side. Higher shell-side heat transfer coefficients were also achieved for crossflow on shell side even at

relatively low shell-side Reynolds Numbers (below 200). When the Wilson's Plot method was employed, experiments with hot brine on the tube side yielded a maximum h_s value of approximately 18000 W/m^2-K which is significantly greater than that obtained from experiments with hot brine on shell side (12000 W/m^2-K).

The tube-side heat transfer coefficients isolated by Conventional Convection Method are comparable to those isolated by the Sieder-Tate correlation. This is shown in Tables E.1-E.4 (values determined by the Conventional Convection Method) and Table E.5 (values determined by the Sieder-Tate correlation). For the majority of the test runs with parallel flow at shell side, the value of RePrD/L fell below 10 and the tube-side heat transfer coefficients were significantly underpredicted by the Sieder-Tate correlation. All runs with crossflow on the shell side yielded RePrD/L values substantially lower than 10 and consequently the tube-side heat transfer coefficients were underpredicted.

According to Table E.3, at low flow rates, the Nu_{T3} value for HEPP3 module with crossflow on the shell side approaches a value of 4.33 for low Nu_w (0.22); similarly the Nu_{T3} value for HEPP3 module with parallel flow at shell side approaches a value of 4.28 for low Nu_w (0.56). Table E.4 also shows that at low flow rates, the Nu_{T3} value for HEPEEK2 module with crossflow at shell side approaches a value of 4.31 for a low Nu_w (1.08); further the Nu_{T3} value for HEPEEK2 module with parallel flow at shell side approaches a value of 4.25 for a low Nu_w (2.03). For both modules, the Nu_{T3} value fell in the range of 3.66 (the limiting Nusselt number for the constant wall temperature condition) - 4.364 (the limiting Nusselt number for the constant heat flux condition) and closer to the upper bound. These results reveal that at lower flow rates, the constant heat flux boundary condition is approached. These results also clearly suggest that the

Conventional Convection Method is valid only at high flow rates since the wall resistance only approaches a constant value or maxima at such points (where Nu_{T3} approaches 3.66 as Nu_w goes to ∞). Thermally developing flow is presumed to be more prevalent than fully developed flow (influenced by shell-side liquid behavior) since the module lengths are small (18.5 cm, 21.5 cm).

The mean Nusselt Number must be accounted for in order to obtain an accurate and complete solution of the thermally developing T3 problem. However, since Equations (2.1)- (2.6) were used for the evaluation of the tube-side and shell-side heat transfer coefficients without employment of an iterative procedure about the wall Nusselt Number, poor isolation results were obtained for the tube and shell- side heat transfer coefficients. The derived solution or the first tube-side or shell-side heat transfer coefficient estimate is more appropriate for the fully developed laminar flow regime. As a result, the isolated shell-side heat transfer coefficients for HEPP3 and HEPP2 were much higher than those isolated by Wilson's Plot. No heat transfer correlation exists which accurately predicts crossflow and parallel flow behavior outside the tube bundle.

Axial heat conduction tends to reduce the thermal effectiveness of heat exchangers. There is an underlying assumption in the utilization of the Conventional Convection method that the axial heat conduction is negligible. This intrinsic assumption is not justifiable since as demonstrated in Tables C.1 to Table C.8, the thermal effectiveness factor for all the tested tubular devices fell significantly below 80% in almost all of the runs.

It is also evident from the experimental results that the temperature difference between the shell inlet and outlet temperatures is generally significant (greater than

10°C). The thermal boundary condition achieved during testing is not a constant wall temperature boundary condition since the shell-side liquid temperature is changing. This is primarily due to the low thermal conductance of the polymeric devices and the low flow rates of the shell-side and tube-side liquids. However, the Conventional Convection Method regards the wall and outside convective resistance as a single term. Based on the three limitations, it can be said that Conventional Convection Method is not necessarily the best method of isolating the inside, outside and wall heat transfer coefficients at low flow rates.

The Wilson's Plot Method was the preferred method for isolating the wall heat transfer coefficient, shell-side and tube-side heat transfer coefficient. The test run results for the HEPP1 and HEPEEK2 modules yielded poor fit (very low regression coefficients). In order to obtain a 'best fit' straight line in the case of constant tube- side flow with shell-side liquid flow variation, all of the resistances other than the inside resistance must remain constant so as to keep the intercept constant.

However, in the case of the data showing a poor fit, h_o is not proportional to the shell-side velocity raised to a power in the vicinity of 0.8 since a significant change in liquid hydrodynamic conditions (augmentation of turbulence) at high flow rates on the shell side causes the power index to differ substantially which in turn impacts the intercept and the heat transfer rate. The tube-side conditions are generally more predictable than shell-side conditions. In general, the isolated tube-side heat transfer coefficients are high. According to Table 4.2, the highest shell-side heat transfer coefficient attained for HEPP2 module with crossflow at shell side is approximately 4800 W/m^2-K; this is substantially lower than the highest shell-side heat transfer coefficient

Table 4.2 Sample Wall, Tube-side and Shell-side Heat Transfer Coefficients Obtained from Utilization of Wilson's Plot Method

Module	Configuration	Re_s	h_t(W/m^2-K)	h_s(W/m^2-K)	h_w (W/m^2-K)	R_t/R_{ot}(%)	R_w/R_{ot}(%)	R_s/R_{ot}(%)
HEPP2	**Crossflow at Shell side: Hot Brine (Shell),Cooling water (Tube)**	39-200	2305-38400	1229-4843	1706	24-3	32-71	44-25
	Parallel Flow at Shell side: Hot Brine (Tube), Cooling water (Shell)	83-490	1986-33900	1433-18425	2481	31- 6	25-83	43-11
HEPP3	**Crossflow at Shell side: Hot Brine (Tube), Cooling water (Shell)**	5-39	1793-6109	1005-7493	2148	28-21	23-61	49-17
	Parallel Flow at Shell side: Hot Brine (Shell), Cooling water (Tube)	316-2567	2902-8580	2793-12336	2418	31-19	37-67	32-13
	Parallel Flow at Shell side: Hot Brine (Tube), Cooling water (Shell)	81-825	1140-9308	1314-17963	2415	42-18	21-72	37-10

attained for HEPP3 module (7500 W/m^2-K) with crossflow at shell side. The highest tube- side heat transfer coefficient isolated for HEPP2 module (crossflow at shell side) is substantially higher (38000 W/m^2-K) than that isolated (6100 W/m^2-K) for HEPP3 module with crossflow at shell side. The results documented in Table 4.2 also show that the shell- side heat transfer coefficient for HEPP2 module with parallel flow at shell side can reach as high as 18000 W/m^2-K, a value higher than that of HEPP3 module with parallel flow at shell side (18400 W/m^2-K). The highest isolated tube-side heat transfer coefficient for the HEPP2 module with parallel flow at shell side is approximately 34000 W/m^2-K. This value is significantly higher than that of the HEPP3 module with parallel flow at shell side (9300 W/m^2-K). The wall heat transfer coefficients for the HEPP2 and HEPP3 modules isolated by the Wilson Plot method (2148 W/m^2-K and 2400 W/m^2-K) are closer to the literature value (2125W/m^2-K) than those isolated by the Conventional Method. This also serves to confirm the accuracy of the Wilson's Plot method over a reasonably wide range of flow rates.

The results for the aqueous-aqueous system in Table 4.2 (Wilson's Plot-based percentages of thermal resistances) suggest that the tube-side resistance was the smallest of the three. The tube-side resistance only contributed up to 21% of the total thermal resistance. Hence, as demonstrated in the case of hot brine flow variation on shell side with fixed tube-side cooling water flow for HEPP3 module, there is insignificant improvement in the overall heat transfer performance by increasing the tube-side Reynolds number. Based on the thermal resistance percentages determined by the Wilson's Plot method, the wall thermal resistance was controlling for all test run configurations with shell-side crossflow arrangement and the majority of test run

configurations with shell-side parallel flow arrangement. It contributed as much as 83% of the total thermal resistance. This is also observed in the trends exhibited in the plots of U against the tube-side or shell- side liquid velocities. The existence of a final plateau in almost all of these plots confirms that the wall thermal resistance is the limitation factor for heat transfer.

Table C.9 demonstrates that the heat-exchanger effectiveness and the NTU, up to almost 97% and 4, respectively are attainable in devices having HTU values as low as 5 cm. These results were achieved under conditions of low tube-side Reynolds numbers. In Figures D.1-D.9, the NTU, HTU and the thermal effectiveness factor are plotted against the tube-side and shell- side Reynolds numbers. Generally high thermal effectiveness factors were attained at high NTU and low HTU values. High thermal effectiveness values (above 0.90) were attained when the tube-side Reynolds numbers were lower than 200. Tables C.1 to C.8 demonstrate that there is an increase in the overall heat transfer coefficient with a significant decrease in NTU and thermal effectiveness. For all test runs, at lower flow rates, the temperature changes and the thermal effectiveness factors were higher. As a result, the NTUs were high and the HTUs were small. According to Table C.9, the module with the lowest HTU value (5 cm) and the highest NTU (4.00) is HEPP2. This HTU value is approximately 20 times lower than the lower limit for conventional metallic shell-and-tube heat exchangers [Zarkadas and Sirkar, 2004]. Table C.9 also demonstrates that the module with the highest HTU (106 cm) and the lowest NTU (0.17) is HEPEEK2. Correspondingly, HEPEEK2 module yielded the lowest maximum thermal effectiveness value (0.58). The majority of test runs with crossflow on the shell side had NTUs and shell-side temperature difference values substantially greater than those values

achieved for test runs with parallel flow on shell side. This is depicted in Tables C.1 to C.9. Parallel flow configuration on shell side gave higher heat transfer coefficients than crossflow configuration at shell side but did not necessarily reduce the liquid temperature that effectively.

The value of F (the temperature correction factor) was approximately one when the terminal temperature differences (differences between the shell-side liquid outlet temperatures and the tube-side liquid outlet temperatures) were large but F did not significantly lower the logarithmic mean temperature difference when the temperatures of the shell-side and tube-side liquids were almost identical. This is demonstrated in Tables C.1 to C.9. Tables C.1 to C.9 also show that the smaller the temperature approach (the difference between the outlet temperature of one stream and the inlet temperature of the other stream), the larger is the heat transfer area required for a given duty. Sinnott [1983] also supports this observation.

Figures F1 to F2 depict plots of Fanning friction factor ($f_{Fanning}$) and Colburn factor (j_H) against Reynolds Number for the tube side of HEPP3 and HEPEEK2 modules, respectively. The Fanning friction values were calculated using the pressure drop values derived after corrections for entrance and exit pressure losses. The Fanning friction factor curves for HEPP3 and HEPEEK2 demonstrate a deviation from the conventional tube-side friction factor. The Fanning friction factor curves indicate that the true tube-side pressure drop values yielded tube-side friction factors that are applicable to the entire laminar flow regime. The slopes of the friction factor curve for HEPP3 and HEPEEK2 are - 0.66 and - 0.57, respectively. These values are substantially lower than the predicted value of the slope of the curve for Hagen Poiseuille flow or laminar flow in micro

channels. These friction factor values derived experimentally being higher than those in theory can be attributed to the inherent surface roughness for hollow fiber surfaces. The surface roughness element is usually excluded for laminar flow through conventional micro channels leading to lower frictional losses and a delayed transition from laminar to turbulent flow regime. It is also evident that Fanning friction factor or coefficient decreases as tube-side Reynolds Number increases. The slope of j_H vs. Re_t plot for HEPP3 and HEPEEK2 is 0.992 and 1.0, respectively. Both of these values fall close to theoretical prediction of -1 for fully developed laminar flow at constant Nu. This suggests that the lengths of the two test modules are not only larger than the thermal entry length but also of sufficient magnitude to support fully developed laminar flow conditions on the tube side.

The specific pressure drop, $\Delta P/NTU$ is a vital parameter in assessing the performance of the heat exchanger. Specific pressure drop values for water/water duties for most heat exchangers fall in the range of 20-100 kPa/NTU and the optimum specific pressure drop values for plate heat exchangers fall close to 30kPa/NTU [Kakac, Shah and Bergles, 1983]. The specific pressure drop for PP-based modules and HEPEEK2 module were as low as 1.29 kPa/NTU and 42 kPa/NTU, respectively for parallel flow on the shell side. The specific pressure drop for PP-based modules and HEPEEK 2 module with crossflow on the shell side were as low as 0.7 kPa/NTU and 15 kPa/NTU, respectively. These values are closer to the lower bound of the range of typical specific pressure drop values for water/water applications presented earlier. It is evident that a greater heat exchange performance is attained by the test modules compared to that by conventional

shell-and-tube heat exchangers and plate heat exchangers at a substantially lower pumping cost.

CHAPTER 5

CONCLUSIONS

Heat exchange performances of solid, polymeric, transverse/parallel flow hollow fiber heat exchange devices constructed out of PP and PEEK materials were evaluated for hot brine-cold water and condensing steam-cold water systems. The modeling and analysis was carried out only for the hot brine-cold water system. Two modeling methods were employed namely, Conventional Convection and Wilson's Plot. The Conventional Convection Method was based on the convective boundary condition at the inside surface of the wall of the heat exchangers and a constant wall thermal resistance assumption. The Wilson's Plot was the preferred method because the isolated wall heat transfer coefficients for the PP-based modules is comparable to that reported for PP in literature; however, the shell-side liquid behavior was not as predictable as that of the tube-side liquid, its range of validity (applicable over a wider range of flow rates) was greater than that of the Conventional Convection Method and the wall and outside convective resistances were not regarded as one single constant term. The following conclusions were established in light of the results and analysis of the different test run configurations used in the hot brine-cold water and steam-cold water systems.

- The maximum overall heat transfer coefficient attained in the polymeric hollow fiber heat exchangers for parallel flow mode at shell side is significantly higher than that achieved for crossflow mode at shell side; the Reynolds Number for crossflow were, however, much lower.

- The fouling free maximum O.D-based overall heat transfer coefficient (1534 W/m^2-K) and CUV ($2.9x10^6$ W/m^3-K) (both values obtained in the HEPP2 module) attained in this study is higher than those previously reported for plastic heat exchangers, hollow fiber exchangers [Zarkadas and Sirkar, 2004] and metallic shell-and-tube heat exchangers(U_o based on fouling factor). The highest attained overall heat transfer coefficient based on the outside area (U_o) for the HEPEEK2 module (1434 W/m^2-K) is in the range of that obtained for PP-based modules (1330-1534 W/m^2-K).

- The maximum CUV value achieved in this study is approximately 19 times higher than that attained in conventional metallic tubular heat exchangers based on fouling factor.

- The wall thermal resistance is controlling for both crossflow and parallel flow on the shell side. It contributed as much as 83% of the total thermal resistance. The tube-side thermal resistance contributed the least to the overall heat transfer resistance.

- In the context of NTUs achieved, shell side with parallel flow configuration is better than shell side with crossflow configuration.

- Due to its higher packing density, the HEPP2 module has the best heat exchange performance in terms of U, CUV and NTU. The HEPEEK2 module demonstrated the worst heat exchange performance in terms of thermal effectiveness, NTU and CUV. HEPEEK2's low heat exchange performance relative to that of the PP-based modules is attributed to the fact that the PEEK fibers were not potted to accommodate regular spacing on the shell side. The irregular spacing promoted considerable bypassing and that lowered the shell-side heat transfer coefficient and consequently the overall heat transfer coefficient.

- The results for hot brine-cold water heat exchange demonstrated thermal efficiencies of up to almost 97% and up to 4 transfer units for devices having a HTU less than 5cm. Those results are attained under conditions of lower tube-side Reynolds numbers.

- The lowest HTU achieved in the polymeric hollow fiber heat exchange devices studied is approximately 20 times lower than the lower limit for shell-and-tube heat exchangers.

- The pressure drop measurements yield tube-side friction factors that are applicable to the entire laminar flow regime.

- A better heat exchange performance is attained in the polymeric hollow fiber heat exchangers studied relative to most metallic heat exchangers at a substantially lower pumping cost. The magnitude of the lowest specific pressure drop attained is 0.7 kPa/NTU, which is substantially lower than that of metallic heat exchangers (20kPa/NTU).

- The maximum U value attained in the condensing steam-cold water system is 1700 W/m^2-K.That value was realized in the HEPP1 module.

The results of this study will be an invaluable asset to the desalination industry. This study confirms that novel solid polymeric hollow fine fiber heat exchange devices with crossflow mode at shell side and parallel flow mode at shell side are superior to metallic shell-and-tube heat exchangers in terms of heat exchange performance on a volumetric as well as weight basis.

APPENDIX A

U VS LIQUID VELOCITY TRENDS

Figures A.1 to A.28 illustrate the plots of U (overall heat transfer coefficient based on inside fiber area) versus linear or interstitial velocity.

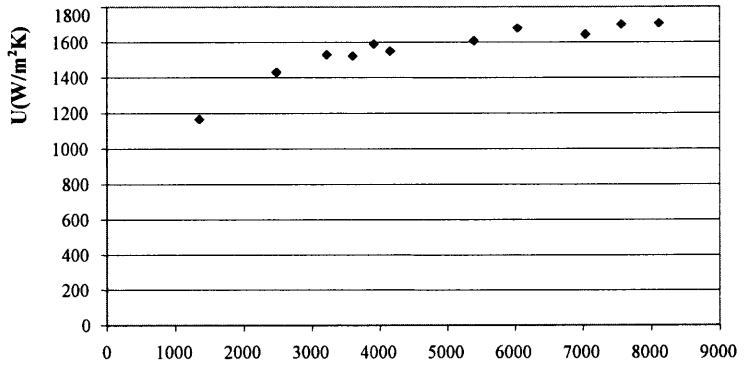

Shell-side (Hot Brine) Linear Velocity Variation: 1346-8110 cm/min (Re_s: 316 -2567)
Inlet Hot Brine (4%NaCl) Temperature: 97^{0}C
Inlet Cooling Water Temperature: 9^{0}C
Tube-side (Cooling Water) Linear Velocity: 10372 cm/min (Re_t: 789)
Shell-side Configuration: Parallel -Flow

Figure A.1 Variation of U with Shell-side Linear Velocity for module HEPP3 with Shell-side Hot Brine flow and Tube-side Cooling Water flow.

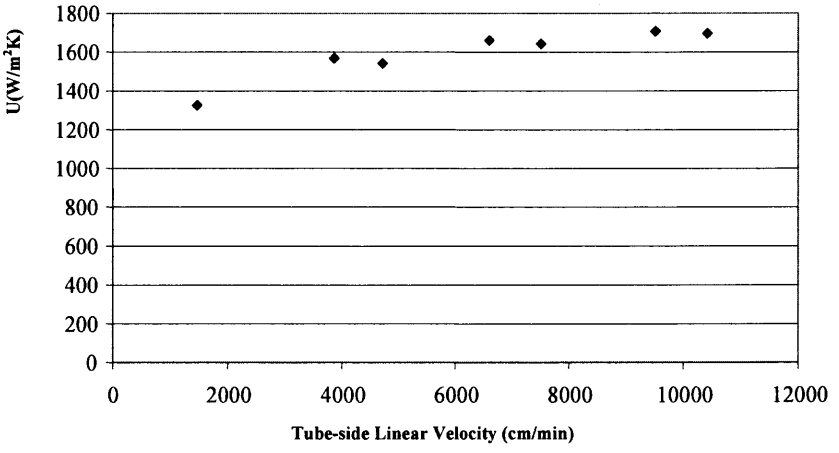

Tube-side (Cooling Water) Linear Velocity Variation: 1469-10422 cm/min (Re_t: 410-828)
Inlet Hot Brine (4%NaCl) Temperature: 97°C
Inlet Cooling Water Temperature: 12°C
Shell-side (Hot Brine) Linear Velocity: 7998 cm/min (Re_s: 2661)
Shell-side Configuration: Parallel Flow

Figure A.2 Variation of U with Tube-side Linear Velocity for module HEPP3 with Shell-side Hot Brine flow and Tube-side Cooling Water flow.

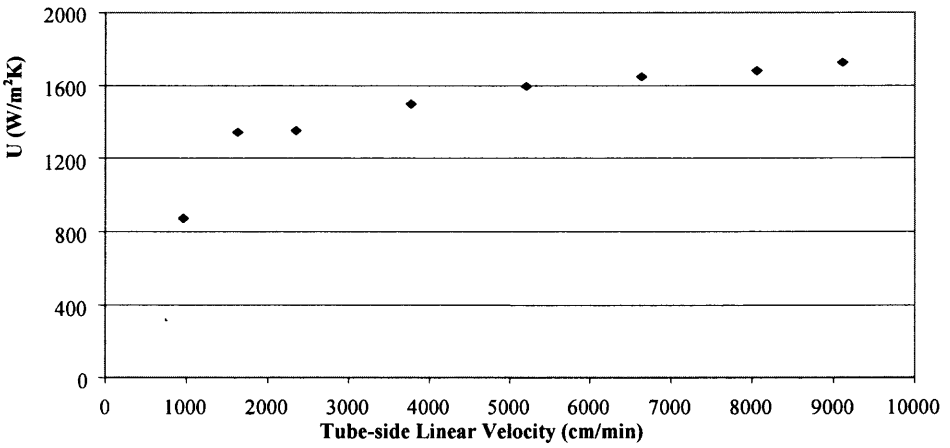

Tube-side (Hot Brine, 4% NaCl) Linear Velocity Variation: 961-9111 cm/min (Re_t:125-1779)
Inlet Hot Brine (4%NaCl) Temperature: 98^{0}C
Inlet Cooling Water Temperature: 10^{0}C
Shell-side (Cooling Water) Linear Velocity: 7820cm/min (Re_s: 650)
Shell-side Configuration: Parallel Flow

Figure A.3 Variation of U with Tube-side Linear Velocity for module HEPP3 with Tube -side Hot Brine flow and Shell-side Cooling Water flow.

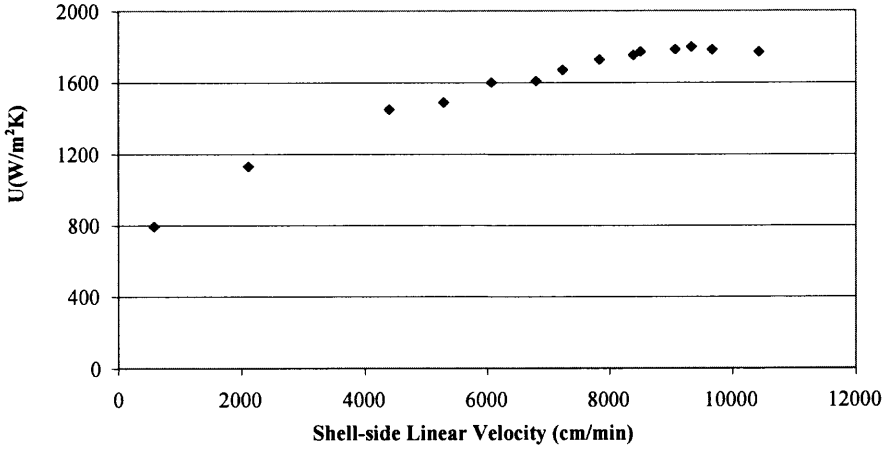

Tube-side (Hot Brine,4%NaCl) Linear Velocity : 9180 cm/min (Re_t:1844)
Inlet Hot Brine (4%NaCl) Temperature: 97^{0}C
Inlet Cooling water Temperature: 11^{0}C
Shell-side (Cooling water) Linear Velocity Variation: 579-10437cm/min (Re_s: 81-825)
Shell-side Configuration: Parallel Flow

Figure A.4 Variation of U with Shell-side Linear Velocity for module HEPP3 with Tube-side Hot Brine flow and Shell-side Cooling Water flow.

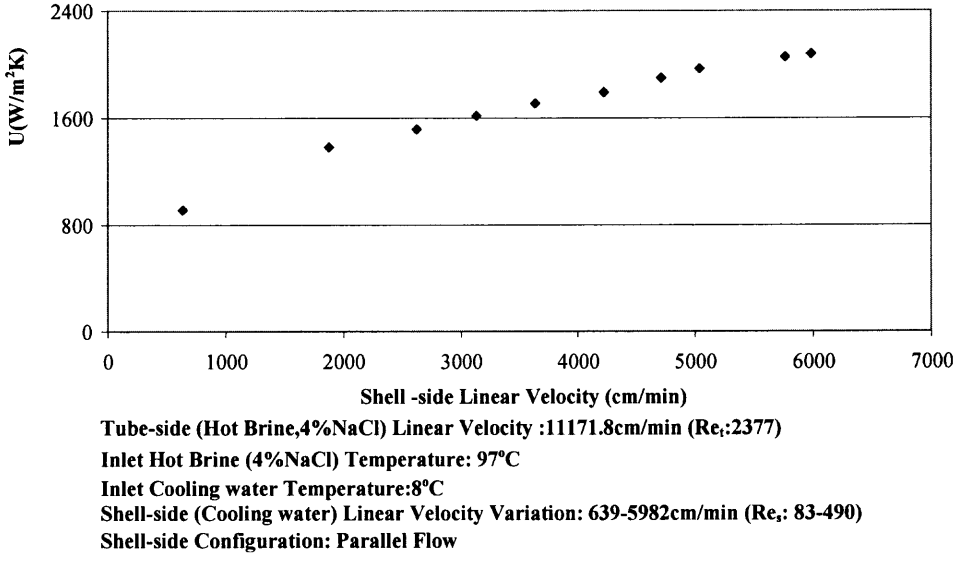

Figure A.5 Variation of U with Shell-side Linear Velocity for module HEPP2 with Tube-side Hot Brine flow and Shell-side Cooling Water flow.

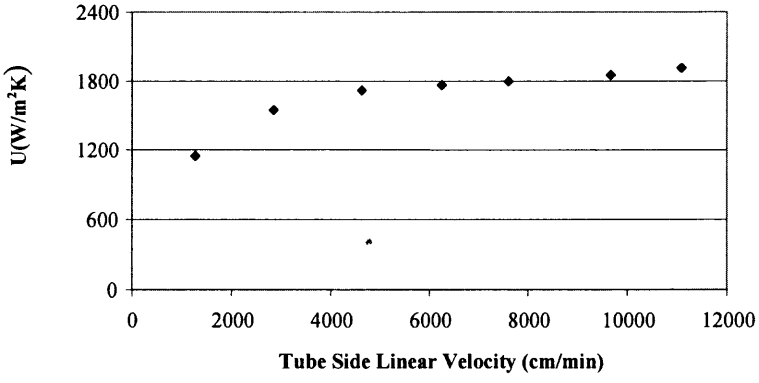

Tube-side (Hot Brine,4%NaCl) Linear Velocity Variation :1265-11089cm/min (Re_t:402)
Inlet (Hot Brine, 4%NaCl) Temperature: 97^{0}C
Inlet Cooling water Temperature :7^{0}C
Shell-side (Cooling Water) Linear Velocity: 4920cm/min (Re_s: 172-2315)
Shell-side Configuration: Parallel Flow

Figure A.6 Variation of U with Tube-side Linear Velocity for module HEPP2 with Tube-side Hot Brine flow and Shell-side Cooling Water flow.

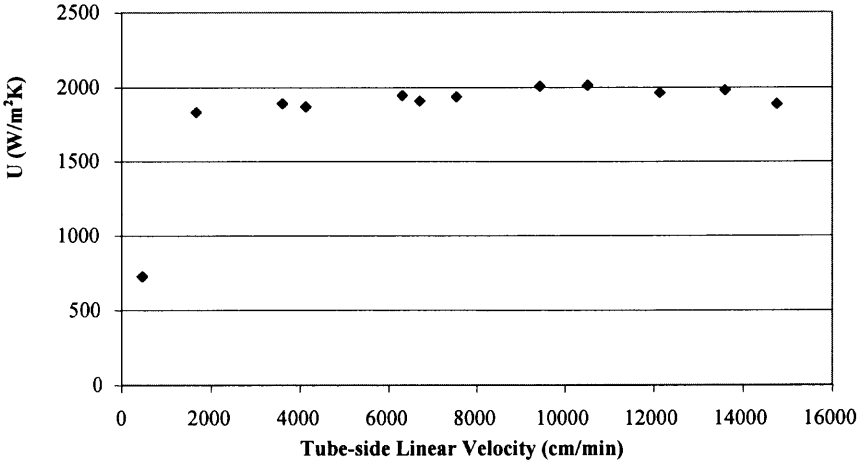

Shell-side (Hot Brine,4%NaCl)Linear Velocity : 11960 cm/min(Re_t:1797)
Inlet Hot Brine (4%NaCl) Temperature: 95^{0}C
Inlet Cooling Water Temperature: 10.6^{0}C
Tube-side (Cooling water) Linear Velocity Variation: 458-14754 cm/min (Re_t: 67-992)
Shell-side Configuration: Parallel Flow

Figure A.7 Variation of U with Tube-side Linear Velocity for module HEPP2 with Shell-side Hot Brine flow and Tube-side Cooling Water flow.

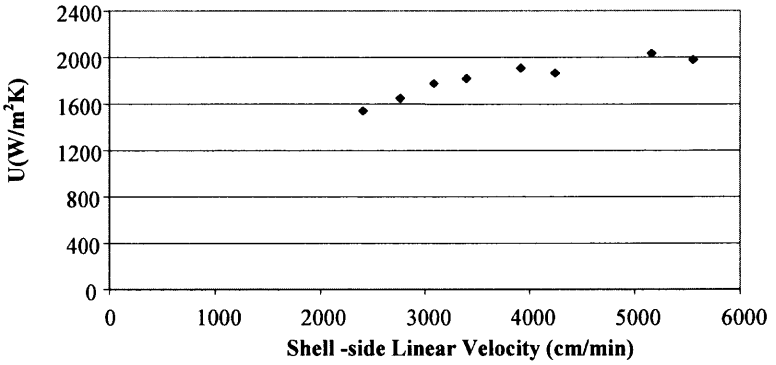

Shell-side (Hot Brine,4%NaCl) Linear Velocity Variation : 2407-5556cm/min(Re_s :667-1649)
Inlet Hot Brine (4%NaCl) Temperature: 96°C
Inlet Cooling Water Temperature: 8°C
Tube-side (Cooling water) Linear Velocity: 10758 cm/min (Re_t : 790)
Shell-side Configuration: Parallel Flow

Figure A.8 Variation of U with Shell-side Linear Velocity for module HEPP2 with Shell-side Hot Brine flow and Tube-side Cooling Water flow.

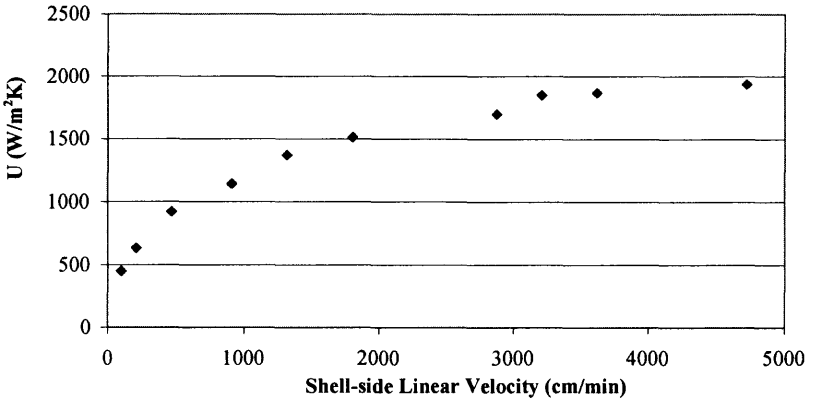

Tube-side (Cooling Water) Linear Velocity: 4251 cm/min (Re_t: 498)

Inlet Hot Brine (4%NaCl) Temperature: 90^0C

Inlet Cooling Water Temperature: 33^0C

Shell-side (Hot Brine,4%NaCl) Linear Velocity Variation :100-4725 cm/min (Re_s : 24-1446)
Shell-side Configuration: Parallel Flow

Figure A.9 Variation of U with Shell-side Linear Velocity for module HEPP1 with Shell-side Hot Brine flow and Tube-side Cooling Water flow.

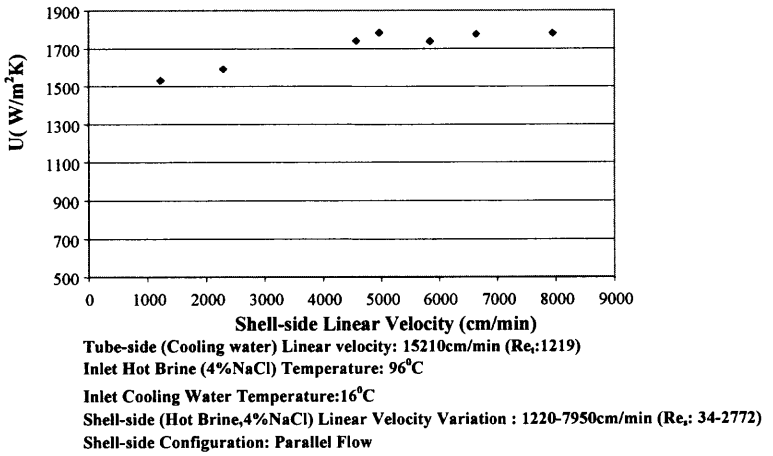

Figure A.10 Variation of U with Shell-side Linear Velocity for module HEPEEK2 with Shell-side Hot Brine flow and Tube-side Cooling Water flow.

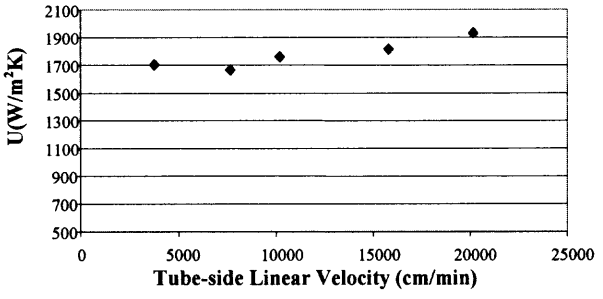

Shell-side (Hot Brine, 4%NaCl) Linear Velocity: 9037cm/min (Re_s:3110)
Inlet Hot Brine (4%NaCl) Temperature: 98^{0}C

Inlet Cooling Water Temperature: 18^{0}C
Tube-side (Cooling Water) Linear Velocity Variation: 3768-20179cm/min (Re_t:433-1571)
Shell-side Configuration: Parallel Flow

Figure A.11 Variation of U with Tube-side Linear Velocity for module HEPEEK2 with Shell-side Hot Brine flow and Tube-side Cooling Water flow.

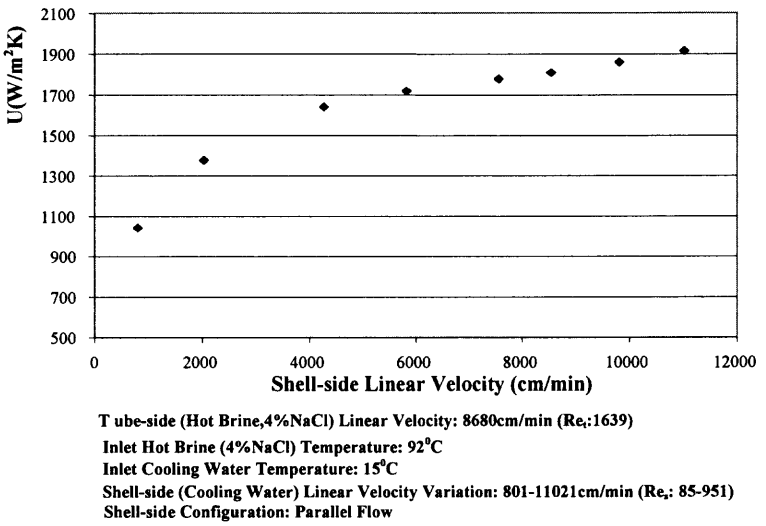

Figure A.12 Variation of U with Shell-side Linear Velocity for module HEPEEK2 with Tube-side Hot Brine flow and Shell-side Cooling Water flow.

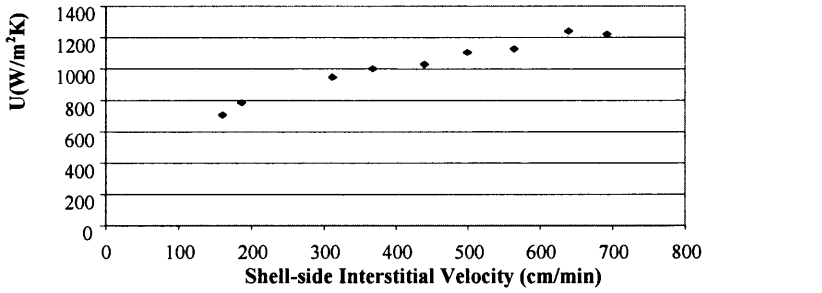

Shell-side (Hot Brine) Interstitial Velocity variation: 160- 693 cm/min (Re_i: 39-200)
Inlet Hot Brine (4%NaCl) Temperature: 91^{0}C
Inlet Cooling water Temperature: 7^{0}C

Tube-side (Cooling water) Linear Velocity: 5039cm/min (Re_t : 600)
Shell-side Configuration: Crossflow

Figure A.13 Variation of U with Shell-side Interstitial Velocity for module HEPP2 with Shell-side Hot brine flow and Tube- side Cooling Water flow.

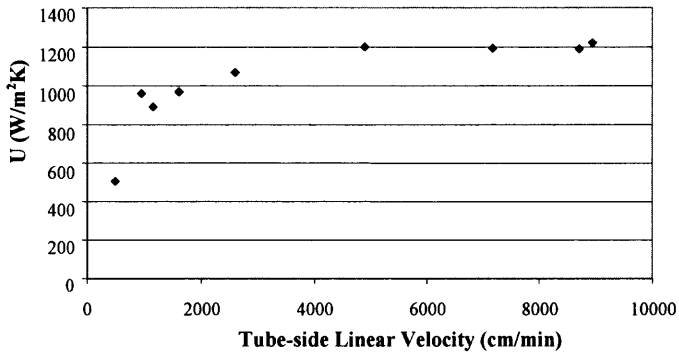

Tube-side (Cooling water) Linear Velocity Variation: 492-8942cm/min (Re_t: 66-639)
Inlet Hot Brine (4%NaCl) Temperature: 93°C
Inlet Cooling water Temperature: 16.4°C
Shell-side (Hot Brine) Interstitial Velocity: 9431cm/min (Re_s: 224)
Shell-side Configuration: Crossflow

Figure A.14 Variation of U with Tube-side Linear Velocity for module HEPP2 with Shell-side Hot Brine flow and Tube-side Cooling Water flow.

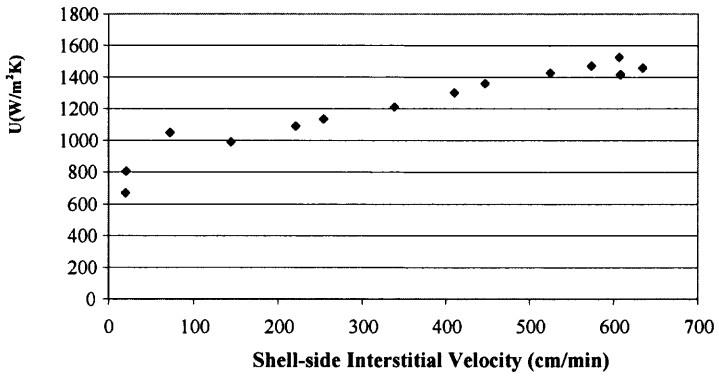

Shell-side (Cooling water) Interstitial Velocity Variation: 258-8403 cm/min (Re_s: 4-50)
Inlet Hot Brine (4%NaCl) Temperature: 94°C
Inlet Cooling water Temperature: 10.5°C
Tube -side (Hot Brine) Linear Velocity: 6316cm/min (Re_t: 2464)
Shell-side Configuration: Crossflow

Figure A.15 Variation of U with Shell-side Interstitial Velocity for module HEPP2 with Shell-side Cooling Water flow and Tube- side Hot Brine flow.

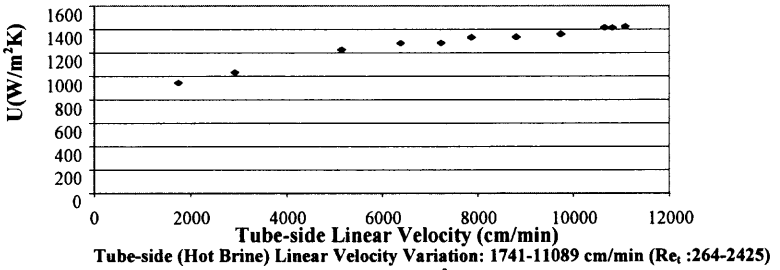

Tube-side (Hot Brine) Linear Velocity Variation: 1741-11089 cm/min (Re_t :264-2425)
Inlet Hot Brine (4%NaCl) Temperature: 96^{0}C
Inlet Cooling water Temperature: 6^{0}C
Shell-side (cooling water) interstitial velocity: 8316cm/min (Re_s:50)
Shell-side Configuration: Crossflow

Figure A.16 Variation of U with Tube-side Linear Velocity for module HEPP2 with Shell-side Cooling Water flow and Tube-side Hot Brine flow.

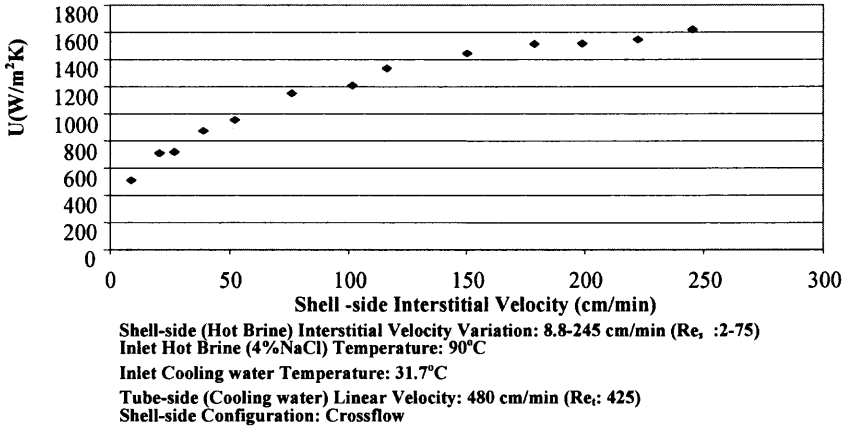

Figure A.17 Variation of U with Shell-side Interstitial Velocity for module HEPP1 with Shell-side Hot Brine flow and Tube- side Cooling Water flow.

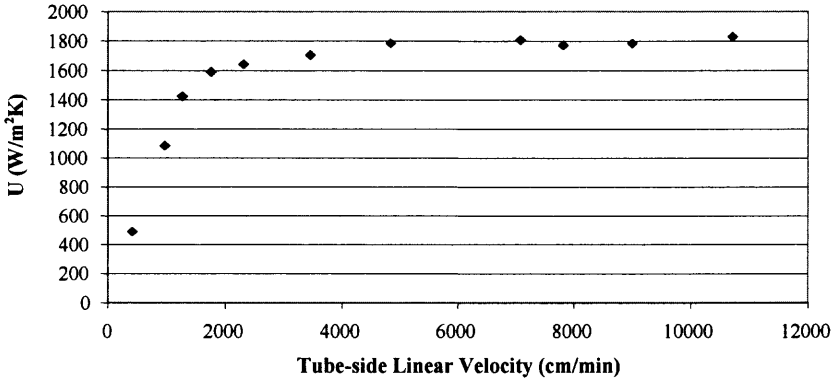

Shell-side (Hot Brine) Interstitial Velocity: 254 cm/min (Re_s: 78)
Inlet Hot Brine (4%NaCl) Temperature: 90^{0}C
Inlet Cooling water Temperature: 35^{0}C
Tube-side (Cooling water) Linear Velocity Variation: 419-8999 cm/min (Re_t: 58-1376)
Shell-side Configuration: Crossflow

Figure A.18 Variation of U with Tube-side Linear Velocity for module HEPP1 with Shell-side Hot Brine flow and Tube- side Cooling Water flow.

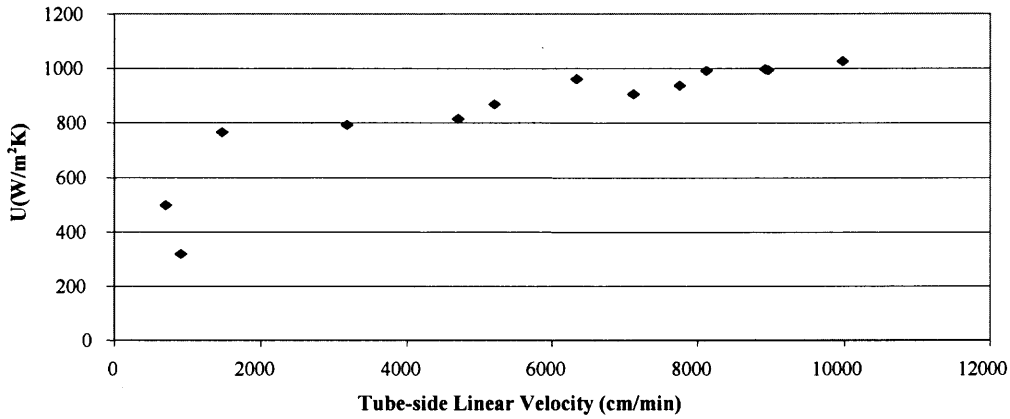

Tube-side (Cooling water) Linear Velocity Variation: 705-9975 cm/min (Re_t: 96-730)
Inlet Hot Brine (4%NaCl) Temperature: 91^{0}C
Inlet Cooling water Temperature: 13^{0}C
Shell-side (Hot Brine) Interstitial Velocity: 283cm/min (Re_s: 93)
Shell-side Configuration: Crossflow

Figure A.19 Variation of U with Tube-side Linear Velocity for module HEPP3 with Shell-side Hot Brine flow and Tube- side Cooling Water flow.

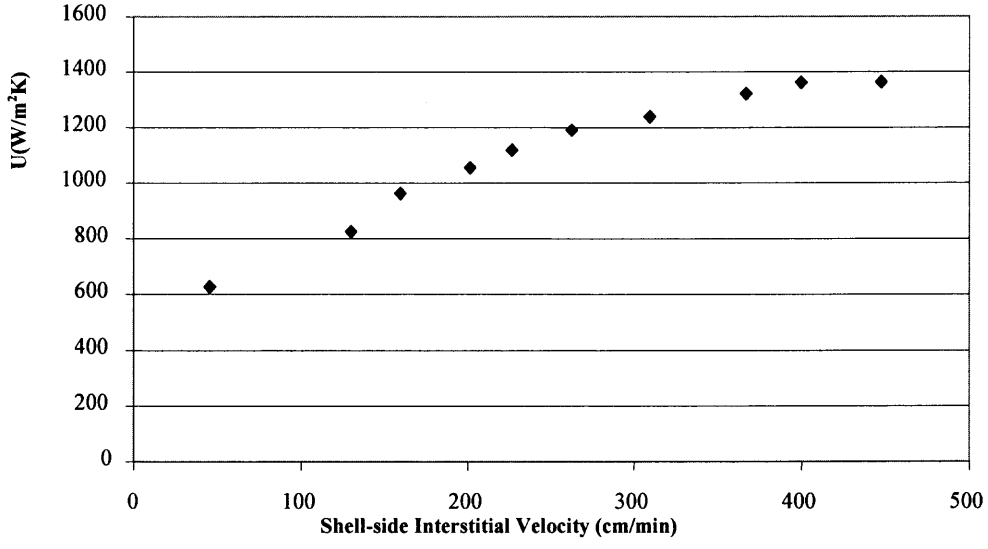

Tube-side (Hot Brine,4%NaCl) Linear Velocity): 9736cm/min(Re_t:2132)
Inlet Hot Brine (4%NaCl) Temperature: 98^{0}C
Inlet Cooling Water Temperature: 10^{0}C
Shell-side (Cooling Water) Interstitial Velocity Variation: 45-447cm/min (Re_s: 5-39)
Shell-side Configuration: Crossflow

Figure A.20 Variation of U with Shell-side Interstitial Velocity for module HEPP3 with shell-side Cooling Water flow and Tube-side Hot Brine flow.

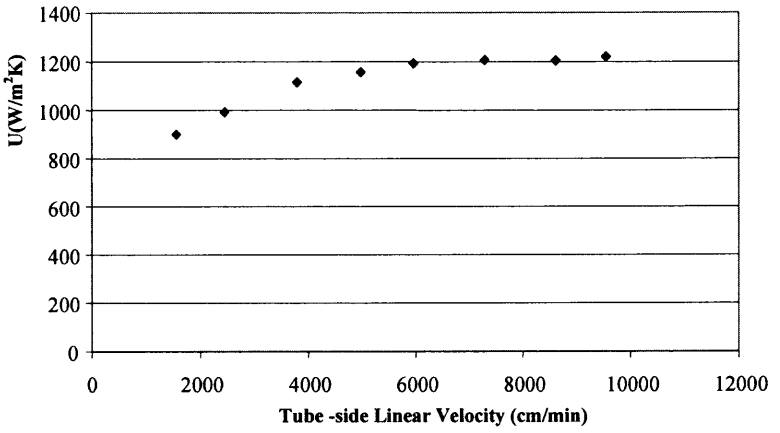

Tube-side (Hot Brine,4%NaCl) Linear Velocity Variation:1555-9547cm/min(Re_t:218-2025)
Inlet Hot Brine (4%NaCl) Temperature: 96°C
Inlet Cooling water Temperature: 8°C
Shell-side (Cooling water) Interstitial Velocity: 312cm/min (Re_s: 24)
Shell-side Configuration: Crossflow

Figure A.21 Variation of U with Tube-side Linear Velocity for module HEPP3 with Shell-side Cooling water flow and Tube-side Hot Brine flow.

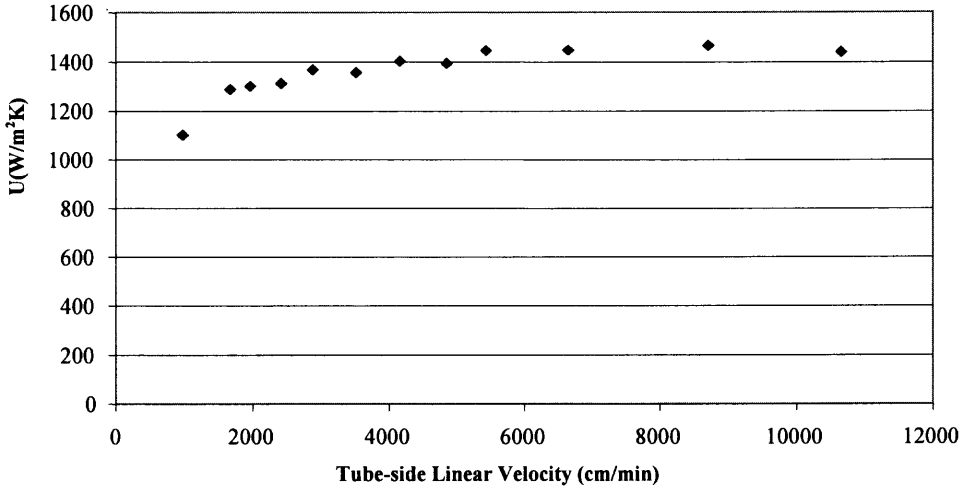

Tube-side (Hot Brine,4%NaCl)Linear Velocity Variation: 982-10650 cm/min (Re_t:153-2232)
Inlet Hot Brine (4%NaCl) Temperature: 89^{0}C
Inlet Cooling water Temperature: 34°C
Shell-side (Cooling water) Interstitial Velocity: 258 cm/min (Re_s:34)
Shell-side Configuration: Crossflow

Figure A.22 Variation of U with Tube-side Linear Velocity for module HEPP1 with Shell-side Cooling Water flow and Tube- side Hot Brine flow.

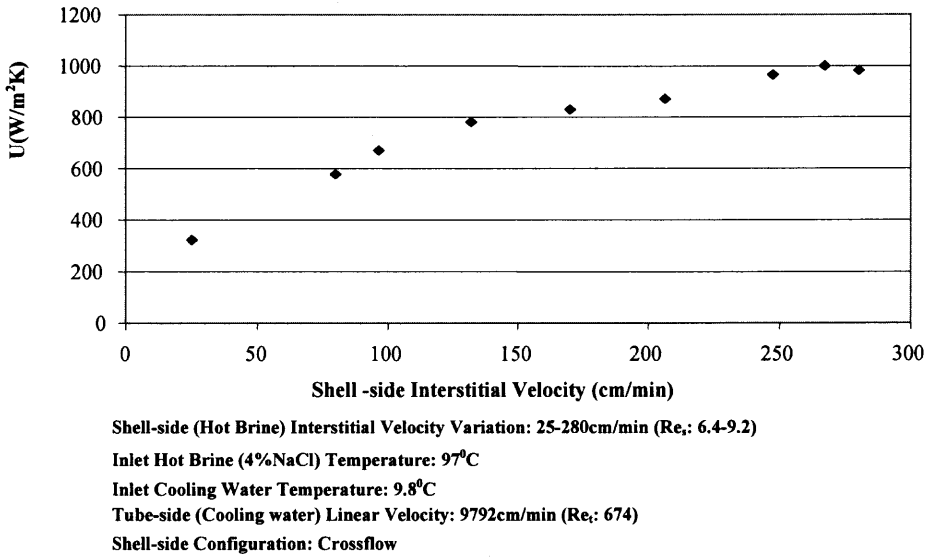

Figure A.23 Variation of U with Shell-side Interstitial Velocity for module HEPP3 with Shell-side Hot Brine flow and Tube-side Cooling Water flow.

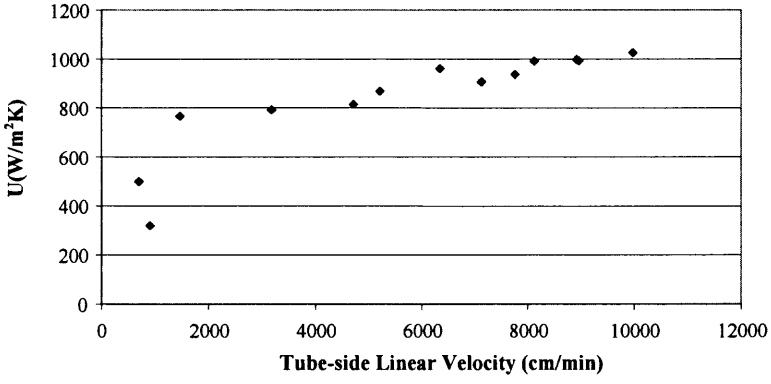

Tube-side (Cooling water) Linear Velocity Variation: 705-9975 cm/min (Re_t: 96-730)
Inlet Hot Brine (4%NaCl) Temperature: 91^{0}C
Inlet Cooling water Temperature: 13^{0}C
Shell-side (Hot Brine) Interstitial Velocity: 283cm/min (Re_s: 93)
Shell-side Configuration: Crossflow

Figure A.24 Variation of U with Tube-side Linear Velocity for module HEPP3 with Shell-side Hot Brine flow and Tube-side Cooling Water flow.

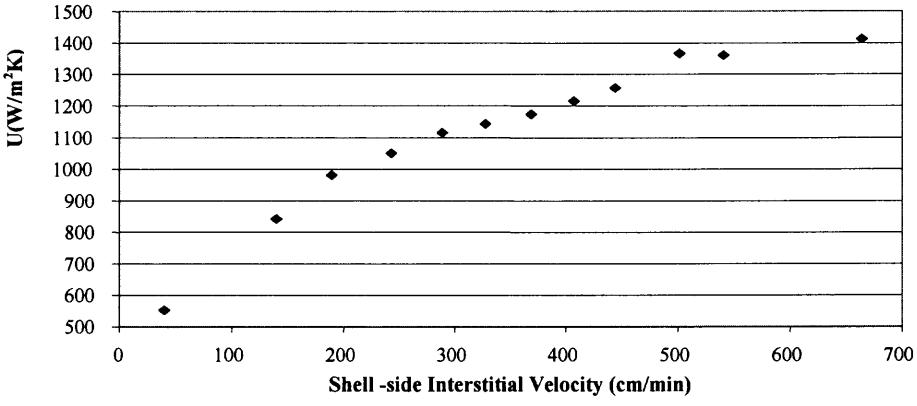

Tube side (Hot Brine,4%NaCl) Linear Velocity : 801cm/min (Re_t:1397)
Inlet Hot Brine (4%NaCl) Temperature: 90 ^{0}C
Inlet Cooling Water Temperature: 15^{0}C
Shell-side (Cooling Water) Linear Velocity Variation: 40-664cm/min (Re_s: 4.4-57)
Shell-side Configuration: Crossflow

Figure A.25 Variation of U with Shell-side Interstitial Velocity for module HEPEEK2 with Tube-side Hot Brine flow and Shell-side Cooling Water flow.

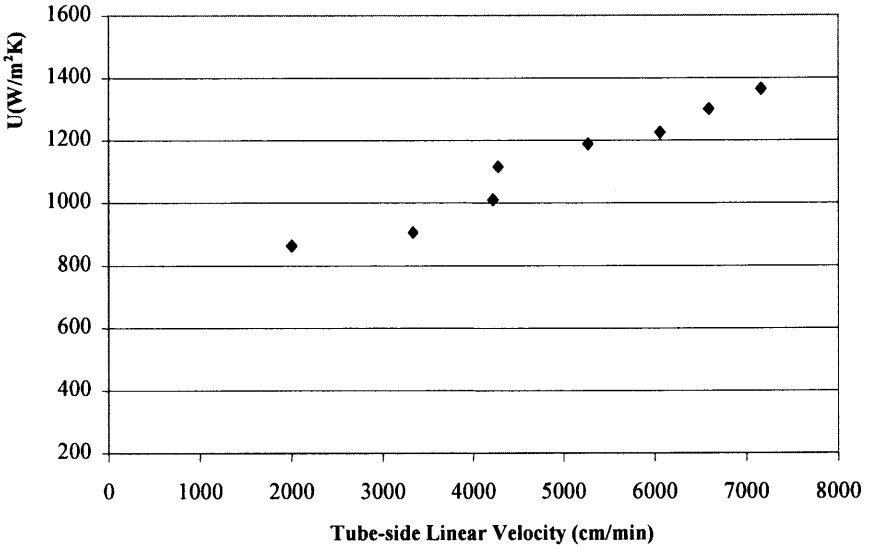

Tube-side (Hot Brine,4%NaCl) Linear Velocity Variation : 2001-7158 cm/min (Re_t:239-1300)

Inlet Hot Brine (4%NaCl) Temperature: 88^{0}C

Inlet Cooling Water Temperature: 14^{0}C

Shell-side (Cooling Water) Linear Velocity: 646 cm/min (Re_s:55)

Shell-side Configuration: Crossflow

Figure A.26 Variation of U with Tube-side Linear Velocity for module HEPEEK2 with Tube-side Hot Brine flow and Shell-side Cooling Water flow.

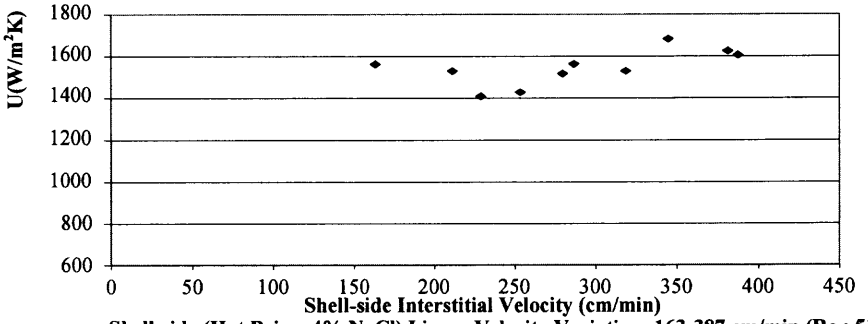

Shell-side (Hot Brine, 4% NaCl) Linear Velocity Variation: 163-387 cm/min (Re_s: 51-130)
Inlet Hot Brine (4%NaCl) Temperature: 97°C
Inlet Cooling Water Temperature: 16°C
Tube-side (Cooling Water) Linear Velocity: 15247 cm/min (Re_t: 1176)
Shell-side Configuration: Crossflow

Figure A.27 Variation of U with Shell-side Interstitial Velocity for module HEPEEK2 with Shell-side Hot Brine flow and Tube-side Cooling Water flow.

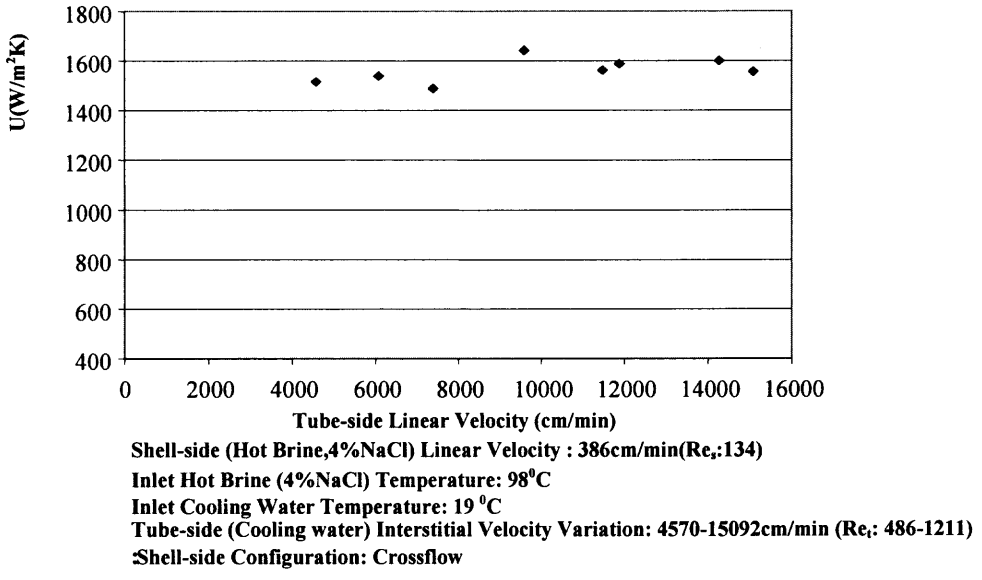

Figure A.28 Variation of U with Tube-side Linear Velocity for module HEPEEK2 with Shell-side Hot Brine flow and Tube- side Cooling Water flow.

APPENDIX B

CUV VALUES IN PLASTIC AND METALLIC HEAT EXCHANGERS FOR AQUEOUS-AQUEOUS APPLICATIONS

Tables B.1 to B.2 show values of experimentally-determined CUV values in plastic heat exchangers and previously reported CUV values for plastic and conventional metallic shell-and-tube heat exchangers.

Table B.1 Comparison of CUV in PHFHEs with Conventional Metallic and Plastic Heat Exchangers for Aqueous-Aqueous Applications

Heat Exchanger	U_C (W/m^2-K)	CUV_C (W/m^3-K)	U_D (W/m^2-K)	CUV_D (W/m^3-K)
Shell and Tube*	2839-5678	$3.0x10^5$-$6.0x10^5$	482-776	$1.2x10^5$-$1.5x10^5$
HEPP1	333-1430	$2.4x10^5$-$1.0x10^6$		
HEPP2	374-1534	$7.1x10^5$-$2.9x10^6$		
HEPP3	236-1330	$4.3x10^5$-$2.4x10^6$		
HEPEEK2	404-1454	$2.8x10^5$-$1.0x10^6$		
PHFHE**	647-1314	$9.0x10^5$-$1.8x10^6$		
PEEK Plate Heat Exchanger***	900	$1.0x10^6$		

* The U_c data corresponds to shell-and-tube metallic heat exchanger with a ¾ in tubes in a 1 inch triangular pitch and a 30° layout. The U_c data were referenced from Perry's Chemical Engineering Handbook and α was taken from [Zarkadas and Sirkar, 2004].

** PHFHE data were taken from Zarkadas and Sirkar, 2004.

*** U_c values were predicted based on the experimentally determined heat transfer coefficient for one side of the heat exchanger and the premise that both sides have virtually the same heat transfer coefficient. The experimentally determined heat transfer coefficient is referenced from Jachuck and Ramshaw, 1994.

U_D values for metallic shell-and-tube heat exchangers were referenced from Zarkadas and Sirkar, 2004.

U_C values for hot brine (4 wt %NaCl)-water system with HEPP1, HEPP2, HEPP3 and HEPEEK2 modules are calculated based on the outside fiber area.

Table B.2 Experimentally-Derived CUV_C for Polymeric Hollow Fiber Heat Exchangers (Aqueous-Aqueous Applications)

Test Run Configuration	CUV_C (W/m^3 –K)			
	HEPP1	**HEPP2**	**HEPP3**	**HEPEEK2**
Crossflow at Shell -Hot Brine (Shell side),Cooling water (Tube side)	$2.61x10^5$-$9.71x10^5$	$7.10x10^5$-$1.74x10^6$	$4.29x10^5$-$1.38x10^6$	$7.56x10^5$-$9.03x10^5$
Crossflow at Shell-Hot Brine (Tube side),Cooling water(Shell side)	$5.85x10^5$-$7.79x10^5$	$9.39x10^5$-$2.14x10^6$	$8.44x10^5$-$1.83x10^6$	$2.88x10^5$-$7.35x10^5$
Parallel Flow at Shell-Hot Brine (Shell side),Cooling water(Tube side)	$2.39x10^5$-$1.03x10^6$	$1.02x10^6$-$2.85x10^6$	$1.57x10^6$-$2.29x10^6$	$2.88x10^5$-$1.04x10^6$
Parallel Flow at Shell-Hot Brine (Tube side),Cooling water(Shell side)		$1.28x10^6$-$2.92x10^6$	$1.07x10^6$-$2.42x10^6$	$5.06x10^5$-$1.03x10^6$

APPENDIX C

SAMPLE HEAT TRANSFER DATA FOR HOT BRINE/ WATER SYSTEM

Tables C.1 to C.8 show sample heat transfer data obtained for HEPP1, HEPP2, HEPP3 and HEPEEK2 modules with hot brine/cold water system and Table C.9 shows the heat exchange performance indicator ranges for each test module.

Table C.1 Sample Heat Transfer Data for HEPP1(Hot Brine on Shell side-Crossflow)

Exp	T_{t1} (^{0}C)	T_{t2} (^{0}C)	T_{s1} (^{0}C)	T_{s2} (^{0}C)	F_t (ml/min)	T_{t2}-T_{t1} (^{0}C)	F_s (ml/min)	T_{s1}-T_{s2} (^{0}C)	Q (W)	U (W/m^2-K)	Effect. Factor	F	NTU	HTU (cm)
HEPP1: Fix Hot Brine flow (Shell side), Vary Cooling water flow (Tube side)														
Exp. No. 1	28.5	86.4	90.0	88.8	47.0	57.9	3783.0	1.2	245	491	0.938	0.984	2.923	6.3
Exp. No. 2	41.0	63.4	90.8	86.2	793.0	22.4	3822.0	4.6	1200	1807	0.244	0.987	0.638	29.0
Exp. No. 3	40.9	61.4	90.8	86.0	876.0	20.5	4000.0	4.8	1262	1770	0.232	0.988	0.565	32.7
Exp. No. 4	45.0	59.8	90.1	85.5	1200.0	14.8	4000.0	4.6	1228	1828	0.166	0.987	0.426	43.4
Exp. No. 5	45.7	62.2	90.3	85.9	1008.0	16.5	4000.0	4.4	1162	1783	0.187	0.987	0.495	37.4
HEPP1: Vary Hot Brine flow (shell side), Fix Cooling water flow (Tube side)														
Exp. No. 1	30.1	40.3	89.0	52.2	474.0	10.2	137.0	36.8	339	510	0.618	1.000	1.074	17.2
Exp. No. 2	30.2	46.1	90.0	65.6	488.0	15.9	322.0	24.4	534	710	0.410	0.989	0.629	29.4
Exp. No. 3	30.2	50.9	90.1	73.0	483.0	20.7	606.0	17.1	695	873	0.347	0.998	0.509	36.4
Exp. No. 4	30.3	53.3	90.5	76.0	483.0	23.0	810.0	14.5	780	954	0.388	1.000	0.561	33.0
Exp. No. 5	30.4	56.7	89.8	78.6	489.0	26.3	1183.0	11.2	890	1151	0.443	0.993	0.660	28.0

Table C.2 Sample Heat Transfer Data for HEPEEK2 (Hot Brine on Shell Side –Crossflow)

Exp	T_{t1} (^{0}C)	T_{t2} (^{0}C)	T_{s1} (^{0}C)	T_{s2} (^{0}C)	F_t (ml/min)	T_{t2}-T_{t1} (^{0}C)	F_s (ml/min)	T_{s1}-T_{s2} (^{0}C)	Q (W)	U (W/m^2-K)	Effect. Factor	F	NTU	HTU (cm)
HEPEEK2: Fix Hot Brine flow (Shell side) , Vary Cooling water flow (Tube side)														
Exp. No. 1	21.2	61.6	98.4	95.6	500.0	40.4	6135.0	2.8	1270	1515	0.476	0.902	0.762	24.3
Exp. No. 2	20.6	54.0	98.3	95.3	664.7	33.4	6192.0	3.0	1387	1538	0.388	0.897	0.577	32.1
Exp. No. 3	20.0	49.0	98.8	95.4	808.2	29.0	6135.0	3.4	1507	1488	0.341	0.923	0.472	39.2
Exp. No. 4	19.7	44.9	98.8	95.1	1049.0	25.2	6135.0	3.7	1673	1643	0.290	0.908	0.395	46.9
Exp. No. 5	19.4	40.6	98.7	94.8	1256.8	21.2	6160.2	3.9	1725	1562	0.249	0.929	0.320	57.8
Exp. No. 6	19.1	39.9	98.6	94.7	1300.4	20.8	6153.8	3.9	1738	1587	0.242	0.923	0.312	59.3
Exp. No. 7	18.0	36.2	98.6	94.4	1561.7	18.2	6085.2	4.2	1839	1600	0.210	0.929	0.264	70.2
Exp. No. 8	17.3	34.4	98.3	94.1	1651.1	17.1	6135.0	4.2	1840	1556	0.198	0.935	0.244	75.8
HEPEEK2:Vary Hot Brine (Shell Side with Crossflow), Fix Cooling water (Tube side)														
Exp. No. 1	16.7	30.2	94.4	88.3	1773.6	13.5	2595.2	6.1	1363	1562	0.142	0.817	0.199	92.9
Exp. No. 2	15.7	30.7	96.1	89.6	1758.5	15.0	3359.5	6.5	1647	1529	0.167	0.896	0.216	85.7
Exp. No. 3	15.3	30.8	97.0	90.2	1687.3	15.5	3638.6	6.8	1736	1408	0.181	0.953	0.220	84.1
Exp. No. 4	15.4	31.4	97.1	90.9	1655.6	16.0	4032.3	6.2	1756	1428	0.186	0.952	0.227	81.4
Exp. No. 5	15.3	32.0	97.1	91.4	1659.3	16.7	4447.7	5.7	1810	1517	0.192	0.938	0.237	78.0
Exp. No. 6	15.5	32.4	97.1	91.5	1673.2	16.9	4559.3	5.6	1836	1563	0.193	0.932	0.241	76.8
Exp. No. 7	15.5	32.8	97.2	92.0	1627.8	17.3	5067.6	5.2	1859	1529	0.201	0.947	0.246	75.1
Exp. No. 8	15.5	33.7	97.0	92.4	1622.5	18.2	5484.5	4.6	1869	1682	0.203	0.908	0.261	71.0
Exp. No. 9	15.5	33.9	97.2	92.7	1608.6	18.4	6066.7	4.5	1940	1625	0.212	0.941	0.263	70.3
Exp. No. 10	15.5	34.0	98.7	95.2	1613.3	18.5	6166.5	3.5	1943	1605	0.208	0.934	0.257	71.9

Table C.3 Sample Heat Transfer Data for HEPP3 (Cooling Water on Shell side-Crossflow)

Exp	T_{t1} (^{0}C)	T_{t2} (^{0}C)	T_{s1} (^{0}C)	T_{s2} (^{0}C)	F_t (ml/min)	T_{t2}-T_{t1} (^{0}C)	F_s (ml/min)	T_{s1}-T_{s2} (^{0}C)	Q (W)	U (W/m^2-K)	Effect. Factor	F	NTU	HTU (cm)
HEPP3: Fix Hot Brine flow (Tube side), Vary Cooling water flow (Shell side)														
Exp. No. 1	97.9	88.2	17.3	35.1	2816.9	9.7	965.9	17.8	1510	627	0.279	0.793	0.424	50.7
Exp. No. 2	97.5	81.3	11.8	26.4	2759.9	16.2	2759.9	14.6	2921	825	0.182	0.938	0.237	90.9
Exp. No. 3	97.5	78.9	10.1	23.6	2792.0	18.6	3386.0	13.5	3335	961	0.204	0.922	0.271	79.3
Exp. No. 4	97.7	76.7	8.9	21.0	2765.0	21.0	4279.6	12.1	3754	1054	0.228	0.928	0.302	71.2
Exp. No. 5	97.3	75.1	8.4	19.9	2775.2	22.2	4815.4	11.5	4001	1117	0.241	0.932	0.320	67.1
Exp. No. 6	97.4	73.7	7.9	18.3	2763.7	23.7	5581.4	10.4	4226	1190	0.254	0.926	0.340	63.2
Exp. No. 7	97.8	72.4	7.5	17.2	2737.2	25.4	6578.9	9.7	4564	1238	0.275	0.942	0.363	59.2
Exp. No. 8	96.8	70.3	7.4	15.8	2742.2	26.5	7802.3	8.4	4733	1321	0.287	0.935	0.383	56.1
Exp. No. 9	97.2	69.8	7.3	15.1	2724.8	27.4	8498.6	7.8	4826	1361	0.293	0.928	0.395	54.5
Exp. No. 10	97.6	70.8	11.9	18.9	2697.8	26.8	9508.7	7.0	4753	1363	0.306	0.944	0.406	52.9
HEPP3: Vary Hot Brine flow (Tube side), Fix Cooling water flow (Shell side)														
Exp. No. 1	97.2	72.3	8.9	18.3	2707.5	24.9	6688.0	9.4	4460	1218	0.277	0.950	0.364	59.1
Exp. No. 2	96.6	69.9	8.4	17.6	2442.9	26.7	6514.6	9.2	4287	1203	0.295	0.943	0.395	54.4
Exp. No. 3	97.2	66.0	7.8	16.7	2067.5	31.2	6688.9	8.9	4252	1206	0.341	0.946	0.469	45.8
Exp. No. 4	96.9	60.8	7.7	16.2	1689.1	36.1	6564.6	8.5	4007	1192	0.394	0.943	0.564	38.1
Exp. No. 5	96.4	55.7	7.7	15.8	1409.8	40.7	6696.0	8.1	3835	1156	0.453	0.959	0.666	32.3
Exp. No. 6	95.5	47.8	7.6	15.0	1074.0	47.7	6557.3	7.4	3434	1116	0.535	0.962	0.843	25.5
Exp. No. 7	94.3	36.0	7.7	13.8	692.2	58.3	6607.9	6.1	2784	992	0.680	0.990	1.192	18.0

Table C.4 Sample Heat Transfer Data for HEPP2 (Cooling Water on Shell side-Crossflow)

Exp	T_{t1} (^{0}C)	T_{t2} (^{0}C)	T_{s1} (^{0}C)	T_{s2} (^{0}C)	F_t (ml/min)	T_{t2}-T_{t1} (^{0}C)	F_s (ml/min)	T_{s1}-T_{s2} (^{0}C)	Q (W)	U (W/m^2-K)	Effect. Factor	F	NTU	HTU (cm)
HEPP2: Fix Hot Brine(Tube side),Vary Cooling water (Shell side)														
Exp. No. 1	97.8	94.1	23.3	84.1	6543.1	3.7	270.3	60.8	1371	806	0.764	0.627	2.611	6.9
Exp. No. 2	98.5	95.3	23.8	85.9	6465.5	3.2	258.6	62.1	1240	669	0.718	0.661	2.391	7.5
Exp. No. 3	98.9	90.8	19.0	66.3	6493.5	8.1	956.9	47.3	3317	1048	0.509	0.734	1.116	16.1
Exp. No. 4	96.9	85.7	10.4	43.6	6383.0	11.2	1904.8	33.2	4589	990	0.358	0.823	0.590	30.5
Exp. No. 5	94.2	81.1	9.1	35.2	6351.9	13.1	2921.1	26.1	5446	1089	0.284	0.849	0.436	41.2
Exp. No. 6	92.7	79.0	8.7	32.1	6322.4	13.7	3359.4	23.4	5648	1134	0.260	0.849	0.395	45.6
Exp. No. 7	93.2	78.0	8.1	27.9	6369.4	15.2	4480.9	19.8	6345	1210	0.218	0.859	0.320	56.3
Exp. No. 8	91.7	75.3	7.8	25.3	6309.2	16.4	5431.8	17.5	6797	1300	0.196	0.863	0.284	63.3
Exp. No. 9	94.5	76.7	7.4	24.1	6268.3	17.8	5917.2	16.7	7195	1359	0.185	0.853	0.270	66.7
Exp. No. 10	91.2	72.9	6.9	21.4	6237.0	18.3	6952.5	14.5	7363	1425	0.192	0.856	0.279	64.6
Exp. No. 11	94.7	74.7	6.2	20.8	6243.5	20.0	7594.9	14.6	8067	1469	0.203	0.867	0.291	61.8
Exp. No. 12	92.1	72.7	5.8	19.7	6217.6	19.4	8053.7	13.9	7969	1415	0.207	0.889	0.288	62.5
HEPP2: Fix Cooling water (Shell side),Vary Hot Brine (Tube side)														
Exp. No. 1	94.4	32.1	5.6	12.6	987.7	62.3	8356.5	7.0	4144	941	0.691	0.967	1.295	13.9
Exp. No. 2	98.1	69.2	6.1	19.3	4101.2	28.9	8333.3	13.2	7827	1284	0.308	0.948	0.423	42.5
Exp. No. 3	97.9	70.4	6.2	19.4	4461.0	27.5	8498.6	13.2	8041	1331	0.292	0.941	0.400	45.0
Exp. No. 4	96.1	71.4	6.2	19.4	4995.8	24.7	8670.5	13.2	8145	1335	0.269	0.948	0.361	49.8
Exp. No. 5	93.4	71.2	6.4	19.5	5524.9	22.2	8645.5	13.1	8084	1359	0.250	0.946	0.331	54.3
Exp. No. 6	97.9	75.8	6.3	20.3	6044.0	22.1	8596.0	14.0	8681	1414	0.234	0.933	0.312	57.7
Exp. No. 7	97.0	75.6	6.4	20.5	6160.2	21.4	8415.1	14.1	8548	1412	0.229	0.931	0.306	58.8
Exp. No. 8	97.2	76.1	6.5	20.6	6289.3	21.1	8356.5	14.1	8565	1423	0.224	0.926	0.300	60.1

Table C.5 Sample Heat Transfer Data for HEPP3 and HEPEEK2 (Cooling Water on Tube side-Parallel Flow)

Exp	T_{t1} (^{0}C)	T_{t2} (^{0}C)	T_{s1} (^{0}C)	T_{s2} (^{0}C)	F_t (ml/min)	T_{t2}-T_{t1} (^{0}C)	F_s (ml/min)	T_{s1}-T_{s2} (^{0}C)	Q (W)	U (W/m^2-K)	Effect. Factor	NTU	HTU (cm)
HEPP3: Fix Hot Brine flow (Shell side), Vary Cooling water flow (Tube side)													
Exp. No. 1	9.3	40.3	97.1	84.8	2955.6	31.0	8064.5	12.3	6506	1695	0.360	0.472	45.5
Exp. No. 2	9.4	43.0	97.4	85.4	2697.8	33.6	7832.9	12.0	6295	1706	0.381	0.521	41.3
Exp. No. 3	10.3	48.4	96.0	84.9	2130.7	38.1	7926.0	11.1	5765	1642	0.454	0.636	33.8
Exp. No. 4	12.0	69.2	97.4	89.0	1095.3	57.2	7884.4	8.4	4378	1568	0.676	1.185	18.1
Exp. No. 5	14.7	90.4	97.0	92.8	416.6	75.7	8119.1	4.2	2221	1325	0.942	2.650	8.1
Exp. No. 6	13.4	62.9	97.5	88.4	1338.1	49.5	7936.5	9.1	4705	1542	0.604	0.953	22.6
Exp. No. 7	11.9	53.9	97.1	86.8	1871.5	42.0	8219.2	10.3	5557	1659	0.502	0.732	29.4
HEPP3: Vary Hot Brine flow (Shell side), Fix Cooling water flow (Tube side)													
Exp. No. 1	9.9	36.6	98.3	76.0	3048.8	26.7	4054.1	22.3	5867	1549	0.313	0.418	51.4
Exp. No. 2	8.7	37.7	97.9	79.8	2986.5	29.0	5258.5	18.1	6204	1608	0.334	0.443	48.5
Exp. No. 3	8.8	39.3	97.8	81.7	2963.0	30.5	5893.9	16.1	6273	1679	0.347	0.474	45.4
Exp. No. 4	8.7	39.6	98.2	83.4	2901.4	30.9	6865.0	14.8	6519	1643	0.361	0.466	46.1
Exp. No. 5	8.6	39.0	96.6	83.1	3021.1	30.4	7380.1	13.5	6532	1700	0.353	0.463	46.4
Exp. No. 6	8.8	40.1	97.0	84.5	2952.7	31.3	7915.6	12.5	6526	1706	0.360	0.476	45.2
Exp. No. 7	8.9	35.1	96.6	70.8	2963.0	26.2	3141.4	25.8	5431	1530	0.300	0.425	50.6
Exp. No. 8	9.0	35.8	96.4	73.0	2911.2	26.8	3510.8	23.4	5479	1523	0.309	0.430	49.9
Exp. No. 9	9.0	37.5	97.9	75.5	2906.9	28.5	3819.2	22.4	5756	1589	0.320	0.450	47.8
Exp. No. 10	9.1	27.1	92.7	51.2	2822.0	18.0	1314.1	41.5	3623	1166	0.485	0.748	28.7
Exp. No. 11	9.1	33.1	96.5	65.3	2926.8	24.0	2415.5	31.2	4989	1430	0.350	0.503	42.8
HEPEEK2: Fix Hot Brine flow (Shell side), Vary Cooling water flow (Tube side)													
Exp. No. 1	20.5	71.7	96.1	94.8	412.2	51.2	12207.5	1.3	1257	1703	0.584	1.153	16.0
Exp. No. 2	19.8	52.0	96.7	94.7	837.3	32.2	12096.8	2.0	1740	1666	0.390	0.553	33.5
Exp. No. 3	18.3	45.7	96.7	94.4	1114.8	27.4	12220.0	2.3	1997	1761	0.329	0.438	42.2
Exp. No. 4	16.6	29.4	97.9	95.3	1500.0	12.8	12282.5	2.6	1731	945	0.204	0.174	106.1
Exp. No. 5	15.9	36.4	98.7	95.5	1728.1	20.5	10791.4	3.2	2381	1814	0.239	0.291	63.6
Exp. No. 6	15.6	33.1	98.7	95.2	2207.5	17.5	10353.8	3.5	2550	1930	0.200	0.242	76.4
HEPEEK2: Vary Hot Brine flow (Shell side),Fix Cooling water flow (Tube side)													
Exp. No. 1	16.2	36.2	98.7	95.2	1734.1	20.0	10256.1	3.5	2400.4	1780	0.241	0.284	65.1
Exp. No. 2	16.4	36.4	98.5	95.0	1719.2	20.0	8559.2	3.5	2192.6	1775	0.223	0.286	64.7
Exp. No. 3	16.2	33.7	92.7	88.1	1641.6	17.5	2955.7	4.6	1454.5	1592	0.166	0.269	68.9

Table C.6 Sample Heat Transfer Data for HEPP1 and HEPP2 (Cooling Water on Tube side-Parallel Flow)

Exp	T_{t1} (^{0}C)	T_{t2} (^{0}C)	T_{s1} (^{0}C)	T_{s2} (^{0}C)	F_t (ml/min)	T_{t2}-T_{t1} (^{0}C)	F_s (ml/min)	T_{s1}-T_{s2} (^{o}C)	Q (W)	U (W/m^2-K)	Effect. Factor	NTU	HTU (cm)
HEPP1: Vary Hot Brine flow (Shell side), Fix Cooling water flow (Tube side)													
Exp. No. 1	30.2	39.2	89.5	56.2	474.0	9.0	129.0	33.3	294	450	0.566	1.002	18.5
Exp. No. 2	30.2	44.1	90.0	65.9	480.0	13.9	268.0	24.1	450	633	0.415	0.681	27.2
Exp. No. 3	30.3	50.9	90.0	73.4	478.0	20.6	600.0	16.6	676	923	0.343	0.544	34.0
Exp. No. 4	30.3	56.2	90.7	79.4	480.0	25.9	1167.0	11.3	873	1142	0.436	0.672	27.5
Exp. No. 5	30.9	60.6	90.0	81.4	474.0	29.7	1687.0	8.6	973	1371	0.503	0.817	22.6
Exp. No. 6	32.7	63.7	89.7	83.0	475.0	31.0	2308.0	6.7	1027	1511	0.550	0.900	20.6
Exp. No. 7	34.5	66.8	89.4	84.1	479.0	32.3	3680.0	5.3	1187	1698	0.656	1.004	18.4
Exp. No. 8	36.2	69.7	90.4	86.3	491.0	33.5	4110.0	4.1	1130	1849	0.618	1.068	17.3
Exp. No. 9	37.3	71.7	90.5	87.0	462.0	34.4	4636.0	3.5	1090	1867	0.645	1.147	16.1
Exp. No. 10	38.1	72.4	90.1	87.3	469.0	34.3	6048.0	2.8	1120	1936	0.669	1.172	15.8
HEPP2: Vary Cooling water flow (Tube side), Fix Hot Brine flow (Shell side)													
Exp. No. 1	25.1	97.2	98.9	97.2	259.7	72.1	9569.4	1.7	1181	723	0.901	3.907	4.6
Exp. No. 2	16.1	66.1	94.5	84.4	2343.8	50.0	12195.1	10.1	8178	1870	0.643	1.107	16.3
Exp. No. 3	9.3	52.6	96.6	83.4	3575.7	43.3	11893.0	13.2	10632	1946	0.490	0.752	23.9
Exp. No. 4	8.5	49.8	97.0	82.9	3804.7	41.3	12371.1	14.1	11299	1908	0.483	0.693	26.0
Exp. No. 5	8.4	46.1	95.5	81.2	4276.5	37.7	12195.1	14.3	11452	1939	0.442	0.626	28.8
Exp. No. 6	8.2	40.7	95.3	80.0	5347.5	32.5	12145.7	15.3	12281	2008	0.379	0.518	34.8
Exp. No. 7	8.0	37.4	93.9	78.2	5958.3	29.4	12072.4	15.7	12465	2015	0.350	0.466	38.6
Exp. No. 8	7.6	33.2	93.7	77.5	6880.7	25.6	12145.7	16.2	12747	1964	0.309	0.393	45.8
Exp. No. 9	7.5	31.2	94.7	77.9	7712.0	23.7	12345.7	16.8	13333	1983	0.284	0.354	50.8
Exp. No. 10	7.2	27.5	90.9	74.4	8368.2	20.3	12295.1	16.5	12755	1888	0.261	0.311	57.9
Exp. No. 11	11.4	90.4	97.2	91.1	947.2	79.0	12145.7	6.1	5046	1833	0.902	2.699	6.7
Exp. No. 12	10.4	70.5	97.1	86.5	2042.9	60.1	12145.7	10.6	8551	1892	0.698	1.285	14.0
HEPP2: Fix Cooling water flow (Tube side), Vary Hot Brine flow (Shell side)													
Exp. No. 1	8.5	30.6	96.4	68.8	6048.0	22.1	4942.0	27.6	9252	1539	0.316	0.444	40.6
Exp. No. 2	7.9	31.9	97.0	70.6	6048.4	24.0	5676.4	26.4	10100	1649	0.297	0.414	43.4
Exp. No. 3	7.8	32.9	96.9	72.0	6243.5	25.1	6335.8	24.9	10765	1774	0.284	0.400	45.0
Exp. No. 4	7.9	34.5	97.2	73.9	6054.5	26.6	6976.7	23.3	11071	1817	0.294	0.413	43.5
Exp. No. 5	8.0	36.2	96.2	75.1	5917.0	28.2	8042.8	21.1	11512	1907	0.317	0.444	40.5
Exp. No. 6	7.9	35.1	96.4	76.1	6109.9	27.2	8720.9	20.3	11733	1864	0.312	0.421	42.8
Exp. No. 7	7.7	36.4	96.1	78.3	6342.4	28.7	10600.7	17.8	12670	2032	0.324	0.442	40.8

Table C.7 Sample Heat Transfer Data for HEPP2 (Cooling Water on Shell side-Parallel Flow)

Exp	T_{t1} (^{0}C)	T_{t2} (^{0}C)	T_{s1} (^{0}C)	T_{s2} (^{0}C)	F_t (ml/min)	T_{t2}-T_{t1} (^{0}C)	F_s (ml/min)	T_{s1}-T_{s2} (^{0}C)	Q (W)	U (W/m^2-K)	Effect. Factor	NTU	HTU (cm)
HEPP2: Fix Hot Brine flow (Tube side),Vary Cooling water flow (Shell side)													
Exp. No. 1	96.7	86.0	12.3	57.7	6396.5	10.7	1313.9	45.4	4357	911	0.566	0.960	18.8
Exp. No. 2	98.0	79.1	10.2	38.4	6465.5	18.9	3853.5	28.2	7877	1383	0.334	0.495	36.4
Exp. No. 3	97.2	75.5	9.0	32.0	6342.5	21.7	5381.2	23.0	8933	1517	0.270	0.388	46.3
Exp. No. 4	97.6	74.2	8.4	29.7	6362.6	23.4	6430.8	21.3	9774	1616	0.256	0.363	49.6
Exp. No. 5	97.8	72.8	7.6	27.7	6369.4	25.0	7462.7	20.1	10580	1709	0.274	0.383	47.0
Exp. No. 6	97.2	70.8	6.9	25.0	6355.9	26.4	8670.5	18.1	11118	1792	0.288	0.402	44.8
Exp. No. 7	97.8	69.8	6.6	23.7	6396.6	28.0	9677.4	17.1	11798	1897	0.301	0.423	42.5
Exp. No. 8	97.0	67.8	6.5	22.4	6289.3	29.2	10344.8	15.9	11924	1968	0.311	0.446	40.4
Exp. No. 9	97.4	66.5	6.3	21.3	6211.2	30.9	11834.3	15.0	12660	2053	0.332	0.471	38.2
Exp. No. 10	93.0	63.2	6.5	20.5	6172.8	29.8	12282.5	14.0	12217	2077	0.338	0.478	37.7
HEPP2: Vary Hot Brine flow (Tube side),Fix Cooling water flow (Shell side)													
Exp. No. 1	98.1	69.4	6.8	23.4	6289.3	28.7	10238.9	16.6	12002	1913	0.311	0.434	41.5
Exp. No. 2	94.8	64.7	6.9	22.7	5484.5	30.1	10033.4	15.8	11102	1852	0.341	0.480	37.5
Exp. No. 3	97.3	60.7	7.0	22.4	4313.4	36.6	10050.3	15.4	10731	1798	0.408	0.592	30.4
Exp. No. 4	97.8	55.6	7.0	21.3	3546.0	42.2	10101.0	14.3	10102	1766	0.464	0.706	25.5
Exp. No. 5	98.1	46.8	7.0	19.8	2624.7	51.3	10000.0	12.8	9036	1717	0.557	0.925	19.5
Exp. No. 6	96.9	33.2	7.0	17.0	1612.9	63.7	10453.0	10.0	7117	1548	0.719	1.350	13.3

Table C.8 Sample Heat Transfer Data for HEPP3 and HEPEEK2(Cooling Water on Shell side-Parallel Flow)

Exp	T_{t1} (^{0}C)	T_{t2} (^{0}C)	T_{s1} (^{0}C)	T_{s2} (^{0}C)	F_t (ml/min)	T_{t2}-T_{t1} (^{0}C)	F_s (ml/min)	T_{s1}-T_{s2} (^{0}C)	Q (W)	U (W/m^2-K)	Effect. Factor	NTU	HTU (cm)
HEPP3: Fix Hot Brine flow (Tube side),Vary Cooling water flow (Shell side)													
Exp. No. 1	97.0	62.0	11.4	19.4	2605.3	35.0	8196.7	8.0	5366	1753	0.356	0.571	37.7
Exp. No. 2	97.5	61.2	10.3	17.8	2582.9	36.3	8310.2	7.5	5340	1772	0.351	0.582	36.9
Exp. No. 3	97.6	60.7	9.9	17.2	2590.7	36.9	9118.5	7.3	5551	1800	0.362	0.589	36.5
Exp. No. 4	96.2	59.5	9.5	16.1	2558.6	36.7	8862.6	6.6	5216	1784	0.348	0.591	36.4
Exp. No. 5	97.3	59.8	9.4	16.0	2531.6	37.5	9448.8	6.6	5384	1783	0.358	0.597	36.0
Exp. No. 6	97.2	59.5	9.3	15.3	2506.3	37.7	10186.7	6.0	5326	1771	0.358	0.599	35.9
Exp. No. 7	97.0	62.1	10.1	20.7	2584.0	34.9	7653.0	10.6	5874	1727	0.390	0.567	37.9
Exp. No. 8	97.2	63.6	11.3	22.7	2570.7	33.6	7067.1	11.4	5723	1671	0.376	0.552	39.0
Exp. No. 9	96.8	65.1	11.7	25.0	2584.0	31.7	5923.0	13.3	5508	1600	0.359	0.526	40.9
Exp. No. 10	95.6	67.7	12.5	28.5	2611.0	27.9	4291.9	16.0	4848	1450	0.323	0.472	45.5
Exp. No. 11	97.1	76.5	14.8	39.3	2702.7	20.6	2060.4	24.5	3624	1131	0.241	0.452	47.5
Exp. No. 12	97.9	85.8	16.1	62.7	2727.3	12.1	565.3	46.6	2015	793	0.135	1.161	18.5
Exp. No. 13	96.9	66.9	8.9	23.7	2672.6	30.0	5159.0	14.8	5365	1490	0.354	0.474	45.4
Exp. No. 14	96.3	63.3	7.9	20.1	2618.9	33.0	6637.0	12.2	5743	1608	0.385	0.521	41.3
HEPP3: Vary Hot Brine flow (Tube side),Fix Cooling water flow (Shell side)													
Exp. No. 1	97.0	62.1	10.1	20.7	2584.0	34.9	7653.0	10.6	5874	1727	0.387	0.567	37.9
Exp. No. 2	96.6	59.6	11.0	21.1	2284.8	37.0	7751.9	10.1	5588	1680	0.423	0.623	34.5
Exp. No. 3	96.5	54.2	10.4	19.9	1883.2	42.3	7672.6	9.5	5241	1648	0.477	0.740	29.1
Exp. No. 4	96.2	46.7	8.9	18.0	1475.6	49.5	7672.6	9.1	4917	1595	0.562	0.912	23.6
Exp. No. 5	95.3	38.1	9.2	17.1	1068.7	57.2	7566.0	7.9	4169	1498	0.665	1.178	18.2
Exp. No. 6	93.6	27.6	10.9	16.6	665.5	66.0	7556.6	5.7	3006	1351	0.798	1.700	12.7
Exp. No. 7	91.9	20.9	11.1	25.3	461.5	71.0	7556.7	14.2	2232	1342	0.872	2.427	8.9
Exp. No. 8	89.9	16.5	10.4	13.2	272.7	73.4	7633.5	2.8	1434	871	0.962	2.662	8.1
HEPEEK2: Fix Hot Brine flow (Tube side),Vary Cooling water flow (Shell side)													
Exp. No. 1	92.0	60.2	14.2	16.9	960.2	31.8	12658.2	2.7	2226	1859	0.440	0.551	33.6
Exp. No. 2	92.2	60.7	14.2	17.2	947.0	31.5	11019.3	3.0	2162	1809	0.432	0.544	34.0
Exp. No. 3	92.0	61.2	14.3	17.7	950.9	30.8	9756.1	3.4	2148	1778	0.429	0.532	34.8
Exp. No. 4	92.3	62.0	14.4	18.3	939.6	30.3	7518.8	3.9	1986	1720	0.401	0.521	35.5
Exp. No. 5	92.5	63.5	14.6	19.7	940.7	29.0	5509.6	5.1	1902	1642	0.384	0.498	37.2
Exp. No. 6	92.6	68.4	15.1	24.2	953.3	24.2	2625.0	9.1	1611	1378	0.323	0.413	44.8
Exp. No. 7	92.6	74.8	15.8	33.4	957.9	17.8	1034.0	17.6	1207	1043	0.244	0.312	59.3

Table C.9 Range of Heat Exchange Performance Indicators in Test Modules for Hot Brine/Cold Water System

Module	U(W/m^2-K)	ε	NTU	HTU(cm)	CUV(W/m^3-K)
HEPP1	450-1936	0.166-0.938	0.354-3.118	6.0-43.4	2.4 x10^5-1x10^6
HEPP2	505-2076	0.185-0.902	0.270-3.907	4.6-66.7	7.1x10^5-2.9x10^6
HEPP3	319-1799	0.135-0.962	0.237-2.668	8.0-91.0	4.3x10^5-2.4x10^6
HEPEEK2	535-1929	0.141-0.584	0.174-2.662	14-106	2.8x10^5-1x10^6

APPENDIX D

HEAT EXCHANGE PERFORMANCE INDICATOR VARIATIONS WITH REYNOLDS NUMBER

Figures D.1 to D.9 show the overall thermal effectiveness factor, NTU and HTU plotted against tube-side and shell-side Reynolds Numbers.

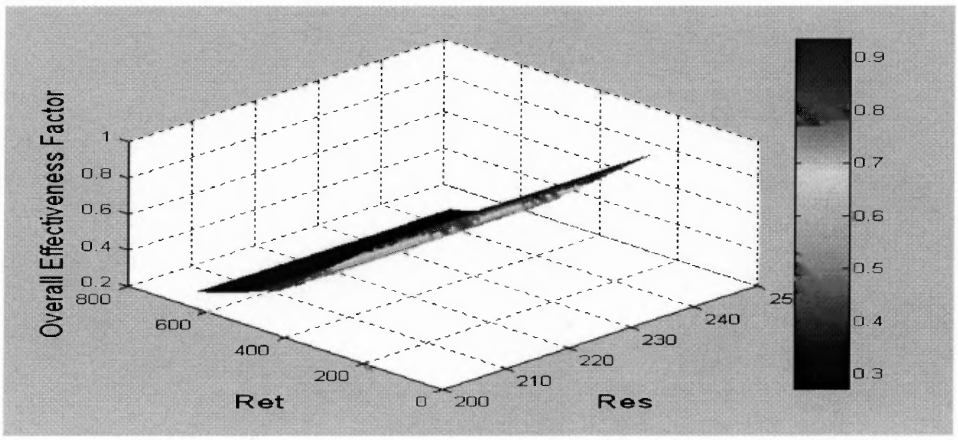

Figure D.1 Overall Effectiveness Factor ε in HEPP2 (Shell side is of Crossflow Configuration) as a Function of Tube and Shell-side Reynolds Numbers.

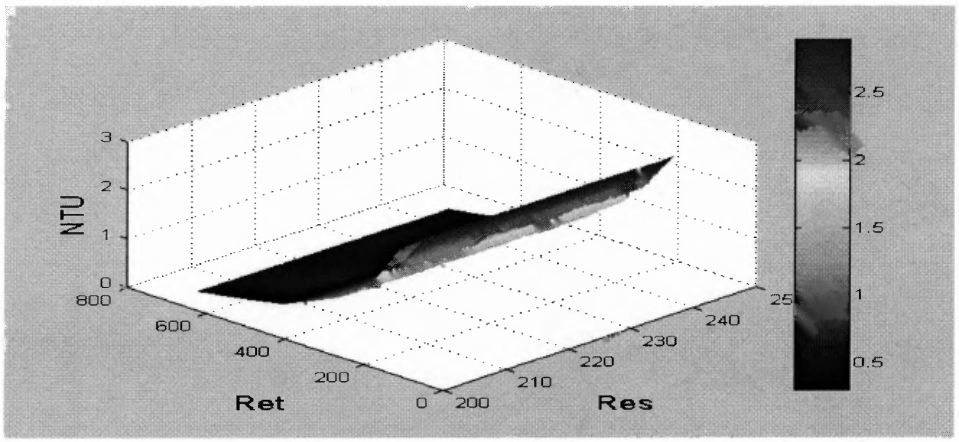

Figure D.2 Experimentally- Derived NTU in HEPP2 (Shell side is of Crossflow Configuration) as a Function of Tube and Shell-side Reynolds Numbers.

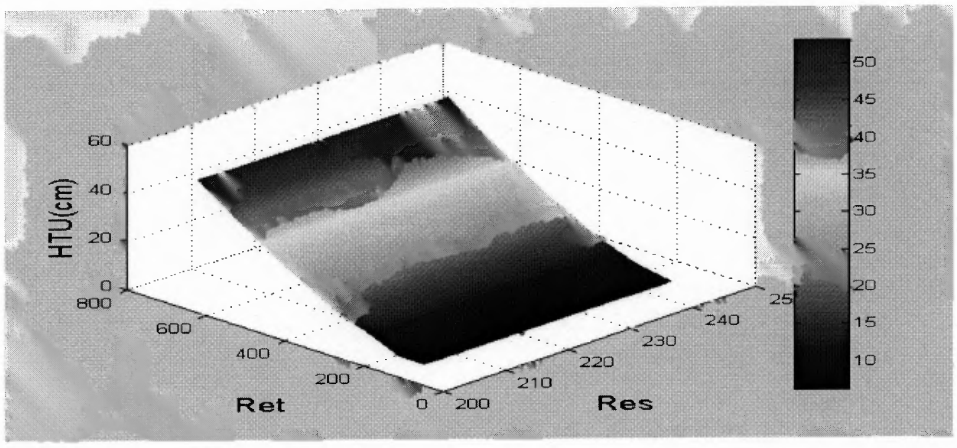

Figure D.3 Experimentally-Derived HTU in HEPP2 (Shell side is of Crossflow Configuration) as a Function of Tube and Shell-side Reynolds Numbers.

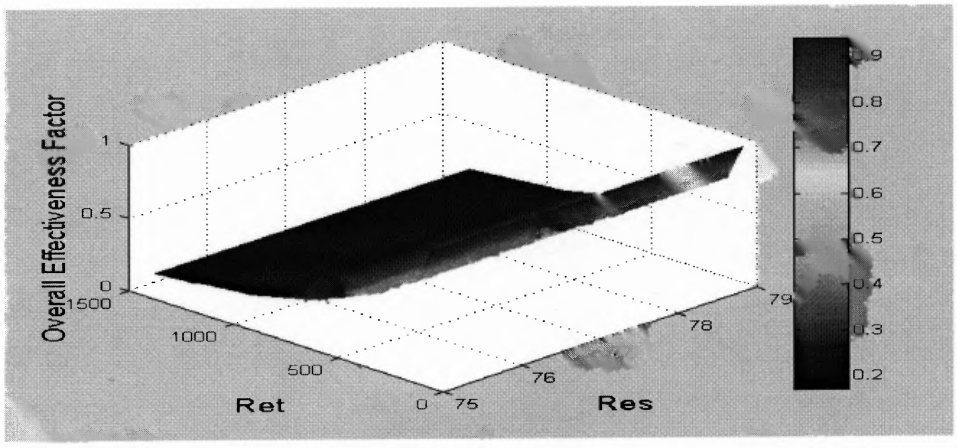

Figure D.4 Overall Effectiveness Factor ε in HEPP1 (Shell side is of Crossflow Configuration) as a Function of Tube and Shell-side Reynolds Numbers.

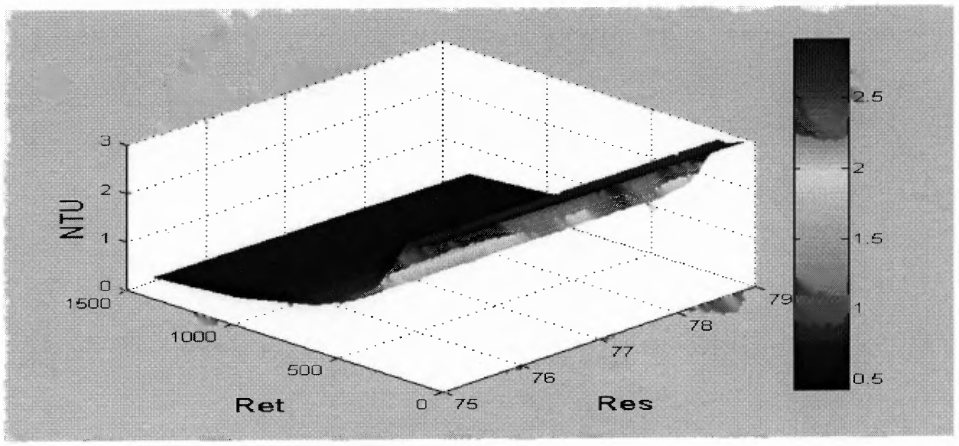

Figure D.5 Experimentally-derived NTU in HEPP1 (Shell side is of Crossflow Configuration) as a Function of Tube and Shell-side Reynolds Numbers.

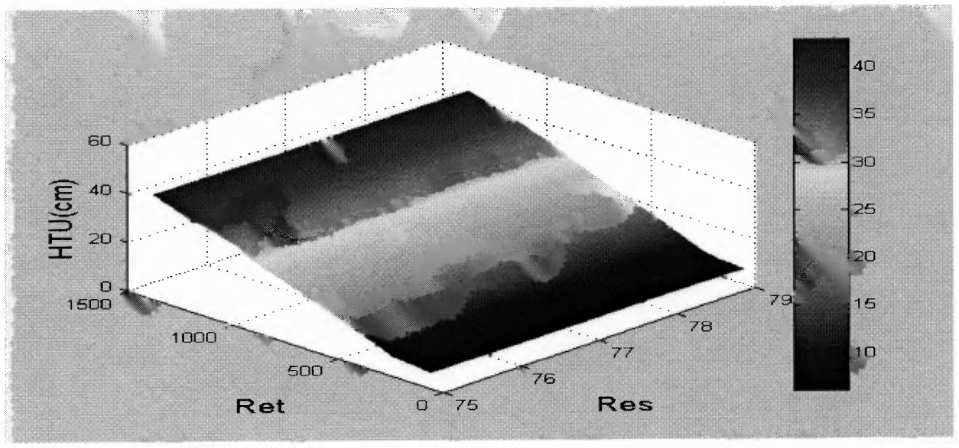

Figure D.6 Experimentally-Derived HTU in HEPP1 (Shell side is of Crossflow Configuration) as a Function of Tube and Shell-side Reynolds Numbers.

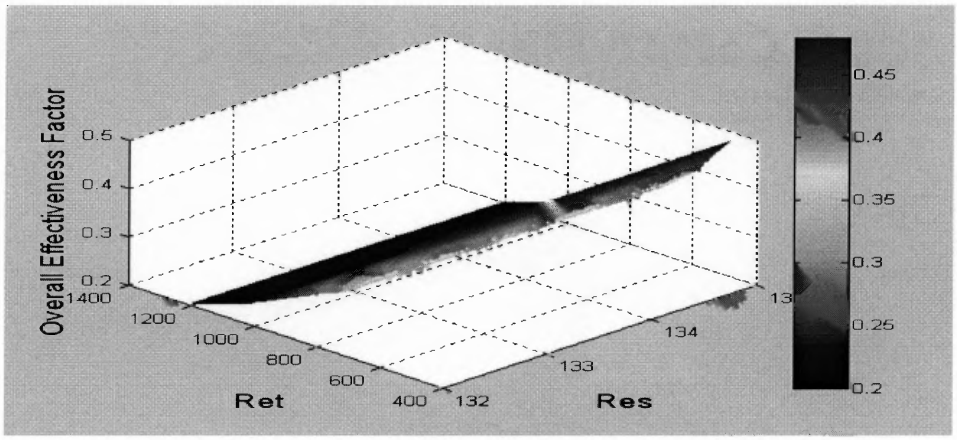

Figure D.7 Overall Effectiveness Factor ε of HEPEEK2 (Shell side is of Crossflow Configuration) as a Function of Tube and Shell-side Reynolds Numbers.

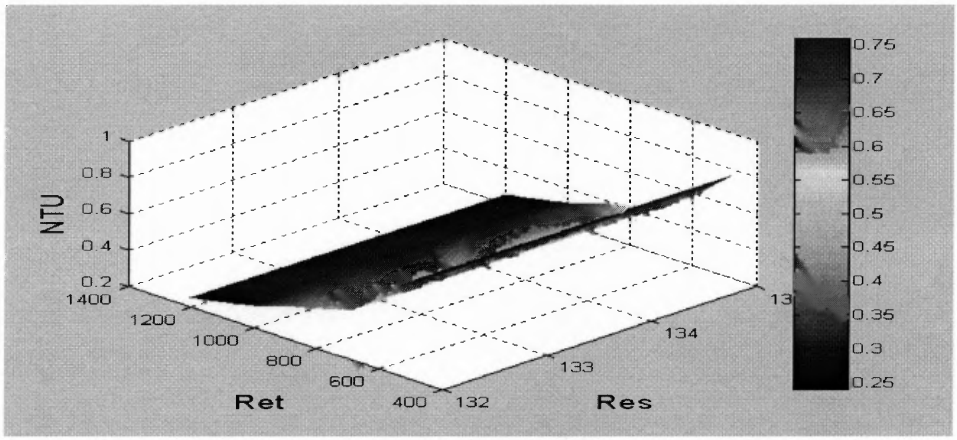

Figure D.8 Experimentally-Derived NTU in HEPEEK2 (Shell side is of Crossflow Configuration) as a Function of Tube and Shell-side Reynolds Numbers.

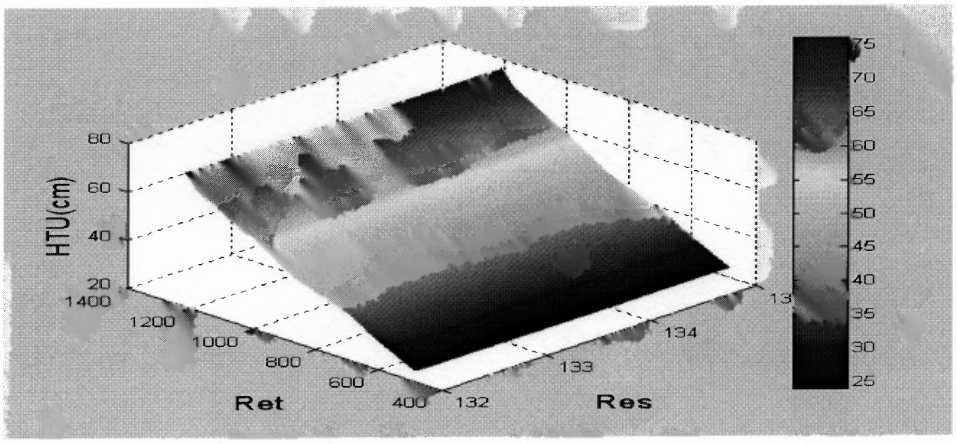

Figure D.9 Experimentally-Derived HTU in HEPEEK2 (Shell side is of Crossflow Configuration) as a Function of Tube and Shell-side Reynolds Numbers .

APPENDIX E

CONVENTIONAL CONVECTION METHOD AND SIEDER -TATE CORRELATION VALUES

Tables E.1 to E.4 show values of h_t , h_s, U_w, Nu_w and Nu_{T3} obtained in the polymeric hollow fiber heat exchange devices using the Conventional Convection Method and Table E.5 shows values of h_t for all the polymeric hollow fiber heat exchangers isolated using Sieder-Tate correlation.

Table E.1 h_t, h_s, h_w, Nu_w and Nu_{T3} Obtained in HEPP1: Conventional Convection Method

Module	Shell-side Arrangement	Configuration	h_t(W/m^2-K)	h_s(W/m^2-K)	U_w (W/m^2-K)	Nu_w	NU_{T3}
HEPP1	**Crossflow at Shell side:**	**Vary Hot Brine (tube), Fix Cooling Water (shell)**	6535-6666	1952-4799	1322-1880	0.85-1.19	4.21-4.25
		Fix Hot Brine (shell),Vary Cooling water(tube)	6325-6606	490-28637	530-2529	0.35-1.69	4.17-4.31
		Vary Hot Brine (shell), Fix Cooling Water (tube)	6314-6357	518-9017	554-2174	0.38-1.43	4.19-4.31
	Parallel Flow at shell side:	**Vary Hot Brine (shell), Fix Cooling Water(tube)**	6316-6349	438-13880	484-2786	0.33-1.82	4.15-4.31

Table E.2 h_t, h_s, U_w, Nu_w and Nu_{T3} Obtained in HEPP2: Conventional Convection Method

Module	Shell-side Arrangement	Configuration	h_t(W/m^2-K)	h_s(W/m^2-K)	U_w(W/m^2-K)	Nu_w	NU_{T3}
HEPP2	**Crossflow at Shell side:**	**Fix Hot Brine tube),Vary Cooling Water(shell)**	6614-6846	761-5822	741-1981	0.47-1.26	4.20-4.29
		Vary Hot Brine (tube), Fix Cooling Water (shell)	6591-6689	1387-4218	1098-1808	0.71-1.14	4.21-4.26
		Fix Hot Brine (shell), Vary Cooling water (tube)	5943-6587	510-2706	547-1536	0.68-1.09	4.21-4.30
		Vary Hot Brine (shell), Fix Cooling Water(tube)	5914-5943	852-2839	803-1567	0.58-1.09	4.22-4.28
	Parallel Flow at shell side:	**Fix Hot Brine (tube),Vary Cooling Water(shell)**	6527-6787	1290-25494	1052-2989	0.66-1.94	4.14-4.26
		Vary Hot Brine (tube), Fix Cooling Water (shell)	6482-6588	2714-28147	1393-2695	0.91-1.70	4.16-4.24
		Fix Hot Brine (shell),Vary Cooling water(tube)	5809-6606		812-3068	0.53-2.16	4.13-4.28
		Vary Hot Brine (shell), Fix Cooling Water (tube)	5849-5884		2084-3114	1.48-2.20	4.13-4.18

Table E.3 h_t, h_s, U_w, Nu_w and Nu_{T3} Obtained in HEPP3: Conventional Convection Method

Module	Shell-side Arrangement	Configuration	h_t(W/m^2-K)	h_s(W/m^2-K)	U_w(W/m^2-K)	Nu_w	NU_{T3}
HEPP3	**Crossflow at Shell side:**	**Fix Hot Brine (tube),Vary Cooling Water(shell)**	6675-6840	690-3573	690-1710	0.43-1.38	4.19-4.29
		Vary Hot Brine (tube), Fix Cooling Water (shell)	6547-6706	1271-2513	1042-1488	0.68-0.94	4.24-4.27
		Fix Hot Brine (shell), Vary Cooling water(tube)	5993-6608	283-1716	335-1236	0.22-0.88	4.24-4.33
		Vary Hot Brine (shell), Fix Cooling Water (tube)	5977-6013	288-1622	340-1200	0.25-0.85	4.25-4.32
	Parallel Flow at shell side:	**Fix Hot Brine (tube),Vary Cooling Water(shell)**	6572-6808	1004-28630	897-2477	0.56-1.57	4.17-4.28
		Vary Hot Brine (tube), Fix Cooling Water (shell)	6455-6593	1199-14932	1006-2340	0.66-1.48	4.19-4.26
		Fix Hot Brine (shell),Vary Cooling water(tube)	5922-6414	345-18065	1670-2387	1.10-1.67	4.17-4.22
		Vary Hot Brine (shell), Fix Cooling Water(tube)	5918-5948	2375-18482	1451-2382	1.04-1.68	4.18-4.23

Table E.4 h_t, h_s, U_w, Nu_w and Nu_{T3} Obtained in HEPEEK2: Conventional Convection Method

Module	Shell-side Arrangement	Configuration	h_t(W/m^2-K)	h_s(W/m^2-K)	U_w(W/m^2-K)	Nu_w	NU_{T3}
HEPEEK2	**Crossflow at Shell side:**	**Fix Hot Brine (tube),Vary Cooling water(shell)**	6707-6900	547-3607	580-1719	0.36-1.08	4.22-4.31
		Vary Hot Brine (tube), Fix Cooling Water (shell)	6620-6708	1175-3565	995-1712	0.65-1.08	4.22-4.27
		Fix Hot Brine (shell),Vary Cooling water(tube)	6067-6317	7308-10649	1993-2240	1.32-1.49	4.18-4.19
		Vary Hot Brine (shell), Fix Cooling Water(tube)	6024-6045	4403-14357	1836-2333	1.28-1.62	4.17-4.20
	Parallel Flow at shell side:	**Fix Hot Brine (tube), Vary Cooling Water(shell)**	5823-6128	1766-21963	1256-2853	0.87-2.03	4.14-4.24
		Fix Hot Brine (shell),Vary Cooling water(tube)	5980-6351	1427-26685	1117-2848	0.78-1.97	4.14-4.25
		Vary Hot Brine (shell), Fix Cooling Water(tube)	6037-6048	6692-40328	2161-2528	1.42-1.74	4.16-4.18

Table E.5 Values of h_t for Polymeric Hollow Fiber Heat Exchangers Calculated Using Sieder-Tate Correlation

Test Run Configuration	**h_t(W/m^2-K)**			
	HEPP1	**HEPP2**	**HEPP3**	**HEPEEK2**
Vary hot brine on shell side, fix cooling water on tube side	4685[a] 4689[b]	6122[a] 5657[b]	5736[a] 5529[b]	6935[a] 6901[b]
Fix hot brine on shell side, vary cooling water on tube side	2196-6388[b]	2282-6688[a] 3089-8067[b]	3156-5786[a] 2480-5629[b]	4527-7582[a] 4804-6920[b]
Vary cooling water on shell side, fix hot brine on tube side		6503[a] 6490[b]	8587[a] 5855[b]	5971[a] 5645[b]
Fix cooling water on shell side, vary hot brine on tube side	2907-6346[b]	3189-6491[a] 3545-6481[b]	4094-8573[a] 3221-5823[b]	3680-5608[b]

[a] – Shell side in Parallel flow Configuration for module [b] – Shell side in Crossflow Configuration for module

APPENDIX F

FRICTION FACTOR AND COLBURN FACTOR CURVES

Figures F.1 to F.2 show plots of the Fanning Friction Factor ($f_{Fanning}$) and j_H against Re_t for experiments with hot brine on tube side and shell side in crossflow mode.

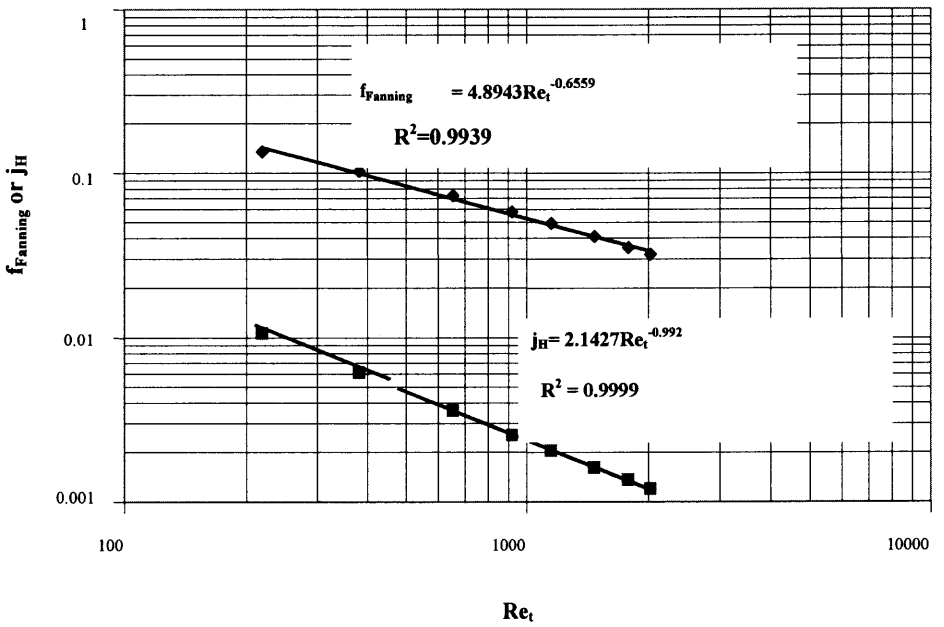

Figure F.1 Plot of $f_{Fanning}$ and j_H vs Re_t for HEPP3 module.

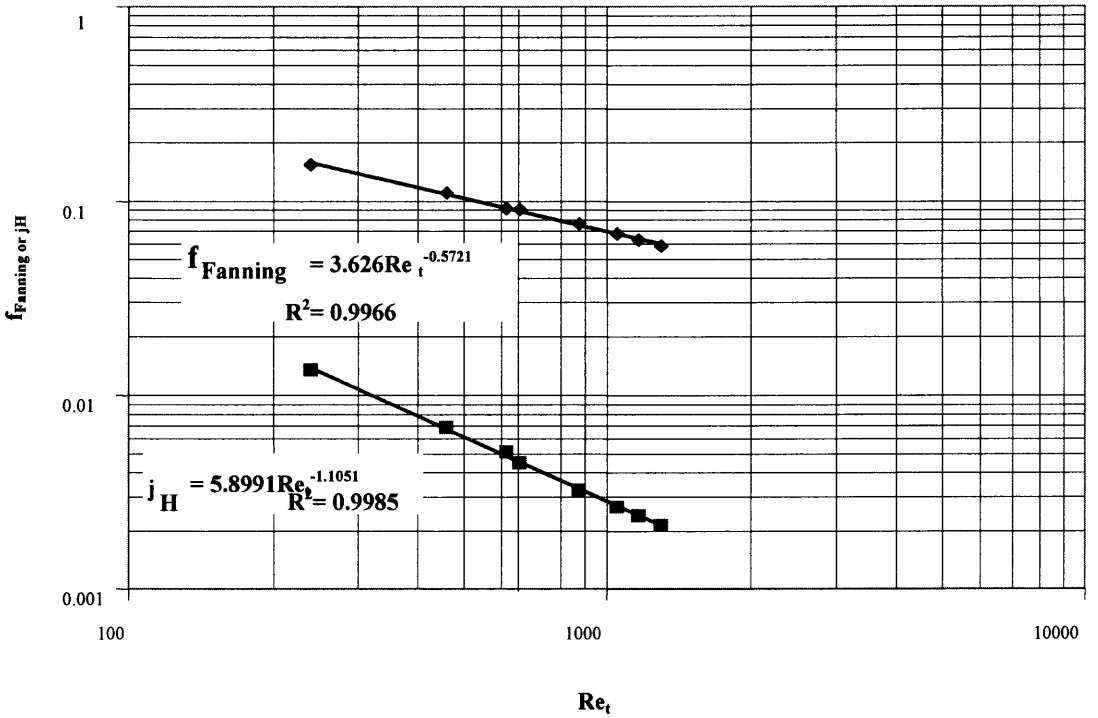

Figure F.2 Plot of $f_{Fanning}$ and j_H vs Re_t for HEPEEK2 module.

APPENDIX G

STEAM/COLD WATER SYSTEM ANALYSIS RESULTS

Tables G.1 to G.5 depict heat transfer data for steam/cold water system

Table G.1 Heat Transfer Data for HEPP1 (Shell side -Crossflow)

Exp	T_{t1} (°C)	T_{t2} (°C)	T_{s1} (°C)	T_{s2} (°C)	F_s (ml/min)	T_{t1}-T_{t2} (°C)	T_{s2}-T_{s1} (°C)	A (m^2)	Q (W/m^2)	m_tCp_t (J/K)	m_sCp_s (J/K)	U (W/m^2-K)
Fix shell-side cooling water flow rate and vary tube-side steam flow rate												
Exp. No. 1	103.6	22.4	20.3	20.6	4518.0	81.2	0.3	0.0195	4842	0.1	314.4	77
Exp. No. 2	105.2	19.4	18.3	22.1	4482.0	85.8	3.8	0.0195	60848	1.7	311.9	939
Exp. No. 3	105.3	16.9	15.1	20.5	4436.0	88.4	5.4	0.0195	85581	2.5	308.8	1283
Exp. No. 4	113.2	37.8	19.6	27.7	4605.0	75.4	8.1	0.0195	133262	4.1	320.2	1621
Exp. No. 5	113.4	35.7	19.6	27.7	4651.0	77.7	8.1	0.0195	134593	4.2	323.4	1693
Exp. No. 6	112.7	35.6	19.7	26.9	4640.0	77.1	7.2	0.0195	119355	4.0	322.6	1609
Exp. No. 7	113.3	33.3	19.7	27.9	4410.0	80.0	8.2	0.0195	129194	3.9	306.6	1609
Exp. No. 8	104.2	20.4	19.7	22.3	4520.0	83.8	2.6	0.0195	41986	1.4	314.5	831
Exp. No. 9	100.1	21.9	19.7	20.3	4520.0	78.2	0.6	0.0195	9689	0.2	314.5	113
Exp. No. 10	101.4	21.2	19.8	20.7	4549.0	80.2	0.9	0.0195	14627	0.4	316.5	239
Exp. No. 11	101.0	20.5	19.8	22.5	4497.0	80.5	2.7	0.0195	43379	1.0	312.9	611
Exp. No. 12	101.9	20.7	19.8	22.6	4532.0	81.2	2.8	0.0195	45335	1.1	315.3	648
Fix tube-side steam flow rate and vary shell-side cooling water flow rate												
Exp. No. 1	117.0	99.3	21.1	72.2	324.0	17.7	51.1	0.0195	59150	2.0	22.3	838
Exp. No. 2	115.6	99.1	21.8	62.5	494.0	16.5	40.7	0.0195	71831	2.5	34.1	992
Exp. No. 3	115.8	99.0	21.8	62.9	496.0	16.8	41.1	0.0195	72831	2.5	34.2	983
Exp. No. 4	115.4	99.4	22.0	56.8	601.0	16.0	34.8	0.0195	74721	2.6	41.6	995
Exp. No. 5	115.1	98.7	21.8	54.0	708.0	16.4	32.2	0.0195	81448	2.5	49.0	953
Exp. No. 6	114.7	98.5	21.5	47.7	989.0	16.2	26.2	0.0195	92574	3.1	68.5	1124
Exp. No. 7	113.7	98.1	21.2	43.3	1270.0	15.6	22.1	0.0195	100274	3.4	88.1	1190
Exp. No. 8	113.1	40.9	20.5	31.0	3563.0	72.2	10.5	0.0195	133658	4.0	247.6	1601

Table G.2 Heat Transfer Data for HEPP1 (Shell Side -Parallel flow)

Exp	T_{t1} (°C)	T_{t2} (°C)	T_{s1} (°C)	T_{s2} (°C)	F_s (ml/min)	T_{t1}-T_{t2} (°C)	T_{s2}-T_{s1} (°C)	A (m^2)	Q (W/m^2)	m_tCp_t (J/K)	m_sCp_s (J/K)	U (W/m^2-K)
Fix shell-side cooling water flow rate and vary tube-side steam flow rate												
Exp. No. 1	53.7	113.1	22.7	34.4	2842.3	59.4	11.7	0.0195	118806	3.5	197.3	1351
Exp. No. 2	39.7	111.5	22.7	34.1	2842.3	71.8	11.4	0.0195	115760	2.8	197.3	1157
Exp. No. 3	23.1	105.7	22.7	29.4	2842.3	82.6	6.7	0.0195	68034	1.7	197.5	1063
Exp. No. 4	49.0	113.0	22.8	34.6	2897.2	64.0	11.8	0.0195	122136	3.2	201.1	1239
Exp. No. 5	43.4	112.4	22.8	34.1	2911.2	69.0	11.3	0.0195	117528	3.4	202.1	1385
Exp. No. 6	22.9	104.6	22.7	27.7	2911.2	81.7	5.0	0.0195	52003	1.3	202.3	825
Exp. No. 7	50.8	112.9	22.7	34.4	2928.3	62.1	11.7	0.0195	122401	4.0	203.3	1550
Exp. No. 8	55.3	113.1	22.8	34.7	2897.2	57.8	11.9	0.0195	123171	3.2	201.1	1226
Exp. No. 9	24.7	107.5	22.7	30.8	3001.0	82.8	8.1	0.0195	86844	1.5	208.5	827
Exp. No. 10	53.7	113.3	22.7	34.4	3001.0	59.6	11.7	0.0195	125442	3.7	208.3	1417
Fix tube-side steam flow rate and vary shell-side cooling water flow rate												
Exp. No. 1	98.6	114.9	22.4	49.1	869.0	16.3	26.7	0.0195	82894	2.7	60.2	997
Exp. No. 2	98.5	116.6	22.4	59.7	500.0	18.1	37.3	0.0195	66630	2.6	34.5	999
Exp. No. 3	98.5	116.8	22.5	64.1	441.8	18.3	41.6	0.0195	65655	2.2	30.5	876
Exp. No. 4	98.5	115.3	22.8	57.2	606.0	16.8	34.4	0.0195	74477	2.5	41.9	965
Exp. No. 5	97.7	116.5	22.5	71.2	304.5	18.8	48.7	0.0195	52979	1.7	21.0	727
Exp. No. 6	98.6	113.5	22.3	44.7	1162.1	14.9	22.4	0.0195	93000	3.1	80.5	1111
Exp. No. 7	81.8	108.6	22.2	36.4	2186.6	26.8	14.2	0.0195	110929	3.7	151.8	1372
Exp. No. 8	54.1	103.7	22.3	34.4	2767.5	49.6	12.1	0.0195	119637	3.6	192.1	1512

Table G.3 Heat Transfer Data for HEPP2 (Shell side -Parallel flow)

Exp	T_{t1} (°C)	T_{t2} (°C)	T_{s1} (°C)	T_{s2} (°C)	F_s (ml/min)	T_{t1}-T_{t2} (°C)	T_{s2}-T_{s1} (°C)	A (m^2)	Q (W/m^2)	m_tCp_t (J/K)	m_sCp_s (J/K)	U (W/m^2-K)
Fix tube-side steam flow rate and vary shell-side cooling water flow rate												
Exp. No. 1	104.6	17.1	17.0	28.5	6233.8	87.5	11.5	0.096	52024	8.5	433.5	1198
Exp. No. 2	104.5	17.1	16.9	25.9	8185.5	87.4	9.0	0.096	53462	8.0	569.4	1063
Exp. No. 3	103.5	17.0	16.9	23.7	10186.8	86.5	6.8	0.096	50269	7.9	708.8	1093
Exp. No. 4	103.4	16.9	16.8	22.1	11952.2	86.5	5.3	0.096	45970	7.8	831.8	1081
Exp. No. 5	104.5	17.1	16.9	30.4	5174.6	87.4	13.5	0.096	50695	8.4	359.8	1128
Exp. No. 6	104.4	17.3	17.1	33.0	4285.7	87.1	15.9	0.096	49451	7.8	297.8	1068
Exp. No. 7	108.2	26.3	17.4	53.0	2000.0	81.9	35.6	0.096	51669	8.2	138.5	869
Exp. No. 8	104.7	19.1	17.4	39.3	2980.6	85.6	21.9	0.096	47370	7.7	206.9	904
Exp. No. 9	103.8	17.2	17.0	22.3	13574.7	86.6	5.3	0.096	52211	8.5	944.7	1115

Table G.4 Heat Transfer Data for HEPP2 (Shell side -Crossflow)

Exp	T_{t1} (°C)	T_{t2} (°C)	T_{s1} (°C)	T_{s2} (°C)	F_s (ml/min)	T_{t1}-T_{t2} (°C)	T_{s2}-T_{s1} (°C)	A (m^2)	Q (W/m^2)	m_tCp_t (J/K)	m_sCp_s (J/K)	U (W/m^2-K)
Fix tube-side steam flow rate and vary shell-side cooling water flow rate												
Exp. No. 1	108.8	76.5	10.8	32.7	6269.6	32.3	21.9	0.096	99641	14.7	436.1	1018
Exp. No. 2	108.8	98.5	11.4	38.3	4246.3	10.3	26.9	0.096	82892	13.1	295.1	900
Exp. No. 3	109.1	99.4	11.9	45.1	3001.5	9.7	33.2	0.096	72315	12.5	208.4	898
Exp. No. 4	108.7	72.7	11.1	31.3	7277.1	36.0	20.2	0.096	106676	12.8	506.3	886
Exp. No. 5	108.4	51.6	10.8	28.1	8664.2	56.8	17.3	0.096	108775	14.5	603.0	1052
Exp. No. 6	108.8	35.4	10.7	25.4	10801.1	73.4	14.7	0.096	115223	15.0	752.0	1152
Exp. No. 7	108.4	96.5	11.4	36.2	4916.0	11.9	24.8	0.096	88475	13.8	341.8	942
Fix shell-side cooling water flow rate and vary tube-side steam flow rate												
Exp. No. 1	108.4	55.8	11.2	29.1	8247.4	52.6	17.9	0.096	107133	13.7	573.9	988
Exp. No. 2	108.3	51.5	11.3	29.0	8333.3	56.8	17.7	0.096	107040	13.5	579.9	990
Exp. No. 3	108.0	50.0	11.3	29.2	8275.6	58.0	17.9	0.096	107499	13.3	575.9	989
Exp. No. 4	107.1	34.5	11.3	28.4	8275.9	72.6	17.1	0.096	102698	12.4	575.9	989
Exp. No. 5	104.1	16.2	11.3	25.1	8298.8	87.9	13.8	0.096	83109	9.6	577.7	926
Exp. No. 6	108.2	41.5	11.4	28.5	8264.5	66.7	17.1	0.096	102557	15.4	575.1	1183
Exp. No. 7	110.3	98.7	11.4	30.6	8174.4	11.6	19.2	0.096	113897	17.9	568.7	1154

Table G.5 Heat Transfer Data for HEPEEK2 (Shell side -Crossflow)

Exp	T_{t1} (°C)	T_{t2} (°C)	T_{s1} (°C)	T_{s2} (°C)	F_s (ml/min)	T_{t1}-T_{t2} (°C)	T_{s2}-T_{s1} (°C)	A (m^2)	Q (W/m^2)	m_tCp_t (J/K)	m_sCp_s (J/K)	U (W/m^2-K)
Fix tube-side steam flow rate and vary shell-side cooling water flow rate												
Exp. No. 1	111.5	37.3	16.4	23.3	3466.2	74.2	6.9	0.0193	86332	3.0	241.2	1166
Exp. No. 2	110.6	28.0	16.2	21.8	4149.4	82.6	5.6	0.0193	83876	3.1	288.8	1289
Exp. No. 3	111.3	23.7	15.9	20.9	5291.0	87.6	5.0	0.0193	95494	3.0	368.3	1276
Exp. No. 4	110.5	21.6	15.8	19.7	6224.1	88.9	3.9	0.0193	87621	3.1	433.3	1363
Exp. No. 5	109.7	20.7	15.7	19.3	6936.4	89.0	3.6	0.0193	90137	3.1	483.0	1391
Exp. No. 6	110.7	19.8	15.6	18.7	7941.8	90.9	3.1	0.0193	88868	3.1	553.0	1406
Exp. No. 7	110.7	19.3	15.6	18.5	8708.3	91.4	2.9	0.0193	91159	3.1	606.4	1425
Exp. No. 8	110.0	19.0	15.5	18.1	9188.4	91.0	2.6	0.0193	86234	3.1	639.8	1471

REFERENCES

1. Bennett, C. O., Myers J. E. Momentum, Heat and Mass Transfer,3rd Edition, Mc Graw Hill Book Company, 1982.

2. Cheremisinoff, N. P. Heat Transfer Pocket Handbook, Gulf Publishing Company, 1984.

3. El-Dessouky, H. T., Ettouney, H. M. Plastic Compact Heat Exchangers for Single-Effect Desalination Systems, Desalination 122 (1999): 271-289.

4. Groll, M.; Mertz, R. Improved Evaporation Heat Transfer Surfaces for cost-effective compact heat exchangers for the process industries, Applied Thermal Engineering 17 (1997): 685-703.

5. Hsu, C. J. Laminar Flow Heat Transfer in Circular or Parallel-Plate Channels with Internal Heat Generation and the Boundary Condition of the third kind, Journal of the Chinese Institute of Chemical Engineers, 2 (1971): 85-92

6. Jachuck, R. J. J., Ramshaw, C. Process Intensification: Polymer film compact heat Exchanger (PFCHE), Chemical Engineering Research and Design,72A (1994), 255.

7. Kakac, S., Shah, R. K., Bergles, A. E. Low Reynolds Number Flow Heat Exchangers, Hemisphere Publishing Corporation, NY, 1983.

8. Kays, W. M., London, A. L. Compact Heat Exchangers,3rd Edition, Mc Graw Hill Book Company, NY, 1984.

9. Kern, D. Q. Process Heat Transfer, Mc Graw Hill Book Company, 1950.

10. Klein and Kessler's "Dialysis'' In Membrane Handbook, Eds., Ho, W.S.; Sirkar, K.K., Kluwer Academic Publishers, Boston, 2001.

11. Lixen, C., Van Dergeld, Cees, W. M. Experimental study of heat transfer and pressure drop characteristics of air/water and air-steam /water heat exchange in a polymer compact heat exchanger, Heat Transfer Engineering 26 (2005): 18-27.

12. Mala, M. Gh., Li, D. Flow Characteristics of water in microtubes, International Journal of Heat and Fluid Flow 20 (1999).

13. Michelsen, M. L., Villadsen, J. The Graetz Problem with axial heat conduction, International Journal of Heat and Mass Transfer 17(1974): 1391-1402.

14. Morcos, V. H., Shafey, H. M. Performance analysis of a plastic shell-and-tube heat exchanger, Journal of Elastomers and Plastics, 27(1995): 200

15. Perry, R. H., Green D. W. Perry's Chemical Engineers' Handbook,7th Edition, Mc Graw Hill, NY 1999.

16. Reay, D. A. The use of polymers in heat exchangers, Heat recovery systems and CHP, 9 (1989): 209-216.

17. Roberson, J. A., Crowe, C. T. Engineering Fluid Mechanics,3rd Edition, Houghton Mifflin Company, Boston 1985.

18. Rose, W. J. Heat Transfer coefficients, Wilson plots and accuracy of thermal measurements, Experimental Thermal and Fluid Science 28(2004): 77-86.

19. Shah, R. Compact Heat Exchangers for the Process Industries, Begell House Inc, 1997: 30.

20. Shah, R. K., London A.L. Laminar Flow Forced Convection in Ducts, Advances in Heat Transfer, Supplement 1, 1978.

21. Sinnott, R. K., Coulson and Richardson's Chemical Engineering, Revised 2nd Edition, Butterworth-Heineman, Oxford, 1983.

22. Weast, R. C. CRC Handbook of Chemistry and Physics, 59th Edition, CRC Press Inc, 1978-1979.

23. Wei, L., Davidson, J., Mantell S. Thermal Analysis of Polymer Heat Exchangers for Solar Water Heating: A Case Study, Journal of Solar Engineering, 122 (2000): 84-91

24. Zaheed, L., Jachuck, R. I. J. Review of polymer compact heat exchangers, with special emphasis on a polymer film unit, Applied Thermal Engineering ,24 (2004): 2323-2358.

25. Zarkadas, D. M., Sirkar, K. K. Polymeric Hollow Fiber Heat Exchangers: An Alternative for Lower Temperature Applications, Ind. Eng. Chem. Res. 43(2004): 8093-8106.

26. Zukauskas, A. Heat Transfer from Tubes in Crossflow, Advances in Heat Transfer, 8 (1972): 93-160.